THE CATALYTIC MECHANISMS OF MYCOBACTERIUM TUBERCULOSIS CATALASE-PEROXIDASE (KATG) AND THE ORIGIN OF ANTIBIOTIC RESISTANCE IN THE KATG[S315G] MUTANT.

by

JAVIER SUAREZ

A dissertation submitted to the Graduate Faculty in Biochemistry in partial fulfillment of the requirements for the degree of Doctor of Philosophy,

The City University of New York

2009

This manuscript has been read and accepted for the Graduate Faculty in Biochemistry in satisfaction of the dissertation requirement for the degree of Doctor of Philosophy.

_____	_____
Date	Chair of the examining committee Dr. Richard S. Magliozzo
_____	_____
Date	Executive officer Dr. Edward J. Kennelly
Supervisory Committee:	_____ Dr. John S. Blanchard
	_____ Dr. Brian Gibney
	_____ Dr. Laura Juszczak
	_____ Dr. Johannes J. P. Schelvis

The City University of New York

ABSTRACT

THE CATALYTIC MECHANISMS OF MYCOBACTERIUM TUBERCULOSIS CATALASE-PEROXIDASE (KATG) AND THE ORIGIN OF ANTIBIOTIC RESISTANCE IN THE KATG[S315G] MUTANT.

by

Javier Suarez

Adviser: Dr. Richard S. Magliozzo

Catalase-peroxidase (KatG) in *M. tuberculosis* is a bifunctional heme protein that exhibits both high catalase activity ($2H_2O_2 \rightarrow 2H_2O + O_2$) and a broad-spectrum peroxidase activity ($2AH + H_2O_2 \rightarrow 2A^{\bullet} + 2H_2O$) and is responsible for activation of isoniazid (INH), a *pro*-drug used to treat TB infections. Resistance to INH is a global health problem most often associated with mutations in the *katG* gene. Nevertheless, there is a big gap in the *M. tuberculosis* literature with respect to the molecular origins of isoniazid resistance due to mutations in KatG. Here, we examined the origin of INH resistance caused by the KatG[S315G] mutant enzyme. Overexpressed KatG[S315G] was characterized by optical, EPR and resonance Raman spectroscopy and by studies of the INH activation mechanism *in vitro*. INH resistance is suggested to arise from a redirection of catalytic heme intermediates into non-productive reactions that interfere with oxidation of INH.

Previous studies have shown the formation of amino acid based radicals in KatG upon reaction with alkyl peroxide. However, the location and the possible function of these radicals are far from being resolved. In this study we tried to gain insights into the loci of radical formation through the analysis of cross-linking during turnover of KatG in the presence and absence of reducing substrate. SDS and Native-PAGE of KatG treated with peracetic acid or hydrogen peroxide under a variety of conditions demonstrate oligomers of molecular weight greater than that of the native dimer. The results are consistent with the hypothesis that cross-linking of KatG can occur in the absence of peroxidase substrates and that under physiological conditions, the activation of INH as well as the stability of KatG may be altered by this process.

One of the most interesting structural features of *Mtb* KatG is the post-translational modification of residues Met 255, Tyr229 and Trp107, the side chains of which form an adduct on the distal side of the heme. Mutation of any of these three residues completely abolishes the catalase activity of KatG. A mechanism accounting for the robust catalase activity and the function of this adduct in catalase-peroxidases (KatG) presents a new challenge in heme protein enzymology. Here, optical stopped-flow spectrophotometry, rapid freeze-quench electron paramagnetic resonance (RFQ-EPR) spectroscopy both at X-band and at D-band, and mutagenesis were used to identify catalase reaction intermediates in *Mtb* KatG. Using rapid-freeze-quench EPR at X-band under catalase activity conditions (excess H_2O_2), a narrow doublet radical signal with an 11 G principal hyperfine splitting was detected within the first milliseconds of turnover. The radical persists in wild-type KatG only during the time course of turnover of excess

H_2O_2 (1000-fold or more). Mutation of Met255, Tyr229, or Trp107, abolishes this radical and the catalase activity. Therefore, a catalytic role for an MYW adduct radical in the catalase mechanism of KatG is proposed.

ACKNOWLEDGMENTS

I would like to express my sincere gratitude to all the people that helped me on the completion of my thesis. Especially, I am very grateful and deeply indebted to my mentor, Professor Richard Magliozzo for his great support, guidance and patience during the past five years. His great knowledge and fervor for scientific research inspired and helped me to overcome a big transition from biology into the field of physical biochemistry and enzymology. Being his student during the completion of my doctoral research was a remarkable experience in my life as a scientist.

I also want to thank all the members of my doctoral thesis committee for their helpful advice and brilliant suggestions regarding my research project. I am pleased to thank professor Hans Schelvis who offered me his laboratory equipment, his advice, guidance and necessary assistance for the study by Raman spectroscopy of one of the mutant enzymes generated for this thesis; and to Professor Gary Gerfen, who provided high field EPR spectrometer as well as his rapid freeze quench equipment for the preparation of very important samples for this study. His advice and expertise was also of great help for the analysis of these samples.

This is also a great opportunity to express my gratitude to all the people working at Dr. Magliozzo's lab, especially to Kalina Ranguelova, Shengwei Yu, Leonid Metlitsky, Abdelahad Khajo, and Xiangbo Zhao, who offered me invaluable help and support during the last five years.

Finally, I would like to thank my friends and family, especially my mother, for their support and encouragement during my Ph. D. studies.

TABLE OF CONTENTS

LIST OF TABLES

LIST OF SCHEMES

LIST OF FIGURES

Chapter I: Introduction

1.1. Tuberculosis, a major global health issue:

Mycobacterium tuberculosis is the etiologic agent of tuberculosis in humans. Humans are the only known reservoir for the bacterium. This bacterium has been present in humans since antiquity. The earliest unambiguous detection of *M. tuberculosis* is in the remains of bison dated 17,000 years ago. Skeletal remains show prehistoric humans (4000 BC) had TB, and spines of Egyptian mummies from 3000-2400 BC show definite pathological signs of tubercular disease (1,2). Fifty years ago *M. tuberculosis* was thought to be nearly eradicated, however, in the last couple of decades it has made a dramatic reemergence partially triggered by the epidemic of human immunodeficiency virus (HIV). Even though this bacteria has been part of human civilizations for a very long period of time, it was not until around sixty years ago that the first effective antibiotic (isoniazid) against tuberculosis was discovered (3).

Currently World Health Organization statistics show that more that one-third of the world's population is infected with the tubercle bacillus and that one in every ten of these individuals will develop the disease at some point of their lifetime. Tubercular infection kills nearly two million people a year and is the leading cause of death due to infectious diseases in adults, and in AIDS patients (4). The infection is usually treatable and isoniazid (isonicotinic acid hydrazide, INH) has been a first-line antibiotic against *M. tuberculosis* since 1952 (3). The management of the disease is complicated by the fact that tuberculosis strains have been steadily acquiring and accumulating mutations that

confer resistance to INH and other drugs (5-8). In recent times, the appearance of multi-drug resistant (MDR-TB, resistant to at least two of the first line antibiotics) and extensively drug resistant tuberculosis (XDR-TB, MDR-TB + resistant to at least one fluoroquinolone + resistant to at least one of the injectable second line drugs) has made the unfortunate patients carrying these strains virtually untreatable (Figure. 1.1). Currently, 20% of the *M. tuberculosis* isolates worldwide are MDR-TB. Among these MDR-TB cases, 4% in the U.S., 15% in South Korea, 19% in Latvia and 24% in South Africa are XDR-TB (9,10). Despite this overwhelming emergence of antibiotic resistant strains, many of the molecular mechanisms altered due to mutations that confer resistance are unknown or poorly understood.

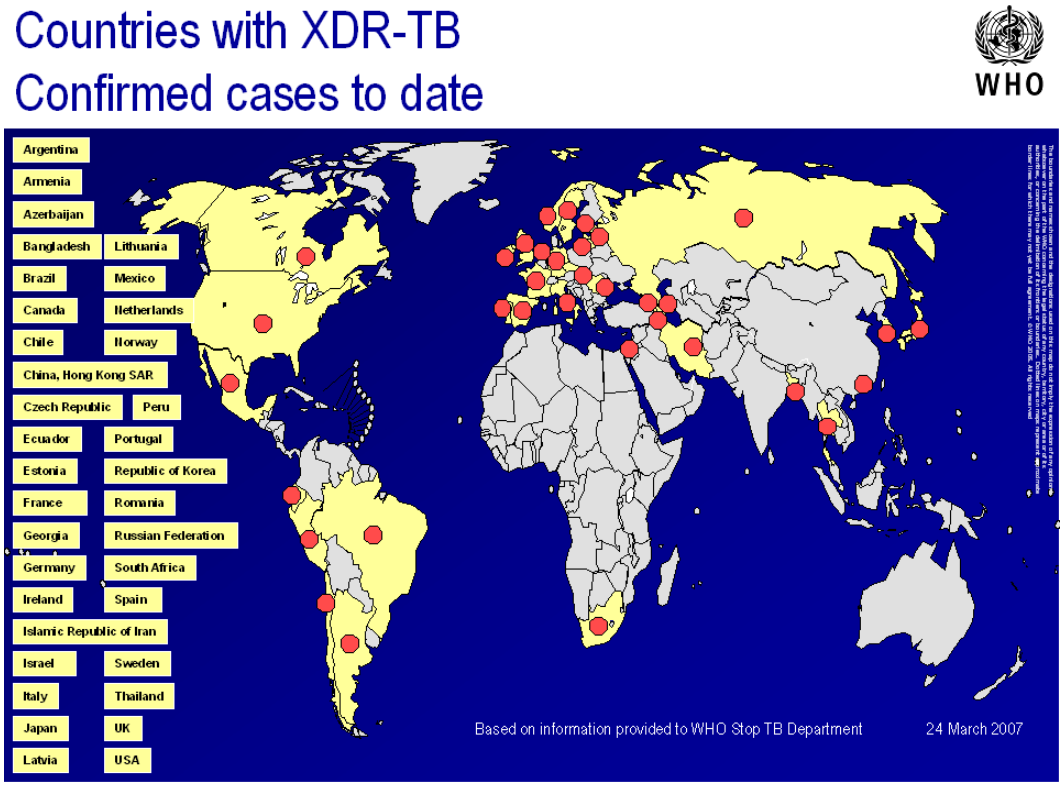

Figure 1.1. World map showing countries with confirmed cases of XDR-TB (red dots). (World Health Organization TB report 2007)

1.2. *M. tuberculosis* cell wall composition and Isoniazid (INH) activity:

The genus mycobacterium has an unusual cell wall structure that differs from that of $Gram^+$ and $Gram^-$ bacteria. Mycobacteria are relatively resistant to conventional staining procedures. Cells stained with carbolfuchsin dye cannot be decolorized with acid-alcohol and are therefore classified as "acid fast" (Ziehl-Neelsen or acid-fast stain technique). This characteristic reflects the unusual composition of the cell wall, which contains an unusual amount of lipids, including the atypical kind of fatty acids called mycolic acids. These lipids may be responsible for the resistance of mycobacteria to environmental stresses such as drying. In fact, mycobacteria can survive for weeks in dried sputum and are very resistant to chemical antimicrobials used as antiseptics and disinfectants (11). Many antituberculosis agents, including ethambuthol, ethionamide and isoniazid (INH) (Figure 1.2) are known to inhibit mycolic acid biosynthesis (12,13).

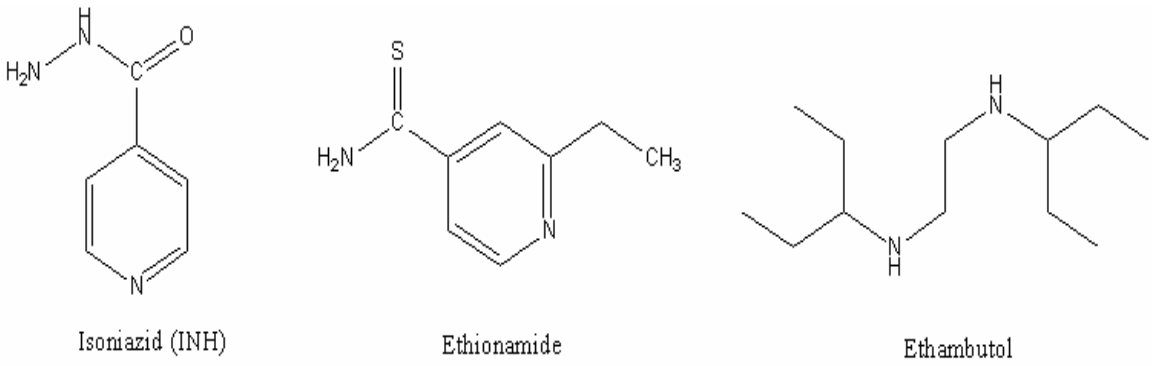

Figure 1.2. First line drugs used in the treatment of tuberculosis known to disrupt cell wall biosynthesis.

Mycolic acids are a homologous series of C_{60} to C_{90} α-alkyl, β-hydroxy fatty acids produced by all mycobacteria and are also found (in shorter chains) in other related

bacteria like *Corynebacterium* and *Nocardia* ssp. In mycobacterial cells, mycolic acids are present either in lipids fractions, extractable by organic solvents, or, for the most part as bound esters or arabinogalactan, a peptidoglycan linked polysaccharide (14,15) (Figure 1.3).

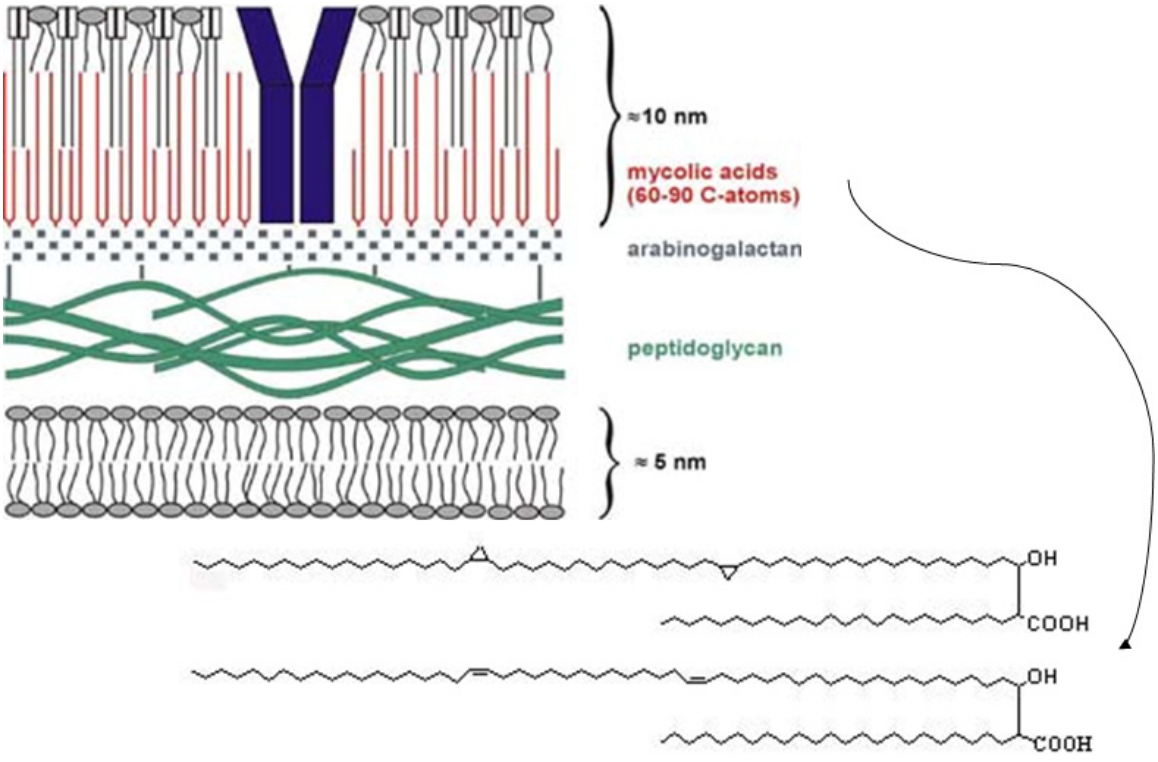

Figure 1.3. Organization of mycobacterial cell wall showing location and chemical structure of mycolic acids. This figure is adapted from Somoskovi, et. al. (16)

The biosynthesis of mycolic acids seems to be a discontinuous process in growing mycobacterial cells. It was shown that mycolic acid synthesis occurs only during the division phase of *M. aurum* (17). Although the mycolic acid biosynthesis pathway is very complex and is not completely defined, evidence to date suggests that normal mycolic acid metabolism is crucial to the survival of *M. tuberculosis*. Some evidence for this fact comes from the work initiated by F. Winder (12) and later by Takayama (18) on

the action of isoniazid (INH), the most efficient and most widely used antituberculosis drug.

1.3. M. tuberculosis catalase-peroxidase KatG, INH activation and resistance:

A member of a new family of bifunctional bacterial heme enzymes (catalase-peroxidase) different from the monofunctional heme catalases was initially isolated from *E. coli* about 30 years ago (19,20). Members of this family of proteins were called KatGs. Shortly after this initial discovery, KatGs were found in several other organisms, like, photosynthetic bacteria *Rhodopseudomonas capsulata* (21) and *Bacillus stearothermophylus (22).* Sequences of these proteins showed they have little homology with typical catalases but high homology with yeast cytochrome *c* peroxidase and ascorbate peroxidase.

As an intracellular parasite infecting macrophages, *M. tuberculosis* is exposed to reactive oxygen species generated by the host NADPH oxidase (Phox) and the reactive nitrogen species (RNS) generated by the inducible nitric oxide synthase (NOS2) (23). Macrophages are capable of inhibiting *M. tuberculosis* replication via NOS2-generated RNS (24), and NOS2 gene-disrupted mice are highly susceptible to *Mtb* infection (25). Since KatG is the only catalase found in *M. tuberculosis* (26), therefore it is expected that survival in macrophages should depend at least in part on this enzyme. One of the first studies showing a relationship between KatG and virulence of *M. tuberculosis* was presented by Middlebrook (27) who showed that isoniazid resistant isolates of *M.tuberculosis* were catalase deficient and markedly attenuated in guinea pigs. This

relationship was further supported by Mckinney et. al (28) who showed that a ΔKatG *Mtb* strain has markedly attenuated ability to replicate and persist in infected macrophages and mice. *Mtb* KatG might be also essential for detoxification of endogenous peroxides generated by bacterial respiration of nonfermentable substrates such as fatty acids which might be the major source of carbon used by *M. tuberculosis* in persistently infected mice (29).

Currently, the most widely studied catalase peroxidases are those from *Synechocystis sp., Burkholderia pseudomallei,* and *M. tuberculosis*. Extensive research on these enzymes shows that they share a very similar catalytic mechanism that differs from that of monofunctional catalases and peroxidases (Figure 1.4 A). KatG's are heme enzymes classified in the Class I superfamily of fungal, plant, and bacterial peroxidases. These enzymes are homodimeric or tetrameric heme proteins that exhibit both high catalase activity ($2H_2O_2 \rightarrow 2H_2O + O_2$) and a broad-spectrum peroxidase activity ($2AH + H_2O_2 \rightarrow 2A^{\bullet} + 2H_2O$) (30,31) (Figure. 1.4-A). In the typical catalase cycle, a molecule of H_2O_2 reacts with the resting protein (ferric) to form a very reactive intermediate called Compound I (Fe(IV)=O Por $^{\bullet+}$) which contains two oxidation equivalents relative to the ferric enzyme; then, Cmpd I reacts with a second molecule of H_2O_2 bringing the enzyme back to the ferric (resting) state. The peroxidase cycle shares the same first step as the catalase cycle, but the highly reactive Cmpd I returns to the resting state by a different pathway involving its reaction with a single electron donor (usually a small aromatic molecule) to form Compound II (Fe(IV)=O Por). Compound II contains oxyferryl heme like in Compound I but without the porphyrin cation radical. A second single electron reduction of Compound II reduces the enzyme back to the resting state.

The main differences between KatGs, and monofunctional catalases and peroxidases, are a very rapid decay of the Compound I intermediate to the ferric resting state apparently without the formation of a typical compound II. This is presumably due to the rapid formation of amino acid based radicals (32,33) and the possible participation of a new catalytic intermediate involving an amino acid based radical in the catalase cycle (32,34). Both aspects of the catalytic cycles in *Mtb* KatG have been extensively studied in our lab in the past and during my doctoral research. Indeed, the first proof for the presence of a catalytically active amino acid based radical during the catalase cycle in any catalase-peroxidase was recently published by us (35) and is presented in chapter 4 of this thesis.

INH is still among the most common antibiotics used against *M. tuberculosis.* Although this drug was introduced in the 1950's, it was not until the last decade that a considerable advance in the understanding of the mode of action of this drug was made (36,37). The most significant advances were made when resistance was analyzed biochemically and genetically. The first evidence that shed light on a possible mechanism of action was the fact that INH resistant strains have either a decrease or a complete lack of catalase activity (38). DNA sequence analysis of these strains revealed the presence of mutations in or deletions of the catalase-peroxidase gene, *katG*. In addition, the introduction of the WT *katG* gene was shown to be sufficient to confer INH sensitivity to INH resistant strains of *M. tuberculosis*. All together, these facts provided a direct association of the KatG protein with INH activation and resistance (38-40).

Further research demonstrated that INH is a "pro-drug" that needs to be "activated" through oxidative reactions by KatG. Activation of INH by KatG was

initially studied by Johnsson et. al. and others (36,41,42), and methods to measure this activation by the formation of the IN-NAD adduct that is a very tight binding inhibitor of INHA have been recently developed (43-45). In these oxidative reactions, INH most likely serves as a one electron donor to Compound I (the first catalytic intermediate of both catalase and peroxidase activity) and Compound II (36). The proposed mechanism of action of this drug can be explained as follows; once "activated" by KatG, INH reacts with NAD^+ to form an IN-NAD adduct which is a potent inhibitor of the *M. tuberculosis* enoyl-acyl carrier protein reductase, InhA (Figure 1.4-B). InhA is an essential enzyme for the synthesis of mycolic acids, which, as mentioned before, are a critical component of the mycobacterial cell wall. Interrupting the synthesis of mycolic acids disrupts the cell wall structure, consequently, killing the bacterial cells (44,46).

As mentioned above, many mutations in KatG have been reported to confer resistance to INH (47,48). Among these KatG mutants, only a few have been overexpressed, purified, and studied in detail in order to look for altered structural and functional features that might be correlated with INH resistance. The majority of studies performed on these mutants (A110V, A139P, S315N, L619P, L634F, D735A, R463L, R104L, H108Q, N138S, S140N, L148R, H270Q, T275P, A350T, D381G, R463G, L587M) often only measured catalase and peroxidase activity in crude extracts. In some, (W321F, S315T, S315G) INH binding and activation (49-52) were evaluated.

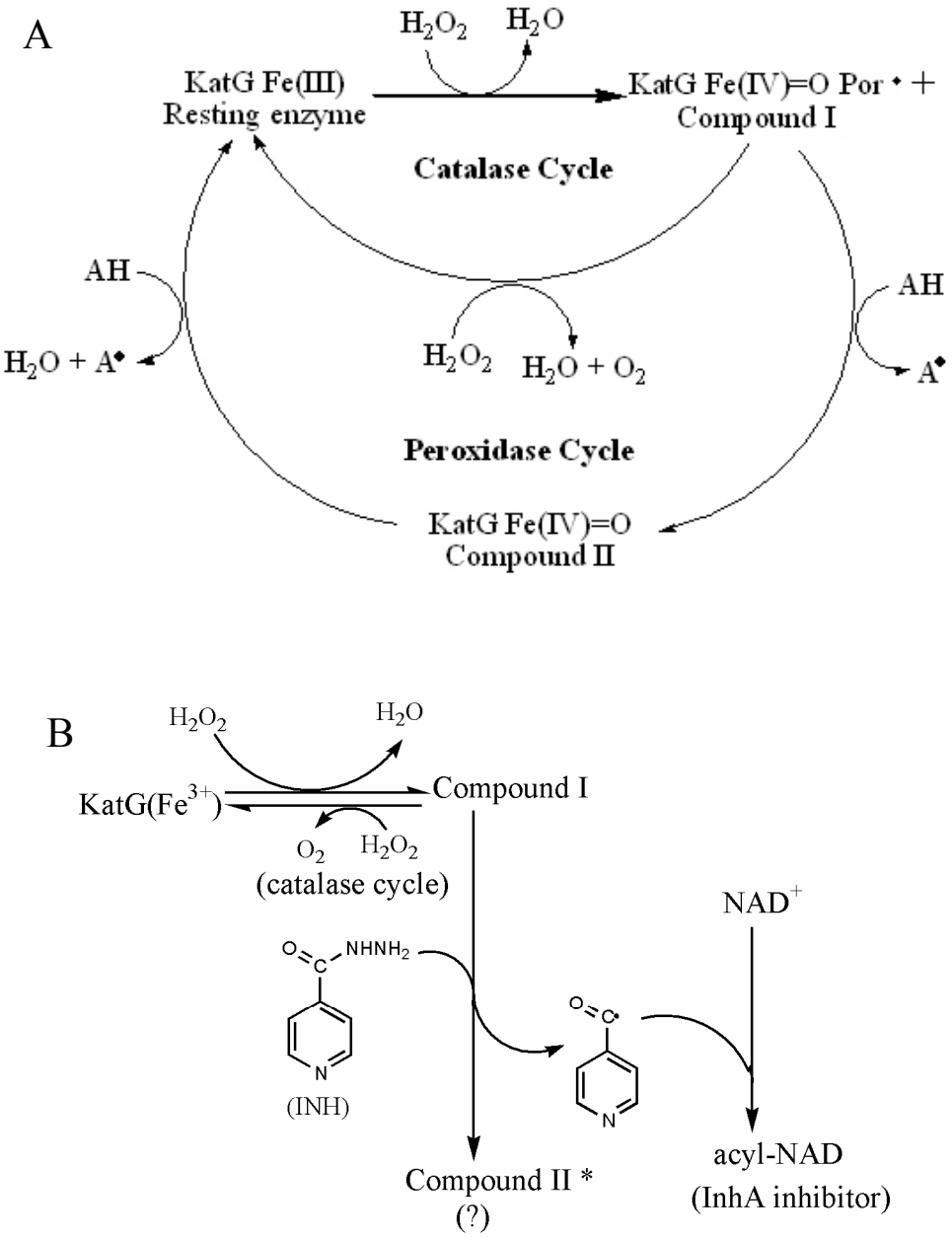

Figure1.4. Catalytic activities of *M. tuberculosis* KatG (A) Classical catalytic cycle of monofunctional catalases and monofunctional peroxidases assumed until recently to also function in KatGs. Evidence for a different catalase mechanism in *M. tuberculosis* KatG is presented in chapter four of this thesis. **(B)** Proposed mechanism of isoniazid activation (taken from ref. 34).

1.4. Structure-function relationships in *M. tuberculosis* catalase-peroxidase KatG:

M. tuberculosis catalase-peroxidase is a homodimeric heme protein (~160KD) containing 740 amino acid residues per monomer. Each monomer (Figure 1.5) is composed of two domains that are mainly α-helical and display a common core structure shared by members of the bacterial and plant peroxidase families. KatG has high sequence homology with prokaryotic peroxidases, including fungal cytochrome *c* peroxidase and plant ascorbate peroxidase (30), and as such possesses substantial peroxidase activity, yet also exhibits catalase activity similar to that of the monofunctional catalases despite having low sequence homology with the latter (53). Typical peroxidases from other sources (plant, fungi and yeast) are composed of ~ 290-350 amino acid residues (54). The doubling in polypeptide size in KatG is the product of gene duplication of an ancestral peroxidase (30). Both halves of KatG show sequence homology to one another and to other members of the superfamily of bacterial, plant and fungal peroxidases. Only the N-terminal domain of the enzyme harbors a functional heme binding site, as a number of the amino acids involved in heme binding and important for catalysis are mutated in the C-terminal domain (30). The heme group is deeply buried in the N-terminal domain. A small substrate access channel connects the surface of the protein with the active site and allows the passage of H_2O_2 and small aromatic molecules.

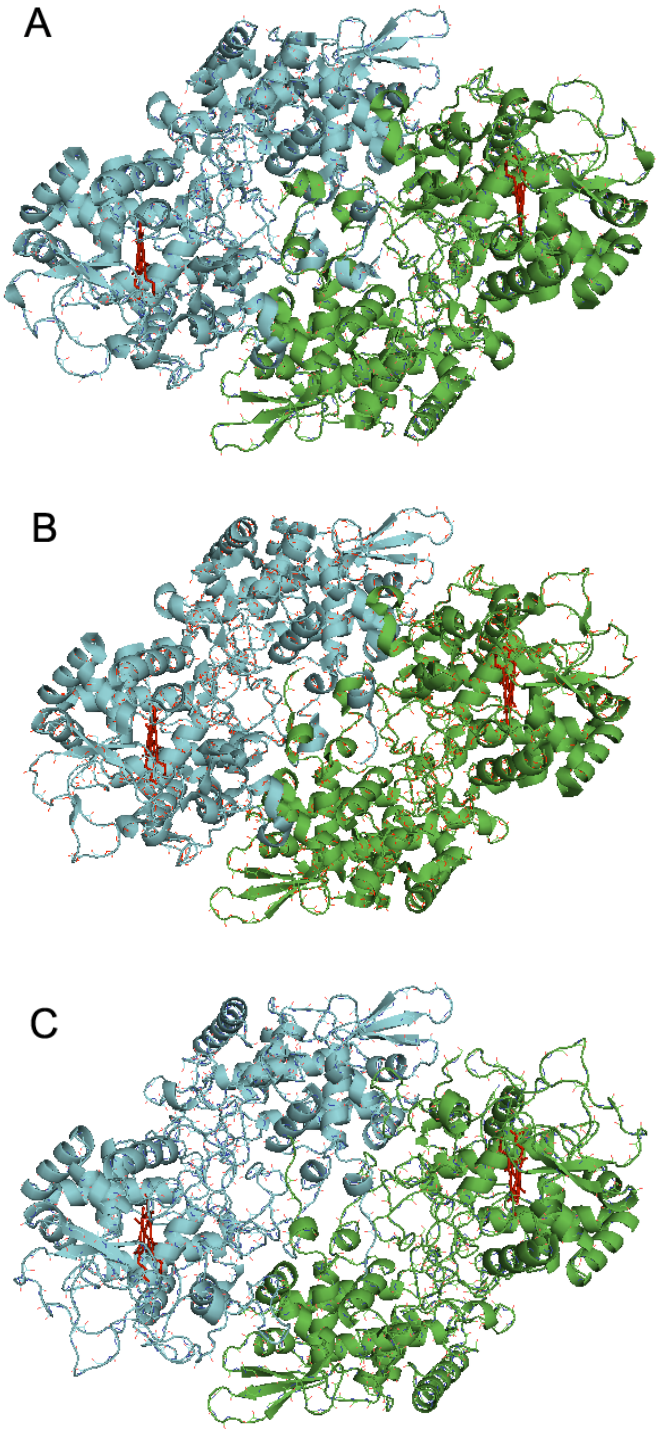

Figure 1.5. Crystal structure of several bacterial KatGs showing the similarity in overall structure within this family of proteins. Structures are colored by protein chains (blue and green) and water molecules are shown in red (dots). Heme groups are shown in red. (A) *M. tuberculosis* (2CCA). (B) *B. pseudomallei* (1MWV). (C) *H. marismortui* (1ITK).

The study of the structure and function of KatG is of great interest because the correlation between unusual features of its structure and particular mechanistic steps is not fully defined or understood. One of the most interesting structural features is the post-translational modification of residues Met 255, Y229 and W107, the side chains of which form an adduct on the distal side of the heme (Fig. 1.6).

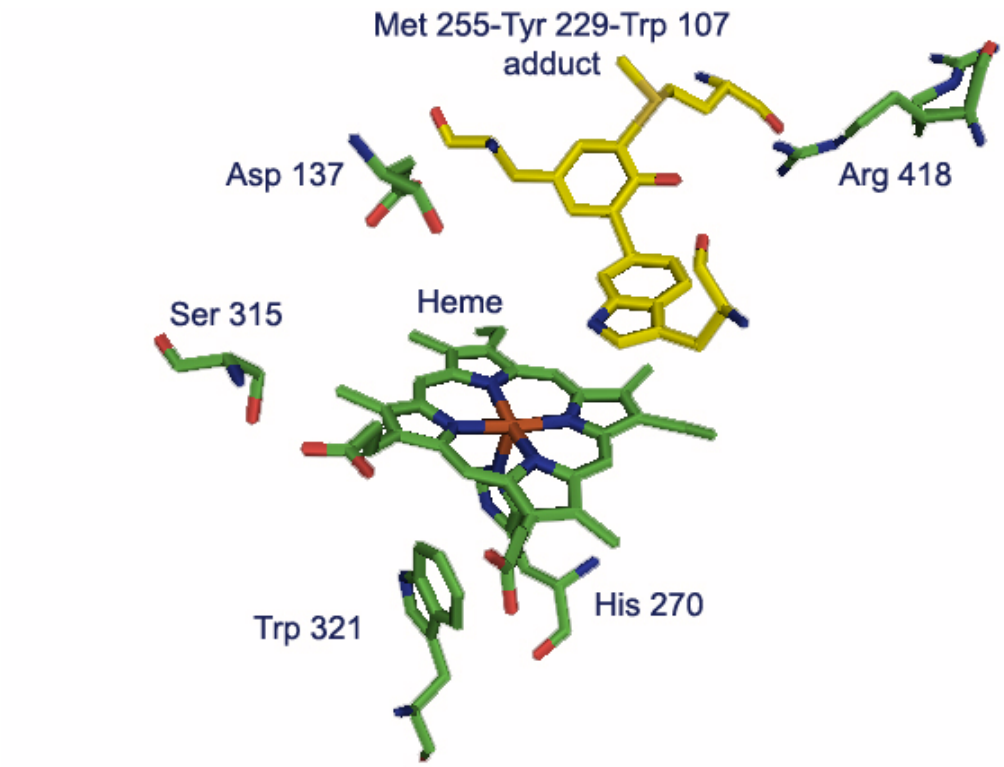

Figure 1.6. The active site (distal side) structure of *M. tuberculosis* KatG (from the coordinates of 2cca.pdb) showing the covalent Met-Tyr-Trp adduct.

Intriguingly, this unusual structural feature is required for catalase but not peroxidase activity (55-58).

1.5. Progress in the understanding of the mechanism of INH resistance conferred by the S315T mutation:

S315T is by far the most common mutation found in clinical isolates of *M. tuberculosis* resistant to INH (found in more than 50% of INH resistant isolates (52)). A great deal of progress has come from our group in explaining how this conservative mutation confers high-level (up to 200 fold) drug resistance. The major findings are: the catalase and peroxidase activity was reduced by 2-fold and 4-fold respectively, while the rate of Compound I formation was unchanged with respect to WT. The INH affinity measured by isothermal titration calorimetry was greatly reduced (~200 fold) compared to WT KatG (49). Additionally, INH activation assays using biomimetic conditions (shown in Figure 1.4 above) demonstrated that KatG[S315T] has a much lower rate of INH activation than the WT protein (59). Also, resonance Raman spectroscopy experiments showed only changes in the relative distribution of different heme spin states and iron coordination and a stronger hydrogen bond environment in the vicinity of heme propionate on pyrrole IV (60,61) but these changes were not correlated with changes in the catalytic ability of the mutant enzyme in INH activation.

The reason for the altered INH binding and rate of INH activation became clear when the 3-dimensional crystal structure of this mutant enzyme was solved (59). In WT KatG, the distal site of the heme pocket is connected to the surface of the protein through a substrate access channel (Figure. 1.7). The residues Asp 137 and Ser 315 delimit the narrowest region of this channel. The size of this access channel is reduced from 6 to 4.7 Å due to the replacement of Ser by Thr in the mutant. The methyl group present in the

threonine residue effectively constricts the accessibility to the heme pocket in the mutant enzyme, therefore, suggested to be a reason for decreasing the INH affinity and activation in this mutant. Beyond these observations for KatG[S315T], there is a substantial gap in the knowledge of the relationship between INH resistance due to the numerous other mutations in the *katG* gene, and the lost function of the KatG enzyme in drug activation. In an effort to fill this gap, the detailed characterization of the origins of isoniazid resistance caused by another mutation in the 315 position of *Mtb* KatG is presented in chapter 2.

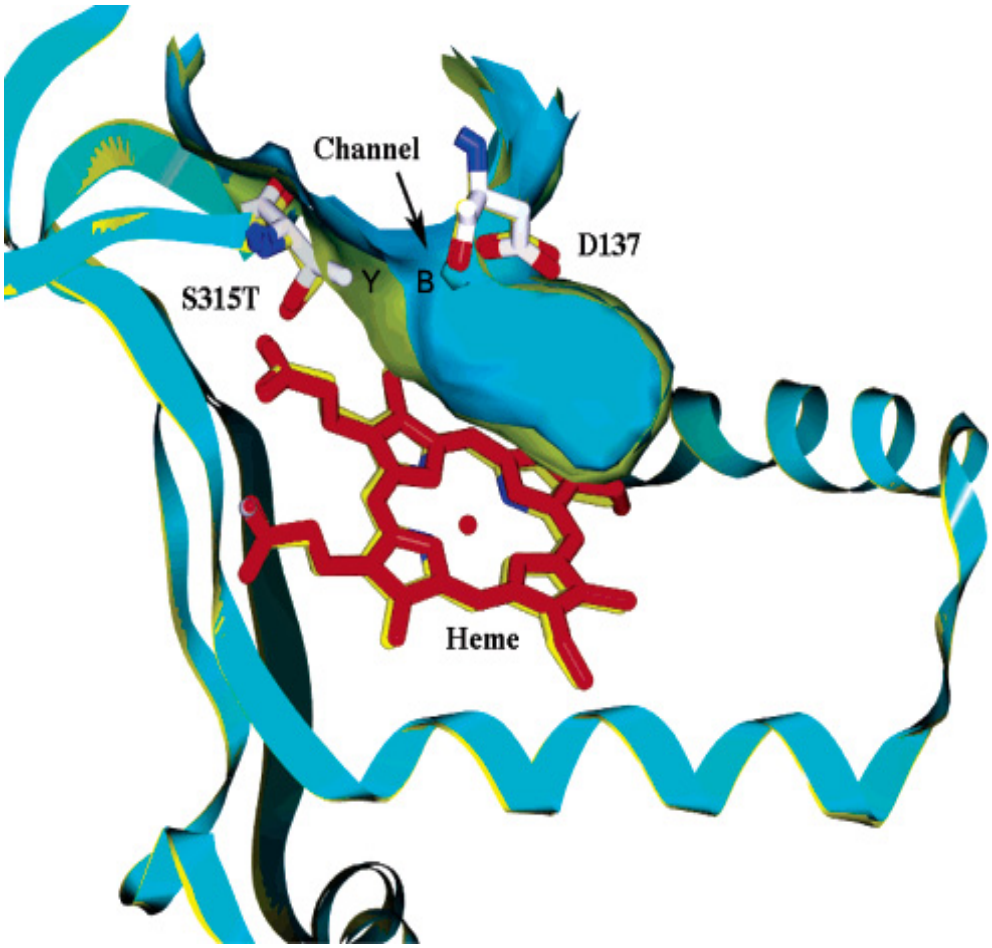

Figure 1.7. Structural comparisons of *M. tuberculosis* WT KatG and KatG [S315T] mutant around the substrate access channel. The reduced size of the channel in the mutant is shown in the blue (B) molecular surface (S315T) when compared with the yellow (Y) molecular surface (WT) (figure taken from ref. 34).

1.6. Formation of tyrosyl and tryptophanyl radicals in *M. tuberculosis* KatG:

Heme proteins are metalloproteins containing a heme prosthetic group either covalently or noncovalently linked to the protein itself. The iron in this prosthetic group is capable of undergoing oxidation and reduction reactions; therefore this metal is the main player in the catalytic activity or binding carried out by these proteins. Myoglobin and hemoglobin are arguably the most widely studied heme proteins due to their abundance and vital function (oxygen binding). Heme peroxidases, catalases, and KatGs (bifunctional catalase-peroxidases) are relative newcomers in the heme enzymes field. Based on the mechanism of reaction of several heme enzymes, the idea that proteins could utilize amino acid based radicals for catalysis started to spread in the middle of the last century (62). Once detection techniques like electron paramagnetic resonance spectroscopy (EPR) became available, amino acid based radicals in heme proteins were found (63). More recently, tyrosyl and tryptophanyl radicals in many other heme and non-heme enzymes such as, Photosystem II (64), bovine catalase (65), turnip peroxidase (66), ribonucleotide reductase (67), prostaglandin H synthase (68), lignin peroxidase (69) and *M. tuberculosis* catalase-peroxidase KatG (70,71) were found. Among these examples, the radicals found in ribonucleotide reductase, prostaglandin H synthase and lignin peroxidase have been associated with catalytic function (72). On the other hand, for the tyrosyl radical found in mammalian catalase (65) and turnip peroxidase isoenzyme 7 (66) a catalytic function has not been identified yet. No amino acid based radical with an assigned catalytic function has been reported in *M. tuberculosis* KatG, until the work in this thesis (see chapter 4).

M. tuberculosis KatG forms the oxyferryl iron porphyrin π–cation radical ([Fe(IV)=O] Por +•) known as Compound I upon reaction with alkyl peroxides. Cmpd I rapidly decays to the resting ferric enzyme even in the absence of added reducing substrates suggesting that endogenous electron transfer reactions take place (73). Recently, the formation of amino acid based radicals in KatG was proven by rapid freeze quench EPR (RFQ-EPR) experiments (70). In this study, after the reaction of the enzyme with peroxyacetic acid (PAA), a transition between a doublet signal found after 6.4 ms, to a singlet is observed (Figure1.8-A). The transition from doublet to singlet in the EPR spectrum is suggested to be a result of the movement of the radical from its original location to other residues (Tyr or Trp) in which there is a different orientation of the phenolic or indolic ring with respect to the β-methylene hydrogens of the amino acids. The kinetics of the radical formation reaction suggested the formation of an amino acid based radical via a catalytic intermediate (Cmpd I). Interestingly, when double mixing experiments (PAA-delay-INH) were performed, these radicals were quenched by INH (Figure 1.8-B) (70). This result suggested that in addition to reacting with Cmpd I, INH could be oxidized by directly reducing the radicals. From these results many critical questions emerge: Where are these radicals located? How many residues are involved in this radical formation? Are these radicals involved in the catalytic function/INH activation by this enzyme?

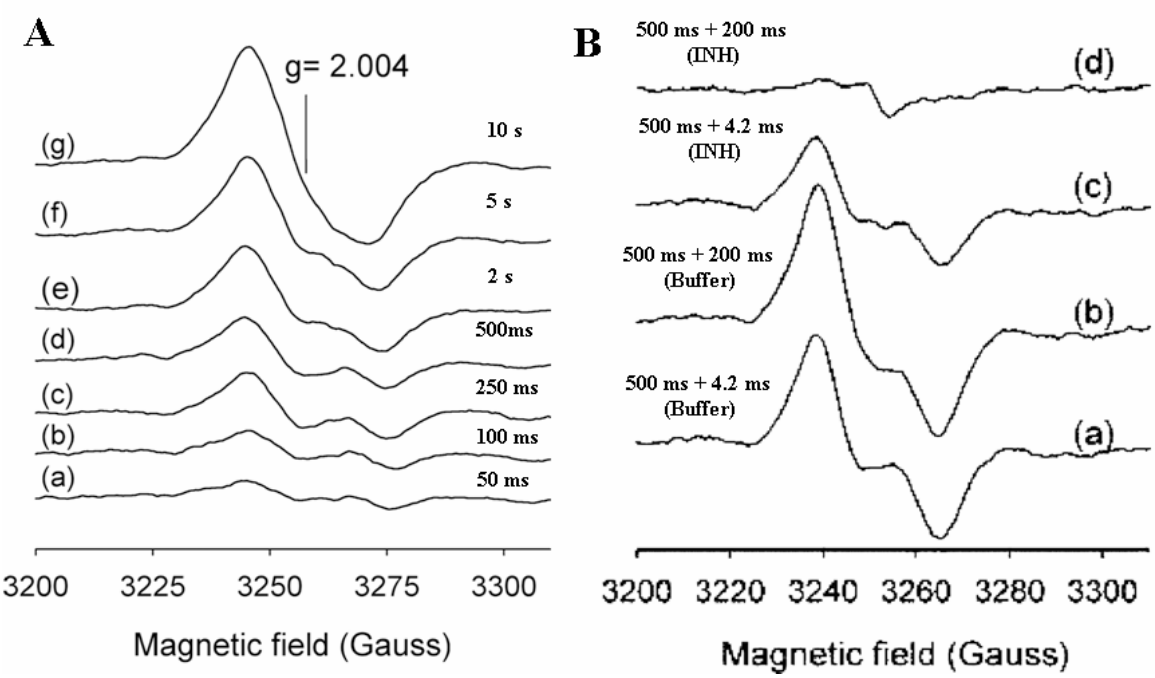

Figure 1.8. Amino acid based radical formation in *M. tuberculosis* KatG (A) Evolution of protein based radicals EPR spectra as a function of time. **(B)** Loss of EPR signals upon addition of INH. Figure taken from (39). Samples in (A) were prepared by mixing resting enzyme with 3 fold excess PAA and then frozen at the indicated times. Samples in (B) were reacted with 3 fold excess PAA for 500 ms in the first reactor, then with phosphate buffer for 4.2 ms (*a*) or 200 ms (*b*) or with INH for 4.2 ms (*c*) or 200 ms (*d*) followed by freeze-quenching.

Recent studies performed by our group provided answers to some of these questions. By a combination of NO trapping, site directed mutagenesis, and RFQ-EPR experiments, residue Y353 (located on the surface of the protein) was identified as a site of radical formation (74). Additional site directed mutagenesis/RFQ-EPR and computational studies suggested the assignment of Y229 and W107 as the primary sites of radical formation followed by Y353 as a secondary site (55,71). Recent results presented in chapter 4 show that this idea has to be reevaluated and that the assignment of the wide doublet signal to Y229 might not be correct. Whether there are more residues in

the electron transfer reactions to Y353 as well as the possible catalytic role of these radicals in KatG still remains unknown but is one of the questions addressed here.

1.7. Protein cross-link formation in *M. tuberculosis* KatG:

In heme proteins and enzymes that can form radicals on surface tyrosines and possibly tryptophans, inter and intramolecular protein cross-links have been observed in several examples such as myoglobin (75), hemoglobin (76), cytochrome *c* peroxidase (77), ascorbate peroxidase (78), and lactoperoxidase (79). In a study of sperm whale myoglobin, the formation of dimers was observed upon reaction with H_2O_2. By tryptic protein digestion and mass spectrometry analysis, an intermolecular cross-link between Y151 and Y103 was identified (75). Also, the formation of dimers and trimers upon reaction with H_2O_2 in bovine lactoperoxidase was observed, suggesting that more than one residue is involved in crosslink formation. Purification and activity assays of the dimers and trimers showed that the enzymatic activity of the higher molecular weight products was not significantly affected.

Although these cross-links appear to be common among heme proteins, beside the studies mentioned above, little is known about the kinetics of formation, the identity of the residues involved and more importantly whether these cross-links have a function or they are just a byproduct of the amino acid based radical formation. Interestingly, the ability of *M. tuberculosis* KatG to form cross-links upon reaction with peroxides had never been tested before the wotk done in this thesis (80) where the recently designed immuno spin-trapping technique was used to prove the formation of protein-protein

crosslinks (Figure 1.9). The inmuno spin-trapping technique uses a novel polyclonal antiserum that specifically and effectively detects protein radicals in their DMPO (5,5-dimethyl-1-pyroline *N*-oxide) nitrone adduct form (81). This immunoassay allow the detection of radical formation in proteins with a greatly increased sensitivity (it requires much less material, μg of protein) when compared with EPR and spin trap EPR techniques alone. Also, the stability of the final oxidation product, DMPO nitrone adduct (a nonradical species), is much higher than that of the paramagnetic DMPO-radical adducts (*t*1/2 of seconds to minutes) required for EPR.

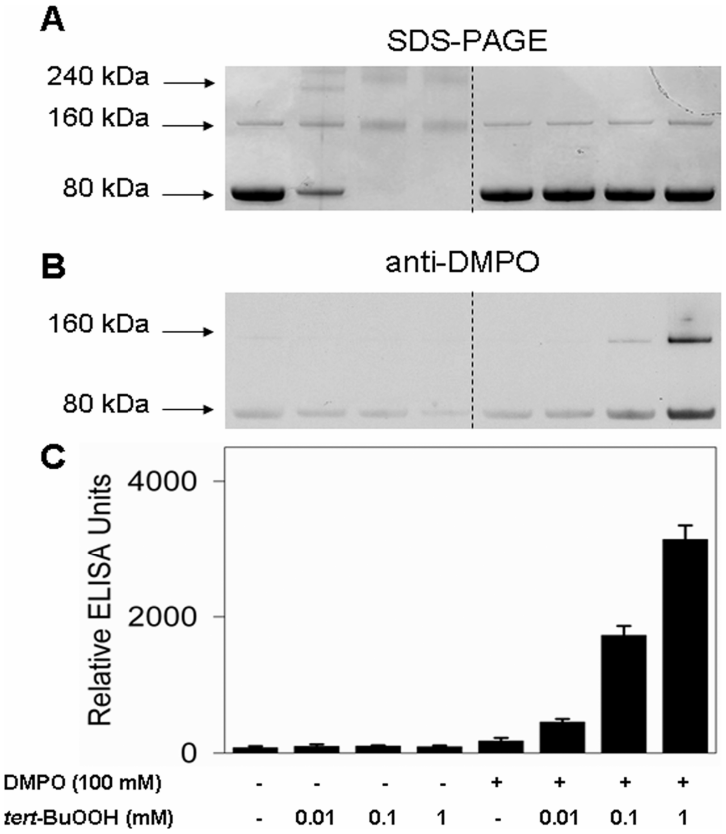

Figure 1.9. Dimerization of *Mtb* KatG by reaction with *tert*-BuOOH in the absence of DMPO and immunochemical detection of protein derived DMPO nitrone adducts. (A) SDS-PAGE and protein staining. (B) Anti-DMPO immunostain as shown with Western blot. (C) Chemiluminescent detection by ELISA of KatG radical-derived DMPO nitrone adducts (figure taken from Ranguelova et. al. 2008 (80)).

In this study, by the use of several techniques like SDS-PAGE, Western blot, immuno-spin trapping, ELISA and EPR, the formation of protein-protein crosslinks (presumably dityrosine crosslinks, as suggested by results shown later in this thesis and in (80)) upon reaction of KatG with alkyl peroxide and a slow flux of H_2O_2 (generated by the Glucose/Glucose oxidase reaction) was shown. This work was initially inspired by the characterization of the crosslink formation process in *Mtb* KatG described in chapter 3.

Chapter 2. Antibiotic resistance in *M. tuberculosis*: Peroxidase intermediate bypass causes poor isoniazid activation by the Ser315Gly mutant of *Mtb* catalase-peroxidase (KatG)

2.1. Introduction.

Replacements at residue Ser315 are the most commonly encountered in the mutated *katG* gene of INH-resistant strains of *M. tuberculosis* (47,48,82). Among these, S315T, which confers high-level drug resistance (up to 200 fold increase in MIC) (52) is the most frequent and is found in more than 50 % of INH resistant isolates. In the case of KatG[S315T], a poor rate of peroxidation/activation of the antibiotic has been defined though the purified mutant enzyme has close to normal catalase activity and peroxidase activity with substrates other than INH (49,83,84). According to the crystal structure of KatG[S315T] (59), the replacement of serine by threonine leads to a structurally modified substrate access channel. This channel leads from the surface of the enzyme to the heme edge at the propionate of pyrrole IV. Residues Asp 137 and Ser 315 delimit the narrowest region of the channel which is reduced in width from 6 to 4.7 Å in the Ser315Thr mutant. The methyl group of threonine effectively restricts accessibility to the heme pocket and apparently interferes with specific interactions required for binding and activation of the drug. While a binding site for INH in KatG is not specifically defined at this time by x-ray crystallography, a recent report about INH bound to cytochrome *c* peroxidase (CCP), a homologous Class I peroxidase, presents what should be an excellent model of drug binding in KatG (85). Hydrogen bonds between the hydroxyl of Ser 185 (315 in *Mtb* KatG), a water molecule and the pyridine nitrogen of the drug are found in

the CCP-INH complex. Thus, it is reasonable that mutations at residue 315 in KatG have an impact on drug binding and activation, but little impact on catalase or peroxidase activity with substrates that may not require the same specific interactions as high affinity INH binding.

Beyond these studies, there is a substantial gap in the knowledge of the relationship between INH resistance due to the numerous other mutations in the *katG* gene, and the lost drug activation function of the mutant enzymes. The main goal of the research presented in this chapter was to examine the origin of drug resistance in the mutant, KatG[S315G] *in vitro*. Here the generation, over-expression, purification and characterization of this mutant found in clinical isolates of *M. tuberculosis* having low level INH resistance with MIC values up to 40 fold higher than for WT strains (8μg/μl *vs*. 0.05μg/μl) is reported (48,82). An interesting aspect of the problem here is that in KatG[S315T], a steric influence on INH binding strongly interferes with activation, while resistance is still present with the glycine replacement of serine, which would not be assumed to interfere with substrate access or binding at the same place in the enzyme.

The application of optical stopped-flow spectrophotometry, isothermal titration calorimetry (ITC), optical titration, electron paramagnetic resonance spectroscopy (EPR) and RFQ-EPR allowed us to probe the functional and structural consequences of the S315G replacement on INH activation by the purified mutant enzyme. Our results strongly suggest that the low-level drug resistance is due to alterations in the peroxidase cycle rather than major changes in specific interactions between the enzyme and INH as reported for KatG[S315T]. Importantly, the results demonstrate the validity of an INH activation model in which peroxidation of the drug is the central feature, since *in vitro*

observations surrounding this activation correlate with the level of INH resistance in *Mtb* strains in the case of both KatG[S315T] and KatG[S315G].

The results presented on this chapter are an adaptation from the article "Antibiotic resistance in *M. tuberculosis*: Peroxidase intermediate bypass causes poor isoniazid activation by the Ser315Gly mutant of *Mtb* catalase-peroxidase (KatG)", by Suarez et. al. (2009). *J. Biol. Chem. 284*, 16146-16155. Low temperature EPR, sample preparation, analysis of the spectra and assignment of the signals were performed by Dr. Kalina Ranguelova.

2.2 Characteristics of the resting mutant enzyme

The KatG[S315G] mutant enzyme used in this study was produced by overexpression in *E. coli* of the mutated *Mtb katG* gene. Purified mutant enzyme from multiple preparations consistently showed a reduced optical purity ratio (A_{405}/A_{280} = 0.40 - 0.45) compared to that of WT KatG (0.50 – 0.55), but similar to that of KatG[S315T] (49). While a significantly higher amount of heme deficient enzyme was consistently found during purification, this form of the enzyme resolves completely from the holoenzyme upon hydrophobic chromatography and therefore, contamination of the holoenzyme with heme deficient enzyme is not the likely origin for the lower extinction coefficient of KatG[S315G]. Another factor that would reduce the optical purity ratio is the presence of a greater proportion of 5-coordinate heme *vs*. 6-coordinate heme relative to the proportions in WT KatG. The blue-shifted Soret peak and red-shifted CT1 (charge-transfer) band (>640 nm) in the optical spectrum of the freshly isolated mutant

enzyme compared to these bands in WT KatG confirms the high proportion of 5-c heme (Fig. 2.1). The accumulation of six-coordinate KatG, spontaneously formed during storage of purified enzymes, leads to a Soret extinction coefficient approximately 30% higher than that of the freshly isolated enzyme and a blue shifted CT1 band (86). Interestingly, while KatG [S315G] samples contained a greater proportion of 5-c heme than was typically found for WT KatG immediately after purification, the conversion to 6-c heme was notably faster than in the WT enzyme. For example, after one week of storage at 4 °C, the population of 6-c heme in the mutant protein doubled, according to resonance Raman spectroscopy (not shown; performed in collaboration with Dr. Johannes Schelvis); for WT KatG, similar changes require more than three weeks and the proportion of 6-c heme in WT KatG has not been found to reach the levels in the mutant even after long term storage. This so-called "aging" of WT *Mtb* KatG has been previously described though specific structural differences between the 5 and 6-c enzyme forms have not been defined beyond the change in heme iron coordination number (86).

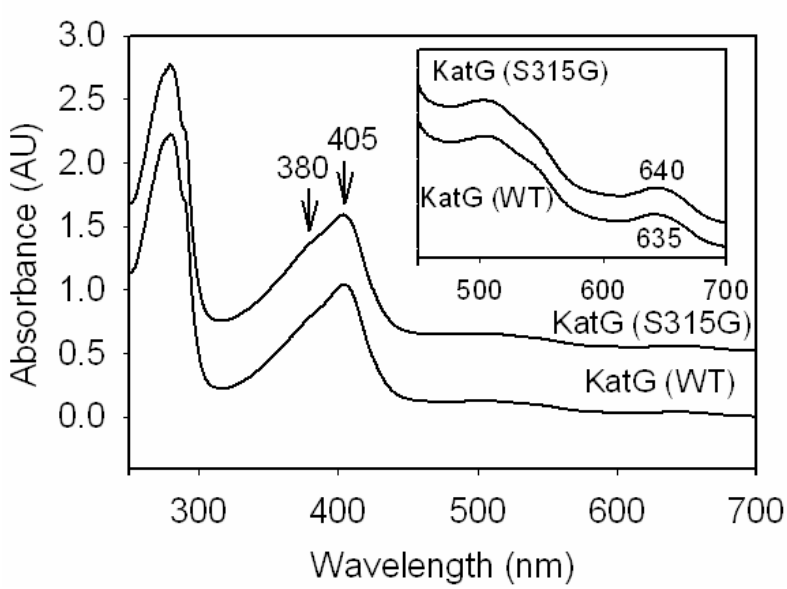

Figure 2.1. UV-VIS spectrum of resting (ferric) WT KatG and KatG[S315G]. 10 μM enzyme was dissolved in 20 mM potassium phosphate buffer pH = 7.2. Spectra are offset for presentation purposes. *Inset*, 3X enlargement of the region from 450 – 700 nm.

Low temperature EPR spectra also revealed a high proportion of 6-c heme in KatG[S315G]. The EPR spectrum of freshly isolated KatG[S315G], frozen immediately after purification, has a rhombic signal (g_1=6.04, g_2=5.54, g_3~2.00) as the majority species (Fig. 2.2). A similar signal (labeled as signal r_2) develops in WT KatG EPR spectra after the enzyme has been stored for a week or two and in the case of KatG[S315T] only after very long term storage (49,87). Also, the mutant has little signal intensity at g-values of 6.3 and 5.1, features that were previously assigned to a 5-c heme signal (r_3) in freshly isolated WT KatG and in KatG[S315T]. Moreover, after only 24 hours of storage, an axial signal ($g_\perp$ = 5.80) also becomes evident in spectra of the S315G mutant. Since during this period of storage no significant changes were observed in the intensity of signals corresponding to 5-c HS species including signal r_3 and r_1 (g_1=6.60, g_2=5.01, g_3~2.00) (86), these observations suggest interconversion of 6-c heme species;

signal r_2 develops into the g = 5.8 axial signal during this brief storage period. After 1 week of storage, signals r_2 and the g = 5.8 signal continued to increase in relative intensity. Signal r3 is not indicated in the spectra of S315G but is also present as in the others.

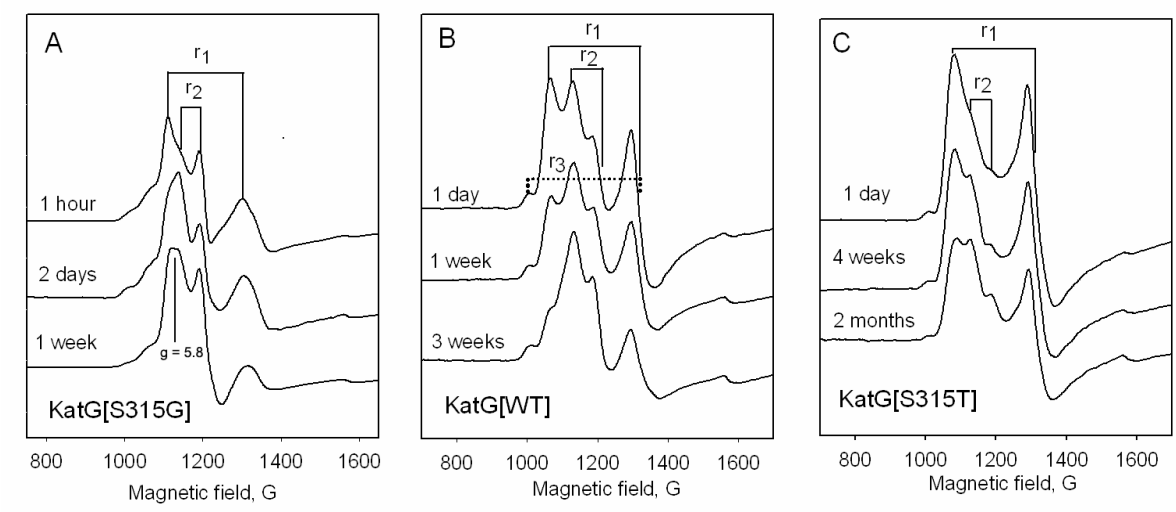

Figure 2.2. Assignment of signals in low-temperature EPR spectra of KatG[S315G] (A), wild-type KatG (B), and KatG[S315T] (C) (87). The features in the *g* = 6 region representing the different heme species for samples of the enzyme frozen after different periods of storage are indicated. Experimental conditions: temperature, 4 K; microwave power, 1mW; modulation amplitude, 4 G; frequency, 9.3867 GHz.

The low temperature EPR spectra in general show a greater abundance of 6-c heme relative to 5-c heme based on estimates from room temperature resonance Raman spectra (based on previously published work including (60,61)) but this type of quantitation is difficult, and its temperature and pH dependence is not yet understood. Despite these difficulties, the important observation based on the results overall is that the dynamics of the structural changes leading to formation of 6-c heme species in KatG[S315G] are very rapid compared to the behavior observed in WT and the KatG[S315T] mutant enzyme (Fig. 2.2). Coordination number has been previously

addressed based on EPR, optical and resonance Raman spectra and on the presence of 6-c heme in the x-ray crystal structure of WT KatG (88) and the assumption here is that 6-c species contain a water molecule associated with heme iron in the sixth coordination position. Whether the rapid changes observed for the mutant are dependent on greater accessibility to the heme pocket alone or in combination with other structural changes will be discussed below as these issues are relevant to the interactions with INH governed by features at the heme edge at the bottom of a substrate access channel. Differences in populations of the coordination states of resting KatG were recently reported to have consequences in ligand binding evaluated using cyanide and alkyl peroxide, and more rapid binding was assigned to 6-c enzyme forms consistent with the participation of active site water in proton transfer steps (87,89).

2.3 Catalytic functions

The catalase and peroxidase specific activities of KatG[S315G] were lower by ~ 60 % (2039 ± 461 UI/mg) and ~ 40 % (0.61 ± 0.15 UI/mg), compared to WT KatG (Table 2.1). Similar reductions in the activities of other KatG mutants including enzymes from INH resistant isolates have been reported (49,50,83,90). However, new insights into INH resistance mechanisms must be specifically gained in each case. Since we suggest there is a high affinity binding site for INH in KatG that could be disrupted by mutations, this binding site may not be common to other peroxidase substrates used in a typical assay. For example, the MIC for INH against a mutant strain of *Mtb* producing KatG[S315T] is more than one hundred times greater compared to the wild-type strain

H37Rv while the peroxidase activity for that purified mutant enzyme is only reduced 3-fold when measured using a standard assay (49). For strains with the KatG[S315G] mutation, the MIC is higher by up to forty fold compared to WT (48), and again for this mutant, the peroxidase activity measured with *o*-dianisidine, the substrate typically used for the steady-state activity assay, is only moderately reduced. Further exploration of the properties of the mutant enzyme reveals structural and catalytic features relevant to understanding the INH resistance mechanism in detail.

Evaluation of the rate of formation of Cmpd I, the oxoferryl:porphyrin π-cation radical intermediate common to both catalase and peroxidase reaction pathways in KatG, is fundamental for characterizing catalytic function of the mutant enzyme. The optical spectrum of Cmpd I formed upon turnover with small excesses of alkyl peroxides (peroxyacetic acid, PAA; chloroperoxybenzoic acid, CPBA; *tert*-butylhydroperoxide, *t*-BOOH) in KatG[S315G] was essentially the same as that reported for WT KatG and showed the characteristic 40-50 % hypochromicity and red shift to 411 nm in the Soret region, and peaks at 550 and 590 nm, together with a shoulder at 665 nm (Fig. 2.3) also very similar to reports on this intermediate in the KatG from other organisms (34,73). In the case of PAA turnover, a second-order rate constant was determined from the linear plot of the k_{obs} values as a function of the concentration of PAA. The rate was ~ 2.5 times faster (7.4×10^4 M^{-1} s^{-1}) than that for WT KatG under similar conditions (Fig. 2.3). This increase may be a special feature of the mutant due to the greater proportion of 6-c heme in its resting state though this small increase does not enhance INH activation (see below) or the peroxidase specific activity as usually assayed.

	KatG[WT]	KatG[S315G]	KatG[S315T]
Catalase activity (U/mg)	3800 ± 344	2039 ± 461	2259 ± 1100
Peroxidase activity (U/mg)	0.9 ± 0.1	0.6 ± 0.15	0.26 ± 0.01
Cmpd I formation (PAA)	3 x 10^4 M^{-1} s^{-1}	7.4 x 10^4 M^{-1} s^{-1}	2.93 x $10^4$$M^{-1}$ s^{-1}
Cmpd I decay (PAA)	~ 80 sec	~ 40 sec	~100 sec
INH dissociation constant (Optical)	1.0 μM	0.7 μM	N.D
INH dissociation constant (ITC)	1.6 μM	1.4 μM	400 μM
Decay of 5-c heme (aging)	~ 3 weeks	~ 1 week	**>** 2 months

Table2.1 Comparison of catalase and peroxidase specific activities and other relevant parameters of WT KatG, KatG[S315T] and KatG[S315G].

The rate of the spontaneous return to the resting enzyme after formation of Cmpd I is also of interest since this process is already known to involve endogenous electron transfers producing radicals on amino acids, as reported for WT KatG enzymes from *Mtb* (70,71) and other organisms (33,71).

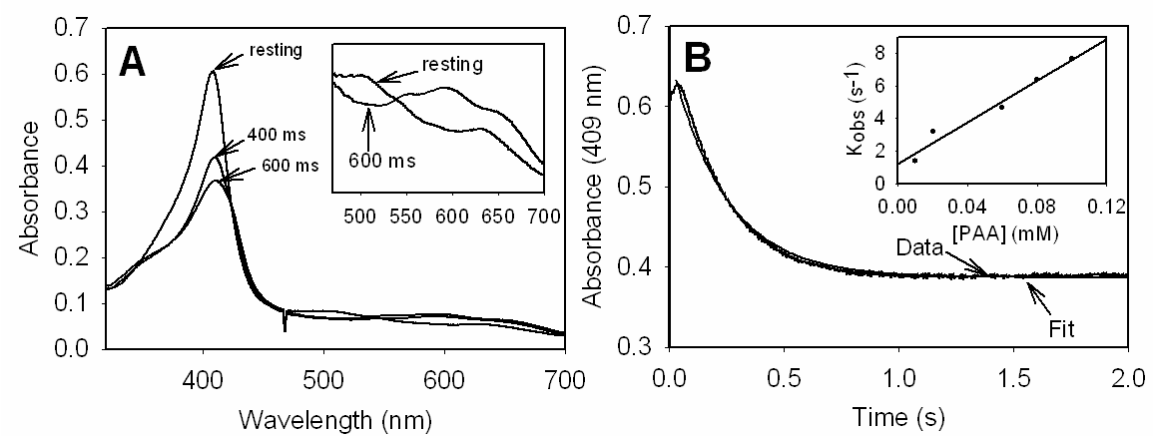

Figure 2.3. Formation of Cmpd I in KatG[S315G]. (A) Absorption spectra showing the formation of Cmpd I after the addition of 25 μM PAA to 5 μM (final concentrations) resting enzyme in 20 mM potassium phosphate buffer, pH = 7.2, at 25 °C; (B) Absorbance *vs*. time recorded at 409 nm. The time course at 409 nm was fitted with a first order exponential decay function for increasing substrate (PAA) concentrations. *Inset*: Linear dependence of the observed rates (k_{obs}) as a function of PAA concentration.

Interestingly, the time course for this return evaluated from the slope during the interval of increasing absorbance at 407 nm *vs*. time after turnover of resting enzyme with a small excess of PAA, was also approximately 2 times faster in the mutant than in WT KatG (Fig. 2.4). This faster return could be evidence for reactions in the mutant enzyme that involve species other than the redox active amino acids, these residues being the same in the mutant and WT enzymes. This observation became very significant in interpretation of the decreased ability of KatG[S315G] to "activate" the antibiotic.

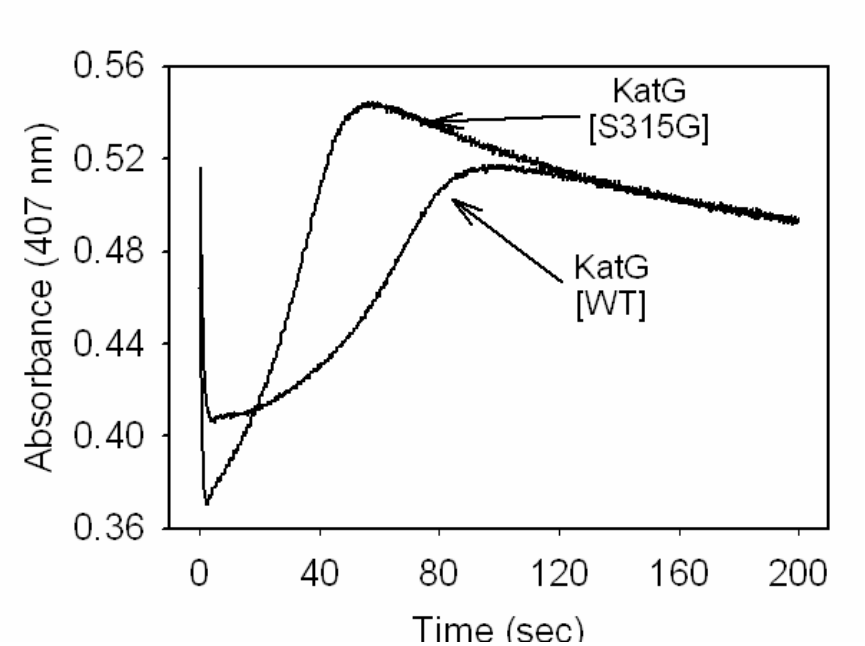

Figure 2.4. Cmpd I formation and decay in WT KatG and KatG[S315G]. Extended time traces (at 407 nm) recorded after mixing 5 μM resting WT KatG or KatG[S315G] with 25 μM PAA (final concentrations) in 20 mM potassium phosphate buffer, pH=7.2 at 25 °C . The initial rapid decrease is followed by the slow return to the starting absorbance value around 0.5.

To test the hypothesis that Cmpd I in the mutant enzyme is more reactive towards peroxide than the WT protein, a double mixing optical stopped flow experiment was used to follow the rate of reaction of Cmpd I with PAA, the same peroxide used in excess to generate this species from resting enzyme. PAA added to pre-formed Cmpd I in KatG[S315G] was more efficient as a reductant than in the case of the WT enzyme (Fig. 2.5) by around 2.5-fold. This observation strongly suggests that the more rapid decay of catalytic intermediates in KatG[S315G] depends on enhanced turnover of peroxide in single electron reactions with catalytic intermediates. One product of this reaction is assumed to be a peroxyl radical of PAA.

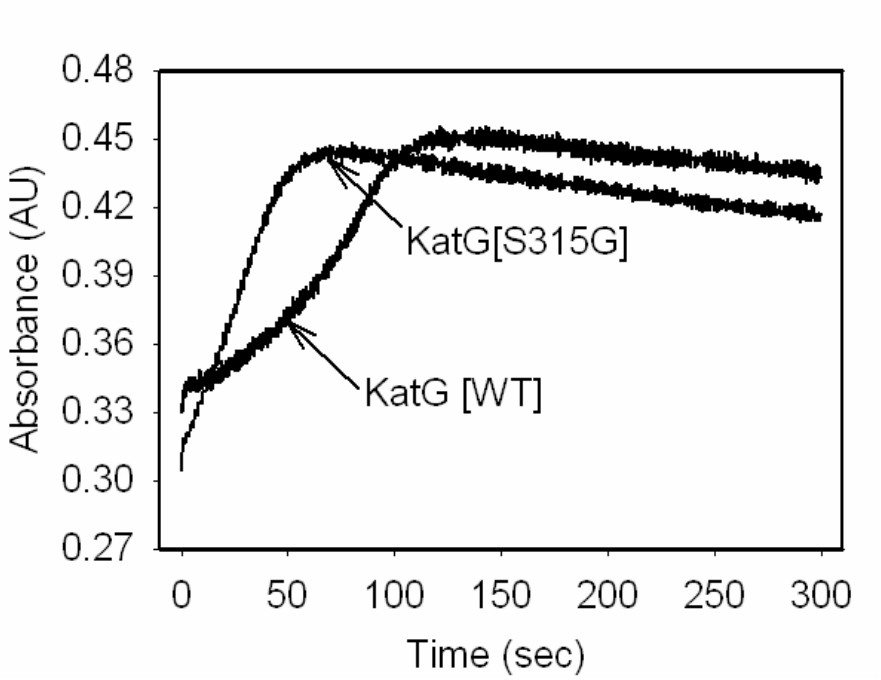

Figure 2.5. Optical stopped flow double mixing reaction of KatG[WT] and KatG[S315G] with peroxide (PAA), 2 s delay, PAA). Absorbance *vs.* time traces at 407 nm are shown beginning after the second mixing step.

RFQ-EPR provided further evidence that PAA could be the species responsible for initiating such decay since evidence for a peroxyl radical, which would be formed from single electron oxidation of PAA by Cmpd I, was consistently found in RFQ-EPR samples (Fig. 2.6). Furthermore, the RFQ-EPR results did not show an increase in the yield of protein based radicals such as the tyrosyl and tryptophanyl radicals assigned in WT KatG (70,71) formed under similar conditions in the presence of PAA. One additional finding relevant to this feature of the reaction with PAA was that anaerobic preparation of RFQ-EPR samples did not alter the identity of the signals observed to any great extent (not shown) consistent with formation of peroxyl radical on an exogenous species rather than from reaction of dioxygen with amino acid radicals, a known source of peroxyl radical in proteins treated with peroxides (91,92). EPR at X-band (9 GHz)

does not allow for the identification of the type of peroxyl radical since all radicals of the type R_2C-OO• have similar spectra (axial signals with g values very close to 2.035 and 2.006).

The spectroscopic observations overall are considered evidence for more facile turnover of catalytic intermediates in KatG[S315G] relative to WT enzyme. Such turnover does not extend to an enhancement of INH activation since the enzyme is the origin of resistance to the antibiotic.

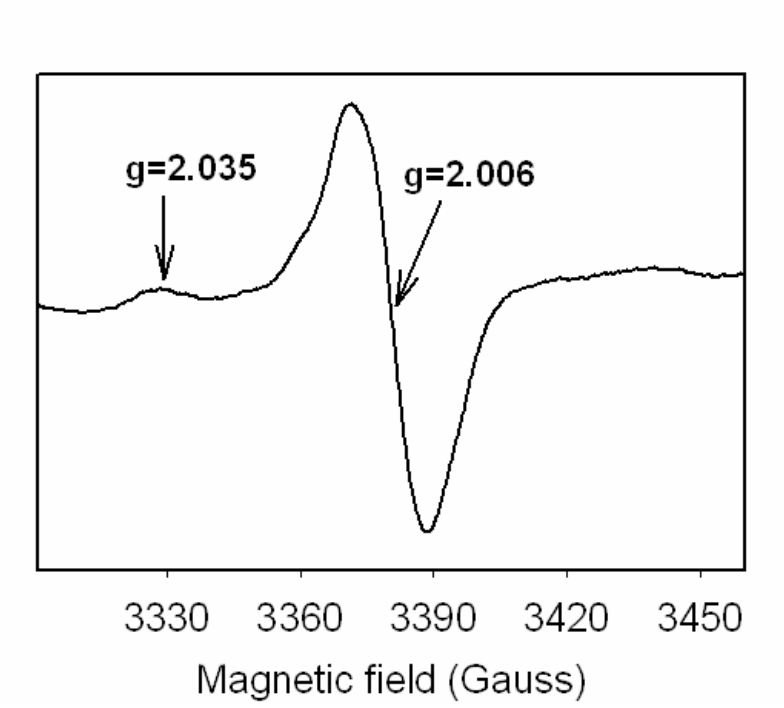

Figure 2.6. RFQ-EPR of KatG [S315G] treated with 3-fold molar excess of PAA. Resting enzyme (100 μM final) was mixed with PAA (300 μM final) and freeze-quenched after 250 ms. This signal is due to a peroxyl radical.

2.4. Is INH a poor substrate of KatG[S315G]?

In order to directly examine the catalytic competence for INH activation by Cmpd I in KatG[S315G], double-mixing stopped-flow experiments were performed according to previously used methods (49). Cmpd I, pre-formed by the reaction of 10 μM WT KatG or KatG [S315G] with 50 μM PAA, was mixed after a 2 sec delay with increasing concentrations of INH (20, 50, 100, 200, 500 μM) after which the absorbance changes at 407 nm were followed. As expected due to the reaction of isoniazid with either Cmpd I or amino acid based radicals, INH accelerated the return to the ferric enzyme in both cases (WT KatG and KatG [S315G]), compared to the rate after the second mixing with buffer alone (Fig. 2.7). Reaction of Cmpd I with INH is considered here to be a required process for activation of the antibiotic through the peroxidase cycle, though other reactions have been considered and described (93-97). For the WT protein, the rate of return after the second mixing step was accelerated two-fold (50 μM INH) and 5-fold (100 μM INH) relative to the rate after addition of buffer alone. For KatG[S315G], the rate of acceleration was only 1.3 fold (50μM INH) and 2 fold (100 μM INH) under similar conditions. These results, together with the lower lifetime of Cmpd I observed in the single mixing experiments tentatively suggest the origin of INH resistance in KatG[S315G] will result from a decreased yield of the initial INH oxidation product (Scheme 2.1, see discussion). Also, as can be seen in Fig. 2.7, the increased absorbance ("overshoot") observed after the consumption of PAA in the single mixing experiment is also present but is more pronounced in the presence of INH because excess INH added in the second mixing step binds to the 6-c heme enzyme product and converts the heme to

the 5-c form (49). A notable feature of the observed time course in this figure and in Figure 2.4 is that the absorbance intensity at 407 nm rises to a value greater than the initial absorbance, before it finally levels off at the starting absorbance value. A similar trend is also observed for WT KatG and KatG[S315T] but the effect is not as pronounced (49). This "overshoot" in the Soret absorbance is evidence that a new species having a greater extinction coefficient than the final product of the Cmpd I decay reaction is produced as the peroxide is nearly depleted. This species is likely 6-c heme containing a water ligand produced during reduction of oxoferryl heme intermediates, which slowly dissociates and regenerates the 5-c state of the starting enzyme. For the mutant, the larger difference relative to WT is due to the fact that the starting heme population had a greater abundance of 5-c than 6-c heme; and the catalytic cycling does not accelerate the "natural" aging process that leads to a stable 6-c species.

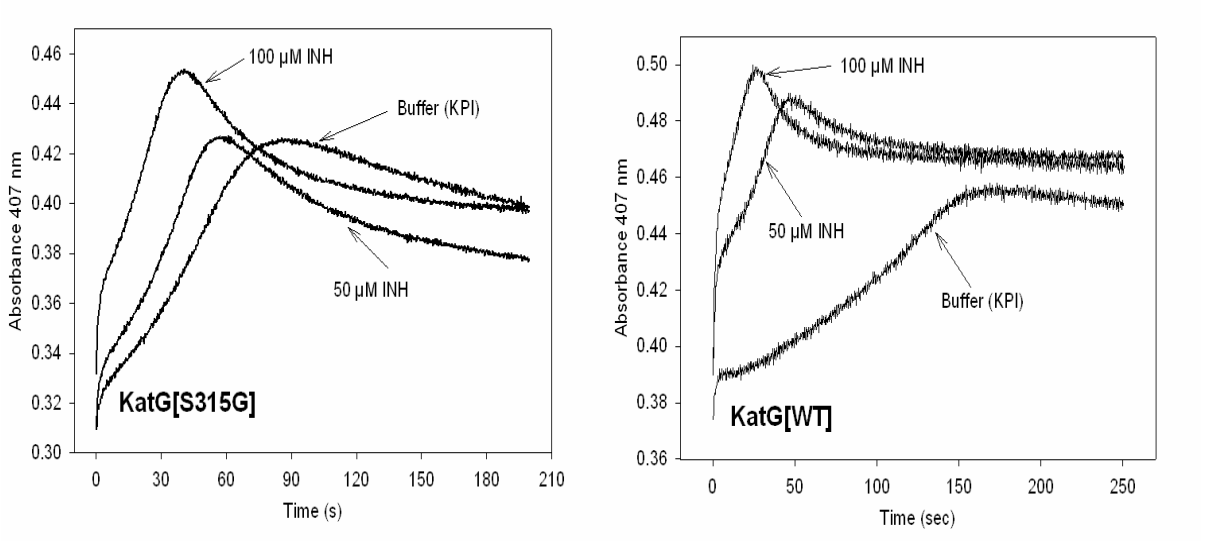

Figure 2.7. Reaction of KatG[WT] and KatG[S315G] Cmpd I with INH. Absorbance *vs.* time traces (at 407 nm) for double mixing stopped-flow experiments are shown. Resting enzymes were reacted with PAA to form Cmpd I, followed by addition of INH. The final concentrations of enzyme and PAA were 5 and 25 uM respectively; the final concentrations of INH are as labeled in the figure for each time trace.

A biomimetic approach outlined in the introduction (Chapter 1) on page 9 and presented in more detail immediately below to examine INH activation provides evidence consistent with these observations and with the low level resistance reported from *in vivo* INH treatment of *Mtb* strains bearing the mutation for KatG[S315G] (59).

2.5. IN-NAD Formation.

According to a consensus model for INH action in mycobacteria, an acyl radical formed upon oxidation of INH by KatG reacts with NAD^+ to form an adduct at the C-4 position of the nicotinamide ring (IN-NAD) (36,44,45,59,98-100). NAD^+ does not bind to KatG nor is it a substrate of peroxidation, suggesting that the rate of formation of IN-NAD measured *in vitro* will depend exclusively on the rate of formation of an INH-derived radical that can react rapidly and non-enzymatically with the nicotinamide ring of NAD^+. Non-enzymatic covalent modification of NAD^+ contrasts with a reported INH-NADH lyase activity assigned as a heme-independent catalytic function of *B. pseudomallei* KatG (97).

The IN-NAD molecule is a potent inhibitor of the *Mtb* enoyl-acyl carrier protein reductase, InhA (44,46,101,102). The ability of WT KatG to produce the IN-NAD molecule in high yield in a physiologically relevant biomimetic reaction system, and the very poor function of the mutant S315T in this reaction, was described in a previous study (59). Here, IN-NAD adduct formation by KatG[S315G] is evaluated using the same biomimetic approach in which dilute H_2O_2 produced enzymatically, initiates

peroxidase catalysis in the presence of excess NAD^+ and INH. In this protocol using WT KatG, the rate of appearance of IN-NAD depended on the concentration of INH up to a saturating amount under conditions in which hydrogen peroxide was generated at 2 μM/minute (59). A maximum rate of formation of IN-NAD by WT KatG was found using 0.5 mM INH. In the case of KatG[S315G], 1 mM INH was required to produce a maximum rate (Fig. 2.8) (both cases in the presence of 50 uM NAD^+ previously shown not to be rate limiting (59)). A decrease in the maximum rate of IN-NAD formation by approximately 30 % was also found (0.3 μM/ min using KatG[S315G] vs. 0.4 μM IN-NAD/min using WT KatG, under saturating INH conditions (1 mM for KatG[S315G] and 0.5 mM for WT KatG). These observations are consistent with the double mixing stopped-flow kinetics results above in which it was shown that INH was an apparently poorer substrate of peroxidase activation in the mutant compared to WT KatG.

Overall, the results are consistent with only small losses in peroxidation of INH in the mutant enzyme as expected from the known low level resistance *in vivo*.

2.6. Optical and ITC titrations.

Changes in specific binding interactions between INH and KatG are important to consider in explaining INH resistance due to mutations in KatG, particularly for replacements at residue 315. This residue is likely to be directly involved in the high affinity binding of the drug to KatG based on the model provided by the CCP-INH complex. In KatG [S315T], for example, changes in affinity for INH and in efficiency of IN-NAD formation (49,59) were assigned to steric effects that hinder high affinity drug

binding; these effects are limited to the region surrounding the propionate of pyrrole IV (49,84) near the bottom of the substrate access channel. INH binding to the ferric enzyme can be monitored by changes in optical spectral features, as first reported in (84) and by isothermal titration calorimetry (ITC). Titration of KatG with INH produces an increase in the absorbance at 380 nm and a decrease at 411 nm consistent with conversion of 6-c heme to 5-c heme species (89). Dissociation constants can be determined from such optical changes. ITC directly measures the heat evolved upon INH binding to KatG and results provide the number of binding sites, and the enthalpy and entropy of binding.

Both optical titrations and ITC results show that less than one equivalent of INH was sufficient to achieve apparent saturation of KatG (Fig. 2.9). This is reasonable if only a fraction of the total available enzyme provides an appropriate binding site for the drug, as reported previously for WT KatG ligand binding (34).

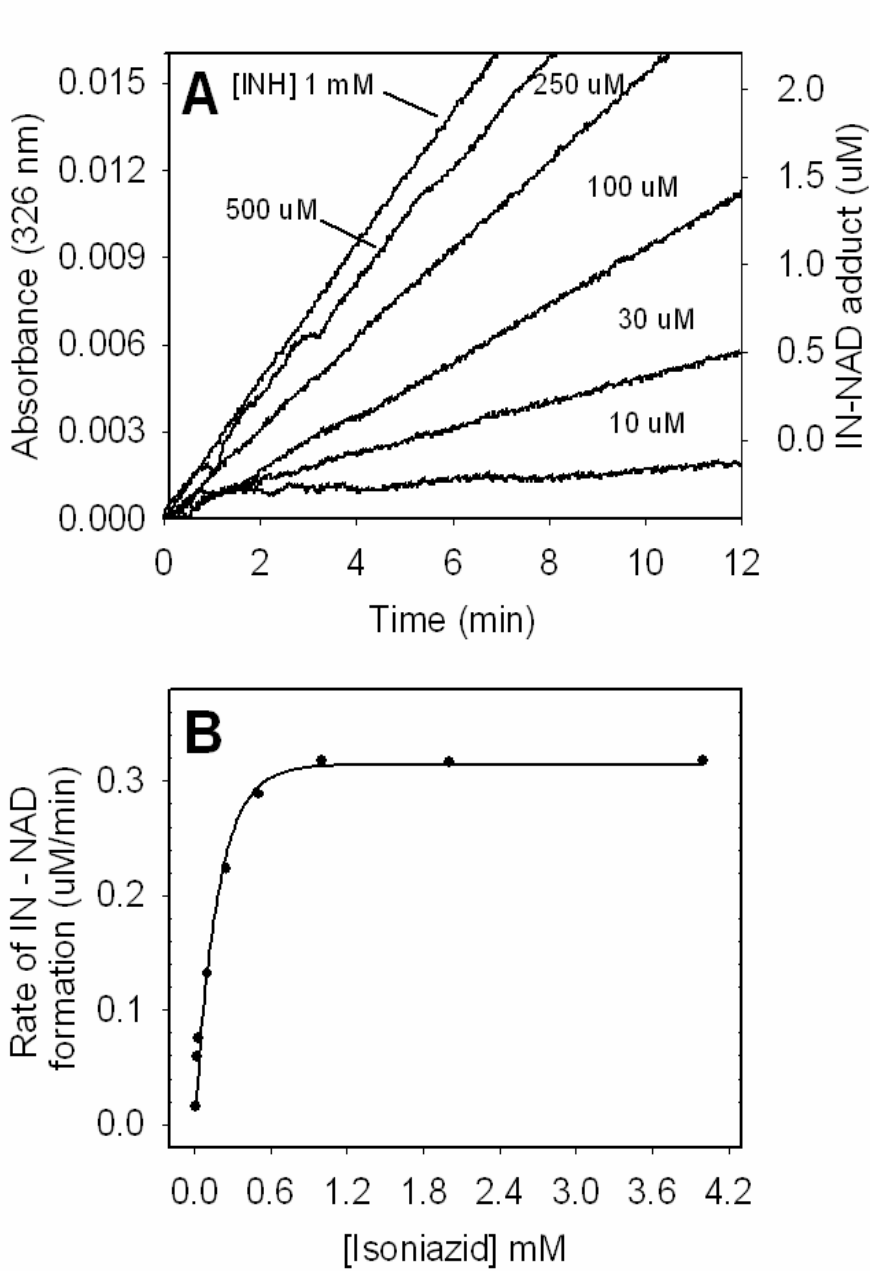

Figure 2.8. Effect of INH concentration on the rate of production of the IN-NAD adduct. (A) IN-NAD adduct formation was followed at 326nm (59). KatG[S315G] (0.5μM), NAD^+ (50 μM), and H_2O_2 (2 μM/min generated enzymatically) were incubated with varying concentrations of INH. (B) Rates of IN-NAD adduct formation as a function of INH concentration.

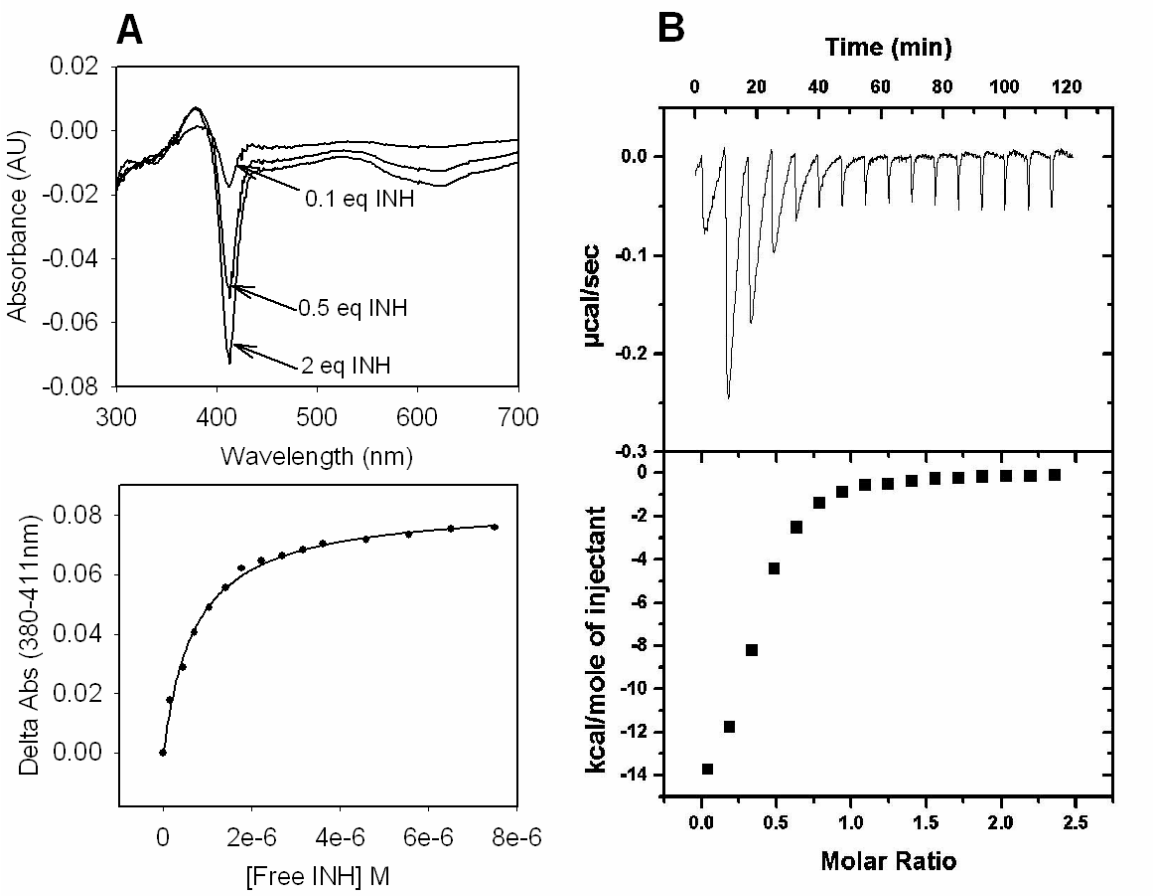

Figure 2.9. Binding of INH to KatG[S315G]. Optical titrations were performed using 5 μM enzyme and increasing concentrations of INH. Difference spectra were obtained by subtracting the spectrum of free KatG from that of the INH-bound enzyme for each increment of addition. INH binding curves were generated by plotting the absorbance difference for the peak minus the trough absorbance values at 380 and 411 nm respectively *vs.* the concentration of free INH. (B) Isothermal titration of KatG[S315G] with INH. ITC experiments were carried out at 25 °C in phosphate buffer pH 7.2 using 10 μM KatG. The top panel shows the isothermal traces measured from a series of injections of INH into enzyme. Heat (integrated values in microcalories per second per injection, *lower panel*) are fitted to a single-binding site model.

For this reason, the *n* value obtained from ITC experiments (~ 0.3-0.4) was used to estimate the concentration of available binding sites to allow calculation of dissociation constants from the optical titration results. Apparent Kd values obtained from the optical and ITC titrations for KatG[S315G] were 0.7 µM and 1.4 µM respectively, very similar to those reported for the WT enzyme (1.0 µM (optical titration)

and 1.6 μM (ITC) (89)). These results argue against poor interaction of the enzyme with INH as the origin of poor activation by KatG[S315G] and lead to greater confidence that the mechanistic changes outlined above including changes in the behavior of Cmpd I should be considered central to the origin of INH resistance.

2.7. Discussion.

To date, the only case in which details about how structural changes in a mutant KatG enzyme impact upon INH activation through the peroxidase pathway have been defined is that of KatG[S315T] (59). Mutations at the 315 position are very common in clinical isolates of *M. tuberculosis* suggesting some unique features of the KatG mutants bearing replacements at this position (47,48,82). Centrally important may be the premise that such replacements do not seriously interfere with the physiologically important roles of the enzyme in *Mtb*, the most important of which is so far believed to be its catalase activity; no obligatory peroxidase function of the enzyme has yet been identified. The Ser315 residue, located at the heme edge, is not a direct participant in catalytic processes such as formation of Cmpd I, but has effects on heme structure reasonably considered to be governed by hydrogen bonding interactions between the propionate of heme pyrrole IV, the backbone N-H of residue His276 and the hydroxyl group of the serine side chain. In addition to these interactions, specific interactions between INH, a water molecule, and residue Ser315 have been identified in a recently published CCP-INH crystal structure (85). Therefore, there are some interesting corollaries between the structural

effects of mutations at residue 315 on the heme pocket (61) and on specific interactions with INH reasonably assumed to be important in activation of the antibiotic by KatG.

One remarkable feature of the KatG[S315G] mutant is the very rapid rate at which 6-c heme evolves from a 5-c form initially found in the freshly isolated enzyme during brief periods of storage after purification. Prior analyses showed this "aging" of WT KatG to be extremely slow in the KatG[S315T] mutant (86,87,89). The process, which was extensive within the first day or two of storage of KatG[S315G], was evident in markers found in optical, resonance Raman and low temperature EPR spectra. The behavior of the mutant is most likely dependent upon changes in the access to the distal cavity through a substrate access channel described in crystal structures of *Mtb* KatG enzymes (59,88) as well as changes in the constraints on the overall architecture of the active site that must accompany interconversion between 5 and 6-c enzyme forms. These constraints likely involve a hydrogen bond between the side chain hydroxyl of residue 315 and the carboxyl of the propionate of pyrrole IV evident in the crystal structure (49,59). The shift of the heme from 5-c to 6-c (86,87,89) will induce changes in macrocycle geometry that require structural adjustments at the heme edge; for example, recent resonance Raman results demonstrate that the heme is more planar in 6-c KatG than in 5-c enzyme (103) and therefore will have different dimensions. The observations on the glycine mutant here are consistent with release of constraints in the absence of the hydrogen bonding hydroxyl of residue 315. Further evidence for this conclusion comes from the behavior of the KatG[S315C] mutant reported elsewhere (87), which also exhibits facile conversion to 6-c heme. In this mutant, the thiol group will form weaker

hydrogen bonds than the corresponding hydroxyl of serine and may therefore impose weaker constraints on heme geometry.

Our previous reports on the origins of INH resistance in KatG[S315T] ascribed it to a decrease of the dimensions of the substrate access channel that interfered with high affinity INH binding (49,59). The publication of the CCP-INH structure illustrates the importance of a key set of hydrogen bonds between the drug and the backbone carbonyl of Ser315, a water molecule, and the pyridine nitrogen of INH that are likely critical for high affinity drug binding and efficient activation by *Mtb* KatG. In the case of the S315G mutant, our results show only small changes in its interactions with INH directly measured by optical and ITC titrations in the resting enzyme. This indicates that the structural parameters for high affinity binding are not seriously altered in the mutant, consistent with little perturbation of the groups required for this, which do not include the side chain of serine 315. However, the stopped-flow and the biomimetic activation results both suggest that the drug is a poorer substrate of the KatG[S315G] mutant enzyme, meaning that less activated drug, likely a radical species, and less IN-NAD adduct would be produced from INH in the peroxidation pathway. In order to reconcile these sets of observations, that is, the apparently normal binding of INH to the resting enzyme but still poor activation, we consider that the interactions between Cmpd I and the drug may be deficient; or, the catalytically important intermediates of the peroxidase cycle including Cmpd I are less efficient due to a change in their structure and or reactivity in the mutant. The optical spectrum of Cmpd I in KatG[S315G] is nearly identical to that in WT KatG, arguing against changes in the structure of this species in the mutant. A change in interaction between Cmpd I and INH is supported by the

kinetics results however only slight changes were observed. The possibility that the function of Cmpd I is in fact altered is supported by the finding that it is more reactive in KatG[S315G] compared to the behavior of this intermediate in the WT enzyme. Recall that the results above showed that the lifetime of Cmpd I in the mutant is about half of that of WT enzyme Cmpd I and that it reacts more rapidly with PAA. Thus, for a given concentration of peroxide, less enzyme intermediate would be available for turnover of INH. Evidence confirming the validity of this suggestion is the finding that the IN-NAD experiments cannot be driven to the rate catalyzed by WT KatG even in the presence of saturating amounts of INH. While a typical peroxidase Cmpd II found in KatG[Y229F] but not any other KatG examined by us was also shown to react with INH (55), this intermediate has not been isolable in WT or other *Mtb* KatG enzymes examined in our approaches, so no insightful comment can be made about the behavior of Cmpd II as a catalytically competent intermediate here. Furthermore, prior work has shown the potential for reaction of INH with protein based radicals in KatG but differences in such reactions would not be expected for the S315G mutant (Scheme 2.1).

In the absence of reducing substrates, the decay of Cmpd I in KatG generates tyrosyl and tryptophanyl radicals (70,71). Then it seems reasonable that endogenous radical formation contributes to the quenching of Cmpd I in KatG[S315G]. However, no direct evidence for an *increased* yield of amino acid based radicals was found in RFQ-EPR experiments in which the resting mutant enzyme is rapidly mixed with alkyl peroxide and frozen; the maximum total yield of radical in the case of the mutant was in fact lower by 60% during the first 200 milliseconds of reaction, compared to the yield in WT KatG (data not shown). Furthermore, an axial EPR signal characteristic of peroxyl

radicals with $g_{\parallel}$=2.035 and $g_{\perp}$=2.006 was the major species detected rather than the doublet and singlet signals characteristic of tyrosyl and tryptophanyl radicals found in WT KatG under similar conditions. Peroxyl radicals can be formed from amino acid radicals initially produced by electron transfers to Cmpd I followed by reaction of these with dioxygen (91,104), or can be evidence for alkyl peroxyl radical formed on PAA acting as a substrate of Cmpd I. The latter idea is supported by the fact that in double mixing stopped-flow experiments, PAA added to pre-formed Cmpd I in KatG[S315G] was more efficient as a reductant than in the case of the WT enzyme. Furthermore, the available amino acids that could reduce Cmpd I and form a radical that could go on to a peroxyl radical are the same in the mutant and WT KatG; in WT KatG the evidence for peroxyl radical is scarce and highly variable (unpublished results), arguing against increased endogenous electron transfers as the origin of a reduced lifetime of the intermediate in KatG[S315G]. Overall, these observations argue that under the artificial conditions with PAA and by extension, in the biomimetic system, INH saturation does not achieve a rate of IN-NAD formation equal to that catalyzed by WT KatG because Cmpd I can also readily react with available excess peroxide. Excess drug would be expected to overcome a simple loss in affinity for binding to Cmpd I, which was not observed (see Scheme 2.1). Therefore, a decreased availability of Cmpd I in any *in vitro* or *in vivo* pathway is reasonably consistent with all the observations we have reported, including poor drug activation, the poor yield of endogenous radicals and the specifically enhanced rate of reaction between PAA and Cmpd I. This enhancement is likely present because of greater flexibility of the substrate access channel near the heme edge, among other potential structural changes. One provocative hypothesis growing out of the results

here, is that the observed decrease in protein-based radicals in KatG[S315G] contributes to reduced activation of INH. This possibility is ruled out since KatG[S315T] exhibits high level resistance yet WT behavior in RFQ-EPR experiments designed to follow formation of protein based radicals (105).

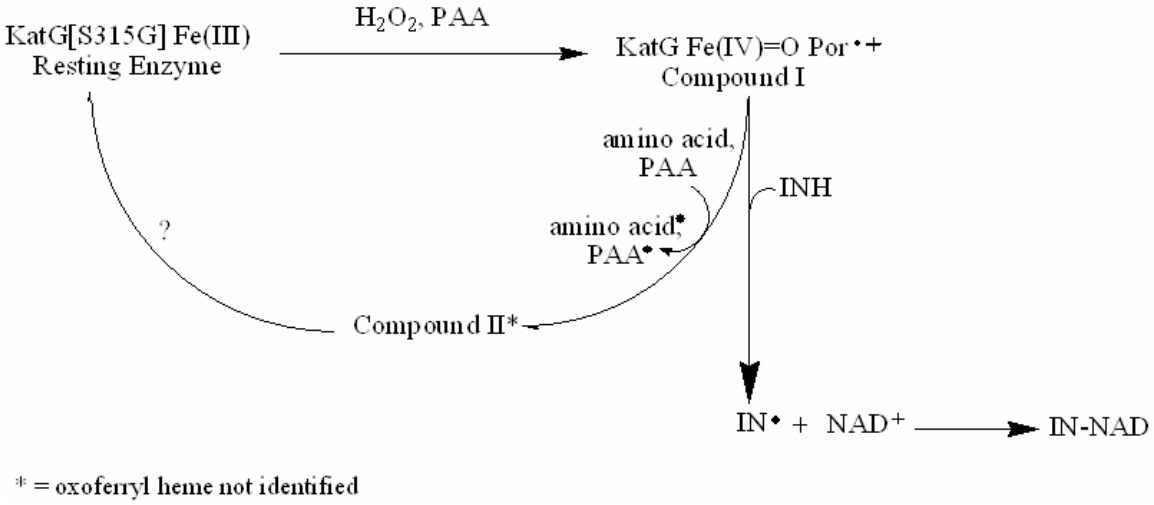

Scheme 2.1. Reaction pathways relevant to INH activation by KatG. Rates of Cmpd I formation using PAA (7.4 x 10^4 M^{-1} s^{-1} (KatG[S315G]); 3.0 x 10^4 M^{-1} s^{-1} (WT KatG) and decay of heme intermediates back to resting enzyme (40 s, KatG[S315G]; 80 s, WT KatG) are faster by a factor of two in the mutant enzyme. Increased rate or efficiency of single electron reactions with peroxide(s) leads to a decreased activation (oxidation) of INH and therefore to a decreased IN-NAD adduct formation, ultimately leading to drug resistance in strains harboring the S315G mutation.

The low level resistance due to the S315G mutation measured *in vitro* (MIC 8 µg/ml vs. 0.05µg/ml for WT) (48) is consistent with our model for drug activation that depends directly on the efficiency of INH peroxidation. We emphasize here that this model is physiologically relevant, as a moderately increased MIC parallels a moderate deficiency in INH activation by the mutant enzyme *in vitro*. For KatG[S315T], a much more dramatic loss in interactions with INH is present, consistent with a greater increase in the MIC (49). Without adjustment of standard dosing in clinical settings, the reduction

in activation is sufficient to lead to failure of INH therapy for patients carrying these S315 mutant *Mtb* strains. These results are consistent with the fact that the mutated KatG enzyme is stable and functional in INH activation but only at drug concentrations that are apparently not attained under normal treatment regimens.

Chapter 3. Protein Crosslinks in *M. tuberculosis* catalase-peroxidase KatG.

3.1. Introduction.

M. tuberculosis KatG forms the oxyferryl iron porphyrin π–cation radical ([Fe(IV)=O] Por +•) known as Compound I upon reaction with alkyl peroxides. Comp I rapidly decays to the resting ferric enzyme suggesting that endogenous electron transfer reactions take place (73). Recently, the formation of amino acid based radicals in KatG was proven by rapid freeze quench EPR (RFQ-EPR) experiments (70). By a combination of NO trapping, site directed mutagenesis, and RFQ-EPR experiments, the residue Y353 located in the surface of the protein was identified as one site of radical formation (74). The location of the amino acid radical sites involved in the electron transfer reactions leading to Y353 as well as the possible catalytic role of these radicals in KatG still remains unknown (except for the possibility of an MYW adduct radical involved in catalase activity; see chapter 4).

The formation of inter and intramolecular protein cross-links upon reaction with peroxides has been observed for several heme proteins such as myoglobin (75), hemoglobin (106), cytochrome C peroxidase (77), ascorbate peroxidase(78), and lactoperoxidase (79). In a study of sperm whale myoglobin, the formation of dimers was observed upon reaction with H_2O_2. By tryptic protein digestion and mass spectroscopy analysis, an intermolecular cross-link between Y151 and Y103 was identified (75). Also, the formation of dimers and trimers upon reaction with H_2O_2 in bovine lactoperoxidase has been observed, suggesting that more than one residue is involved in crosslink formation. Purification and activity assays of the dimers and trimers (79) showed that the

enzymatic activity of the higher molecular weight products was not significantly affected. Thus, cross-link formation upon reaction with peroxides appear to be common feature among heme proteins In which CmpdI produces tyrosyl radicals in the surface.

Several radical signals are observed using EPR spectroscopy of KatG treated with peroxides. A unique "narrow doublet" signal has been observed when the protein is treated with excess H_2O_2 (catalase activity conditions). This radical is only present during turnover of excess peroxide and decays very rapidly (~200 ms at pH= 7, ~ 1.5 sec at pH= 8.5) when all H_2O_2 is degraded (see Chapter 4 for an examination of this reaction). When the protein is treated with alkyl peroxide (PAA or t-butyl peroxide) a mixture of different radical species is observed; first a wide doublet EPR signal appears within milliseconds and after minutes of incubation with peroxide, a narrow singlet spectrum is observed (70). This transition has been assumed to be a product of the formation of amino acid based radicals on tyrosines and tryptophan residues in KatG. (Fig. 1.6 shows EPR spectra of the radicals observed when the protein is treated with PAA**)**

Here, we demonstrate the dimerization and oligomerization of *Mtb* KatG during turnover with peroxyacetic acid or hydrogen peroxide under a variety of conditions. Also shown here is that quenching of radicals by the addition of several peroxidase substrates including INH, eliminates crosslink formation. Concentration dependence experiments strongly suggest that the sites of crosslink formation are solvent exposed and preliminary fluorescence data suggest that the crosslinks are most likely dityrosines. The fact that excess hydrogen peroxide does not produce dimerization/oligomerization but a slow flux of H_2O_2 (and alkyl peroxide) do, suggests that there are two different pathways for

radical formation in *Mtb* KatG that differs depending on the peroxide. The latter observations illustrate the important finding that radicals are likely formed through internal electron transfers from heme intermediates such as Cmpd I but that in the presence of high concentrations of hydrogen peroxide, propagation of radicals to surface radicals is interrupted.

3.2. Crosslinking of *M. tuberculosis* KatG treated with alkyl peroxide:

The formation of dimers and trimers of KatG treated with PAA (5, 10, 20, 40, 80, and 160 fold excess) is evident in SDS-PAGE and native gels (Fig. 3.1. A and B). In the case of t-butyl peroxide, a much higher concentration (up to 1000 fold excess) and incubation time (1 hour) was needed to get comparable results to the ones obtained with the PAA treatment (data not shown).

As can be seen in Fig. 3.1, 40 fold excess PAA was enough to get the maximum yield of crosslink formation in fifteen minute reactions. This "saturation" behavior is consistent with the formation of endogenous radicals from a high-valent heme intermediate followed by covalent bond formation between two radical sites. However, another possible mechanism is the oxidation of surface amino acids on one enzyme by a heme intermediate of another. The fact that there are two higher molecular weight products (dimers and trimers) can be explained by the presence of at least two sites of cross-link formation. Interestingly, protein smears were observed for the products of all the treatments in both SDS and native even when low concentrations of peroxide were used. This can be explained by the formation of fragmented oligomers (croslinked

protein presumably broken down by oxidation reactions) of multiple molecular weights. The fact that the same higher molecular weight products (mostly dimers and trimers) are present in the SDS and native gels is evidence that the oligomerization of KatG is a product of covalent bond formation either between two different protein molecules or two subunits of the same dimer (or both). This covalent bond formation can be explained by the reactions between amino acid based radicals already proven to form in KatG, for example, on residue Y353 (70,71). Another interesting observation from the SDS and native gels is the fact that the formation of the two higher molecular weight products (dimers and trimers) is not evenly distributed. The majority of the products (also the first ones to appear at lower concentration of peroxide) are dimers, followed by the formation of trimers. This supports the model mentioned above in which surface amino acid based radicals are responsible for the crosslink formation. A series of experiments described below further support this model.

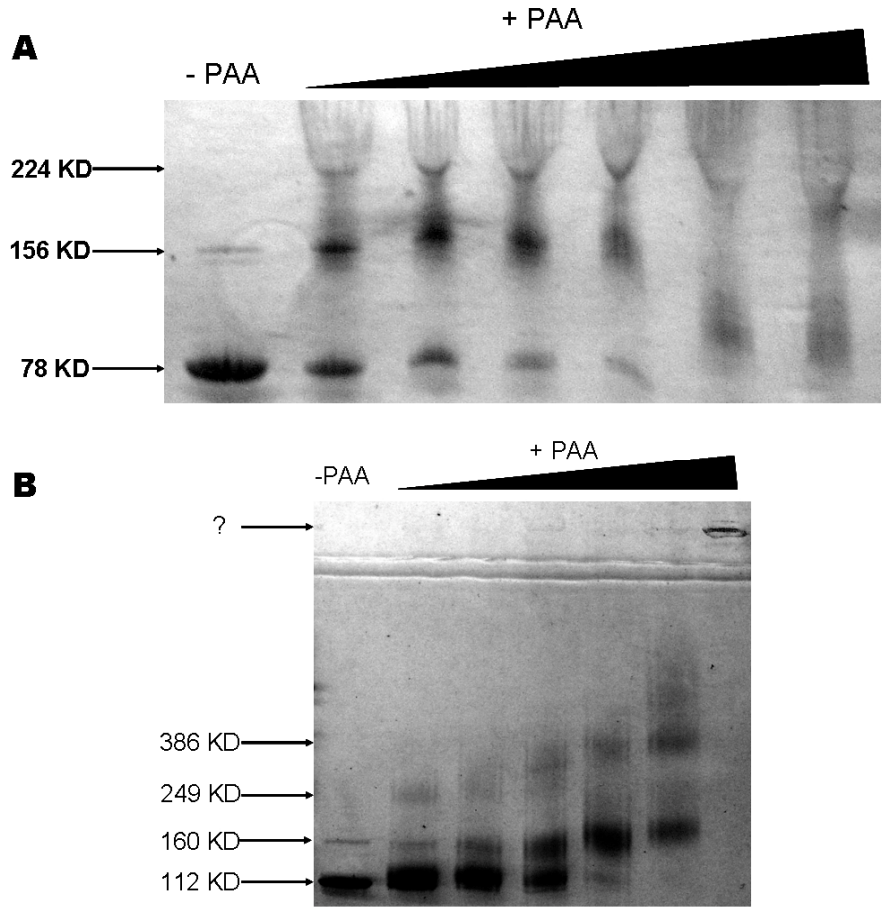

Figure 3.1. Native and SDS electrophoresis of Crosslinked *M. tuberculosis* KatG. SDS (A) and Native (B) PAGE of KatG treated with increasing concentrations of PAA. PAA:KatG ratios 5:1, 10:1, 20:1, 40:1, 80:1, 160:1.

3.3. Inhibition of crosslink formation by peroxidase substrates:

A concentration dependent inhibition of crosslink formation was observed when increasing concentrations of INH (5, 10, 20, 50, and 100 fold excess) were added to KatG treated with 40 fold excess PAA as above. Complete inhibition was observed when 50 fold INH (relative to heme) was added (figure 3.2A). Other peroxidase substrates (ABTS, furoic acid hydrazide, ascorbic acid, benzoic acid hydrazide, and NADH) also inhibit crosslink formation (figure 3.2B). INH was shown earlier by EPR spectroscopy to

quench radicals formed in KatG (70). These other substrates either inhibit amino acid based radical formation by preventing their formation by reducing Compound I more rapidly than the internal electron transfer reaction rates, or they directly quench the surface amino acid radicals after they are formed. One interesting fact that can be observed here and in the previous gels is the presence of crosslinked enzyme (dimers) in the untreated control enzyme.

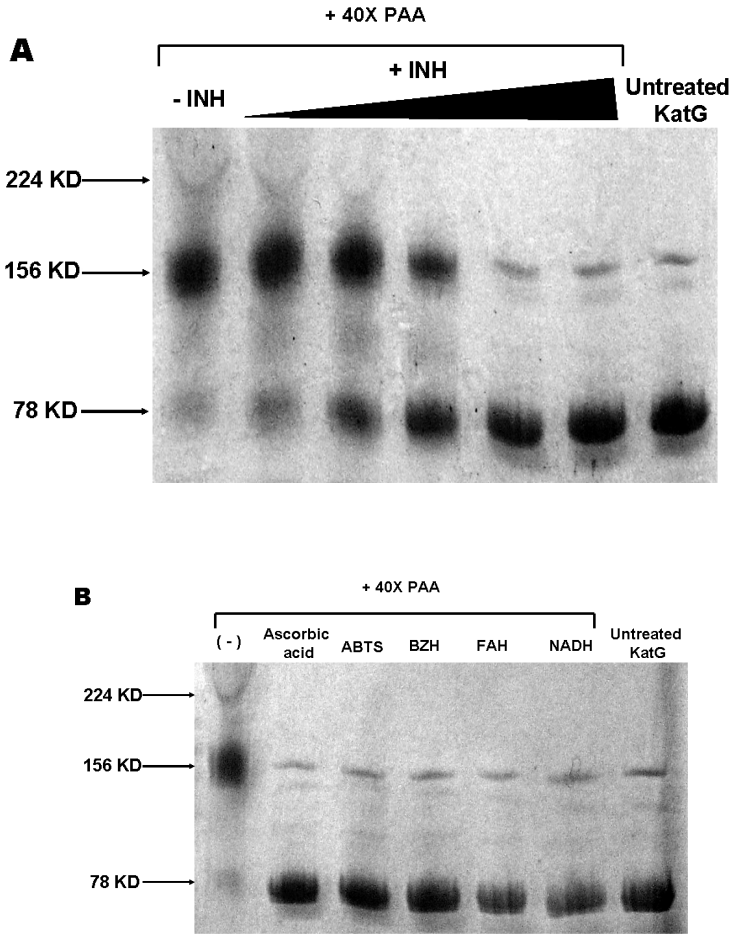

Figure 3.2. SDS PAGE of WT KatG treated with PAA in the presence of several peroxidase substrates. (A) SDS PAGE of KatG treated with 40X excess PAA and increasing concentrations of isoniazid. INH:KatG ratios 5:1, 10:1, 20:1, 50:1, 100:1. **(B)** SDS PAGE of KatG treated with 40X excess PAA and 50 X excess of several peroxidase substrates: ascorbic acid, 2,2'-azino-bis(3-ethylbenzthiazoline-6-sulfonic acid) (ABTS), benzoic acid hydrazide (BZH), furoic acid hydrazide (FAH), nicotinamide adenine dinucleotide (NADH).

3.4. Crosslinking of *M. tuberculosis* KatG treated with a slow flux of H_2O_2.

KatG did not form dimers or trimers during reaction with excess hydrogen peroxide. However, oligomerizaion was found when the protein was exposed to a slow flow of H_2O_2 generated at rates of approximately 100 uM and 200 uM per min from the glucose/glucose oxidase reaction (Figure 3.3). The fact that crosslinks were only formed under slow flow of H_2O_2 and were absent in the presence of high concentrations of hydrogen peroxide, can be explained as follows: When excess H_2O_2 is added, the catalase cycle is favored, meaning that heme intermediates turn over rapidly enough that amino acid based radicals are not formed. Hydrogen peroxide is believed to react with resting *Mtb* KatG following a classical catalase mechanism for the first step involving the formation of Cmpd I (73). Under a slow flow of H_2O_2, once Cmpd I is formed, a sufficient time can pass before it reacts with another H_2O_2, allowing oxidation of nearby aromatic residues. In other words, under these conditions where a 10-fold excess H_2O_2 per minute with respect to protein is being produced, every KatG molecule is expected on average to encounter a molecule of H_2O_2 every 6 sec. In the case where 20X excess H_2O_2 per minute is produced, KatG should react with a H_2O_2 every 3 sec. Cmpd I lifetime is much shorter than this so, according to these conditions no catalase turnover should occur and potentially Cmpd I should be reduced only by single electron oxidation of aromatic amino acids within KatG. This amino acid based radical formation presumably starts an electron transfer chain leading to the surface of the protein ultimately allowing the crosslink formation (See Scheme 3.1 in discussion). Importantly, these results prove that crosslinks can be formed when hydrogen peroxide or alkyl peroxides are used to initiate

turnover of the ferric enzyme and suggest that Cmpd I is an obligatory intermediate for radical and then crosslink formation.

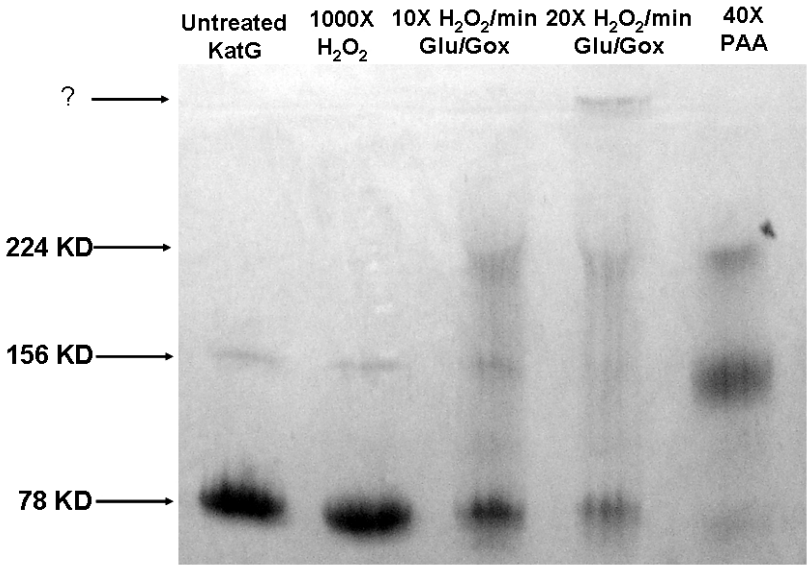

Figure 3.3 SDS PAGE of KatG treated with PAA or H_2O_2 under different conditions.

3.5. Concentration dependence of crosslink formation.

The analysis of experiments described above was performed using SDS-PAGE showing dimer and trimer as well as oligomer formation. Under denaturing conditions, the crosslinked dimer and native dimer have the same molecular weight, and therefore they are indistinguishable in the gel. Based on these facts, two scenarios are possible, one being that the sites of crosslink formation are located on the surface of the protein; and the other being that one site is located on the surface and the other at the subunit

interface. Both sites being on the interface are not possible because this will generate only dimers.

The major interactions at the interface of the two subunits of KatG occur between the N-terminal domains of each chain (107). Inspection of the 3-dimensional crystal structure of *Mtb* KatG showed that the contact between the subunits at the interface seems to be stabilized by stacking interactions between Y28 and Y197 and between W38 and W204 from opposite monomers (88). These facts further suggest that it is reasonable to expect that one of the cross-links formed in KatG could be located in the interface between subunits of the dimer. To address this possibility, we evaluated the cross-link formation process as a function of protein concentration since the inter-subunit cross link yield would not be expected to change while cross links between surface residues would increase with protein concentration. As can be seen in Figure 3.4, the yield of dimers and trimers increases when the concentration of KatG in the reaction with PAA is increased, as would be expected if the sites of cross-link formation were on the surface of the protein. To further confirm these results, site directed mutagenesis of Y197, Y28 and W204 to phenylalanine was performed. The mutant proteins Y197F, Y28F and W204F were able to form dimers and trimers in similar yields to those observed in WT KatG under the same conditions (not shown). In sum, these results suggest that there are at least two sites of cross-link formation in WT KatG and that these sites are located on the surface of the protein and not only in the interface between the two protein subunits (Figure 3.4).

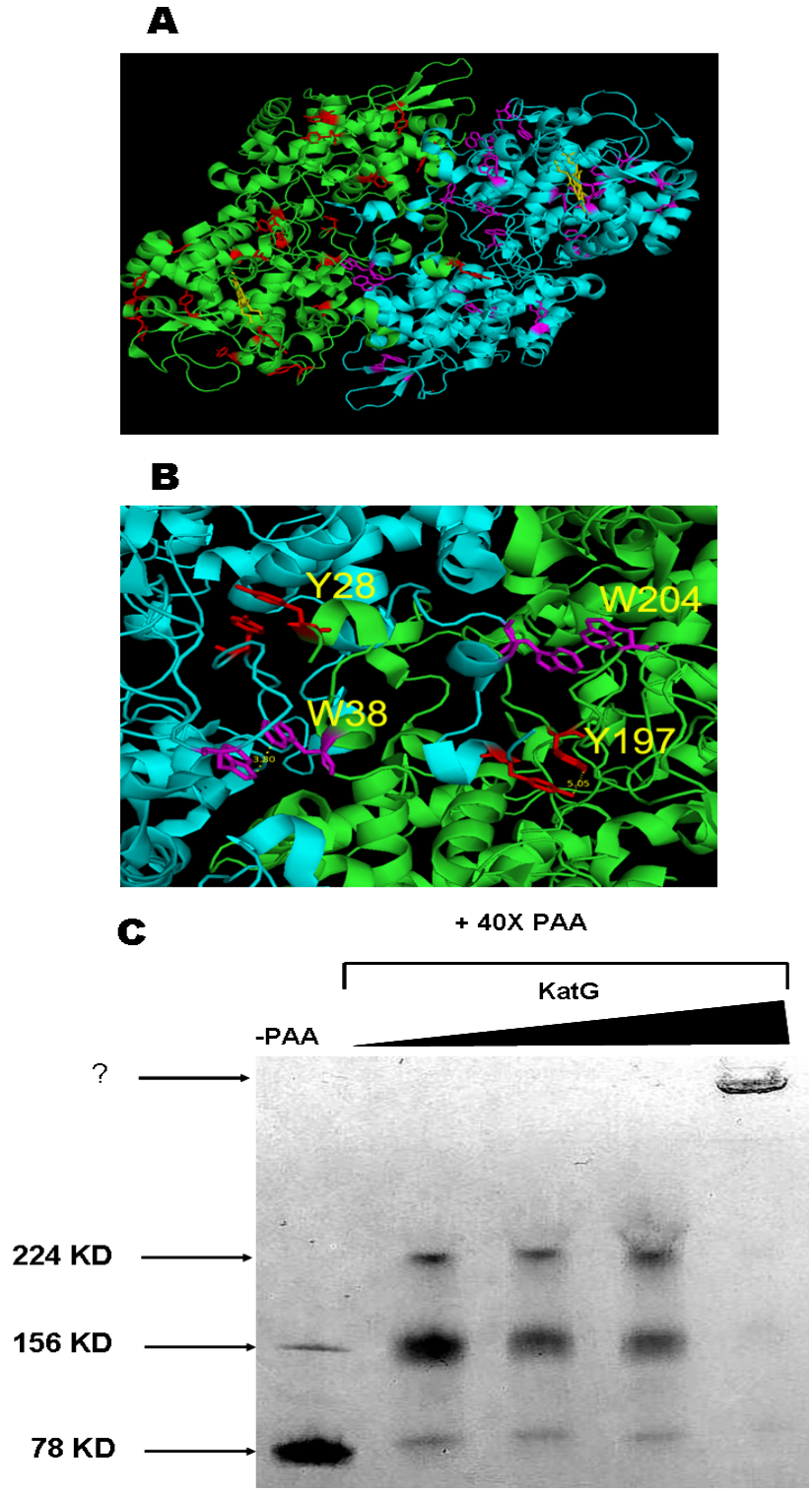

Figure 3.4. Concentration dependence of crosslink formation in WT KatG. (A) 21 tyrosine and 24 tryptophan residues in KatG. (B) Tyrosine and tryptophan residues located at the subunit interface (C) SDS PAGE of KatG treated with 40X excess PAA. KatG concentrations: 10, 20, 40 and 80 uM.

3.6. Catalytic activities of KatG multimers.

In order to address the potential physiological impact of KatG crosslinks on enzyme function, native homodimer was separated from dimers and trimers by gel filtration chromatography and catalytic activities were determined. The UV/vis spectrum of the crosslinked protein (dimer) was severely altered especially in the Soret region where a decreased in the absorbance of ~50% (relative to the WT untreated protein) was observed. This damage is presumably due to oxidative reactionsduring multiple turnovers. Also, analysis of the catalytic function of the PAA treated protein showed that the catalase and peroxidase activity of the higher molecular weight products is severely reduced with respect to the untreated monomeric enzyme (~17% and ~28% of the untreated protein respectively, based on heme concentration in all cases). Interestingly even the monomeric treated protein showed a reduced catalase (~25% of the untreated protein) and peroxidase (~42% of the untreated protein) activity. These results show that the integrity of the protein and/or the heme cofactor are being damaged by the treatment with PAA. More experiments are necessary to understand this question. In any case, it is important to take into account that these experiments suggest that the study of KatG in the presence of high concentration of alkyl peroxides is very risky and that one has to be careful in the interpretation of data obtained under these conditions due to the fact that they undoubtedly damage KatG. A large amount of literature on the function of KatG must be considered with caution based on the present observations. For example, in a recent article published by Singh et al. (96) a [Fe(IV)=O Trp*] intermidiate analogue to CCP Compound I was detected in *M.tb* KatG using a high concentration of PAA (40-fold

excess) and a long incubation time (~15 sec). Based on the results presented here, the catalytic relevance of this intermediate as well as other experiments done by others under similar conditions must be reevaluated.

3.7. Identification of the possible residues involved in crosslinks.

In a previous study, tyrosine 353 was identified as a site of radical formation in *M. tuberculosis* KatG (74). Y353 is located in the surface of the protein, suggesting that this amino acid residue could be involved in crosslink formation. For this reason we tested the Y353F mutant for its ability to form dimers and trimers upon reaction with PAA. Unexpectedly, this mutant formed cross-links in the same yield as the WT enzyme (data not shown), suggesting that in WT KatG, Y353 may still be involved in crosslink formation but in the mutant, a different (and possibly nearby) surface residue is involved. *M. tuberculosis* KatG has 13 tyrosines (Y155, Y426, Y95, Y339, Y337, Y304, Y353, Y210, Y608, Y678, Y597 and Y638) and 6 tryptophan residues (W90, W328, W351, W149, W438 and W689) located on the surface of the protein. A careful analysis of these residues using various protein viewers (Rasmol, Spdb viewer, Pymol) software and the Consurf server http://consurf.tau.ac.il/ (server for the identification of functional regions on the surface of proteins) allowed us to identify Y95, Y210, Y304 and W351 as the most likely residues to be involved in cross-link formation in KatG (excluding other potential sites for radical formation such as cysteine thiols).

Reaction of the mutant Y304F with PAA followed by SDS-PAGE analysis of the products as above showed no difference in the oligomerization pattern compared to WT

KatG. These results may indicate that neither Y353 nor Y304 are involved in cross link formation but other possibilities, such as multiple crosslink formation or crosslink formation at alternative residues occurs in the mutants. We cannot conclude that a particular residue is not involved in the cross-link formation in the WT protein just by site directed mutagenesis studies because the radical can be formed on other nearby oxidizable residues in the mutated enzymes. Consequently, structural and sequential analysis of peptides from the oligomeric enzyme has to be pursued in order to identify the residues involved in the cross-link formation in KatG.

As mentioned in the introduction to this chapter, several heme and metalloproteins have been reported to form covalent crosslinks (75,77-79,106). In many of these cases the amino acid residue involved in the crosslinks had been identified as tyrosine (75,79). In the case of *M. tb* KatG the presence of tyrosines and tryptophan radicals has been demonstrated. Based on high-field EPR data from our group (71) a distribution of approximately 80% tyrosine 20% tryptophan radicals was observed in a rapid freeze quench sample prepared 200ms after mixing with peroxide. Based on the fact that tyrosine radicals are the major species observed and that dityrosines are by far the most common type of crosslink found in proteins treated with peroxide, we decided to check for the presence of dityrosines in our samples of KatG treated with PAA.

Dityrosines are known to fluoresce with an emision maxima around 400 nm when they are excited at 315 nm in alkaline conditions (76,79,108). The fluorescence spectrum of KatG treated with 40X PAA was obtained (borate buffer pH 9) and compared with the untreated protein. The fluorescence intensity at ~410 nm of the peroxide treated KatG was approximately ten times greater compared with the native

enzyme. This result strongly suggests the presence of tyrosine cross links in the products of peroxide treatment **(Fig. 3.5)**.

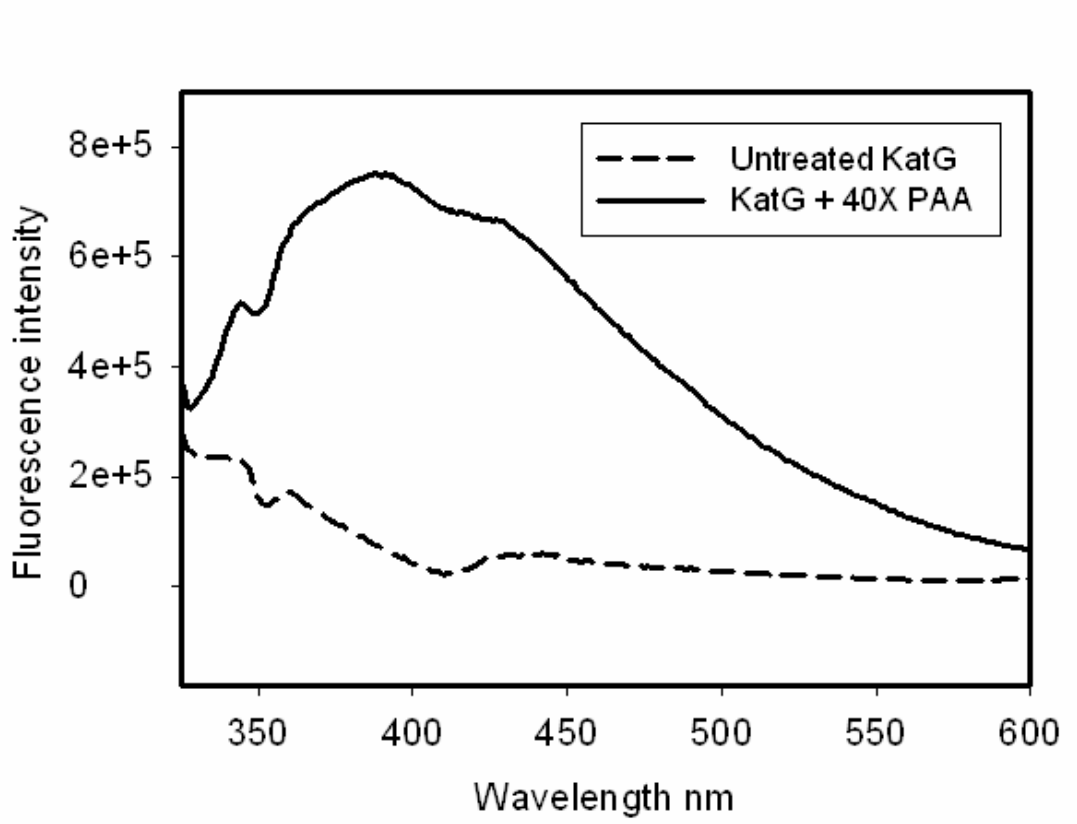

Figure 3.5. Fluorescence spectra of KatG treated with 40X PAA compared to untreated KatG. λ Excitation= 315 nm.

3.8 Discussion.

In this chapter we proved that *M. tuberculosis* KatG forms higher molecular weigh products during turnover in the presence of alkyl peroxides or dilute hydrogen peroxide generated slowly by the glucose/glucose oxidase reaction. This crosslink formation can be rationalized by the following mechanism: Reaction of KatG with alkyl peroxides forms Cmpd I (Rate of Cmpd I formation: 2.9×10^4 M^{-1} s^{-1}) which in the absence of H_2O_2 or peroxidase substrates, decays as amino acid based radicals are formed (most likely tyrosines and tryptophan, but potentially any oxidizable residue). The fact that a slow flow (conditions considered here to be physiologically relevant) of H_2O_2 leads to crosslink formation strongly supports the suggestion that the crosslinks can form *in vivo* and that Cmpd I is an obligate intermediate for the crosslink formation. Once Cmpd I is formed in the absence of exogenous electron donors it can oxidize amino acids in the protein. This creates an (unknown) electron transfer pathway that eventually leads to the protein surface (Y353 and other residues). These surface AA based radicals can either oxidize another protein molecule or an electron donor available in solution, or in the situation in which it finds another protein carrying a surface amino acid based radical, form a crosslink (See Scheme 3.1).

The addition of INH and other peroxidase substrates to reactions of KatG with alkyl peroxide (PAA) completely inhibits the crosslink formation process. This interesting observation can be explained by these peroxidase substrates acting as single electron donors to Cmpd I thereby preventing the formation of amino acid based radicals

altogether. Another plausible explanation is that these substrates directly reduce amino acid based radicals and in this way inhibit the crosslink formation process.

Previously, it was shown that INH directly reacts with Cmpd I I (49), but we also proved that already formed amino acid based radicals are quenched by INH (70). Therefore, the inhibition of crosslink formation by peroxidase substrates could involve both processes, reduction of Cmpd I as well as direct quenching of AA based radicals.

Based on the fact that the major interactions at the interface of the two subunits of KatG occurs between the N-terminal domains of each chain (107) and that residues Y28, Y197, and W38, W204 from opposite monomers seem to stabilize the homodimeric protein by stacking interactions (88), it was reasonable to expect intramolecular cross links to be formed if tyrosine radicals formed at those residues.

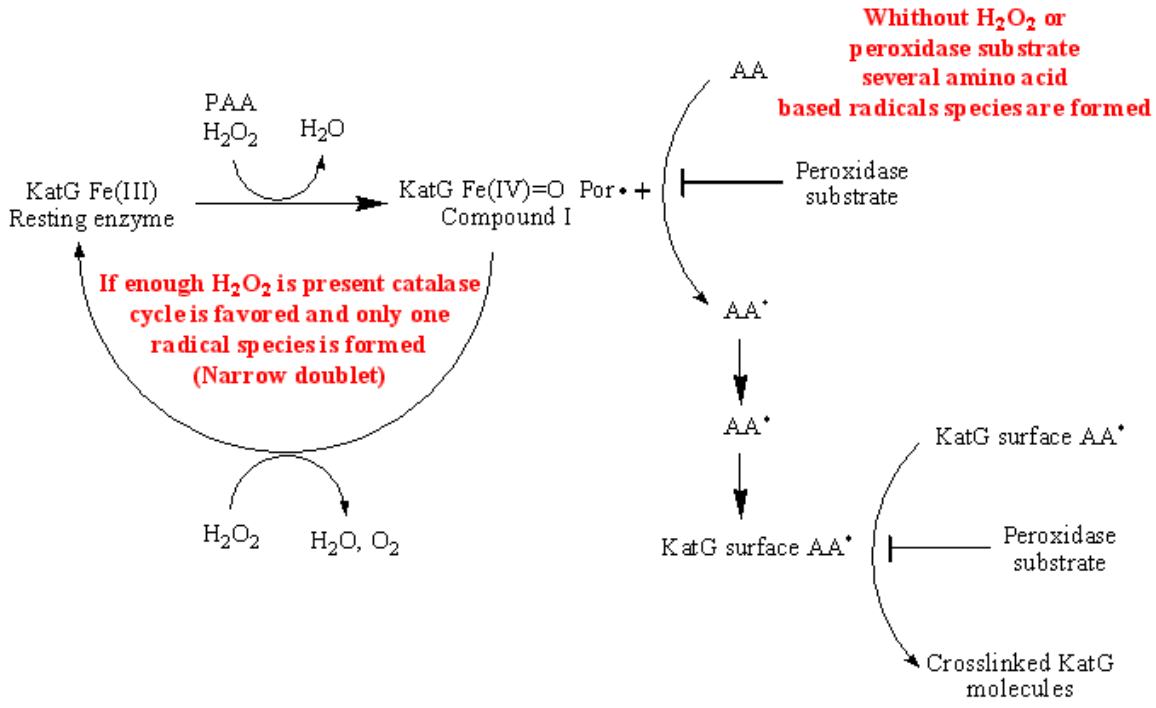

Scheme 3.1. Proposed mechanism of crosslink formation in *M. tuberculosis* KatG.

However, concentration dependence experiments performed in this study clearly show that this is not the case. The yield of crosslinked enzyme is directly dependent on the protein concentration proving that this process is diffusion dependent and therefore surface residues in two different protein molecules must be involved in the crosslinks. The main products of crosslinking are dimers and trimers (and some even higher molecular weight products when the concentration of PAA or KatG is high); consequently there are at least two different sites of radical formation on the surface of KatG. Interestingly, in the concentration dependence experiments, when a very high concentration of protein was used (80μM) an oligomer of undetermined size (so big that it did not go into the gel) is formed (Figure 3.3). This further confirms that the crosslink formation is due to radicals located in the surface of the protein, not the interface.

In an attempt to characterize the higher molecular weight products formed upon reaction with alkyl peroxide and H_2O_2 (slow flow), reactions of KatG with both peroxides were performed and the higher molecular weight products were purified by gel filtration chromatography. Reaction of KatG with excess alkyl peroxide produces oxidative damage of the polypeptide and the heme moiety since crosslinked KatG presents an abnormal optical spectrum (absorbance in the Soret region is reduced about 50%). Also, the catalase and peroxidase activity of the higher molecular weight products is severely reduced with respect to the untreated monomeric enzyme. Interestingly even the monomeric treated protein showed a reduced catalase (~25% of the untreated protein) and peroxidase (~42% of the untreated protein) activity. This can be explained by the fact that the very harsh conditions generated by excess peroxide produce oxidative

damage that lead to heme and protein modification as had been shown for myeloperoxidase and HRP which are damaged by hydrogen peroxide.

The loci of amino acid residues involved in the KatG crosslinks remain unproven but fluorescence results demonstrate the presence of dityrosines. Dityrosine crosslinks are commonly found in proteins exposed to UV-irradiation (109), γ-irradiation (110), aging (111) exposure to oxygen free radicals (oxidative stress) (75,112), nitrogen dioxide, peroxynitrite, and lipid hydroperoxides (112). Dityrosines have been proposed to act as an oxidative stress marker. Concentration of dityrosines was found to be 100-fold higher in low density lipoproteins isolated from atherosclerotic lesions than in normal ones. Also, urine samples from patients suffering from systemic bacterial infections showed dityrosine levels twice as high as those found in healthy individuals (113). Interestingly, incubation of oxidatively modified proteins (containing dityrosines) with proteolytic enzymes resulted in increased selective proteolysis of the modified proteins (114,115). Also, selective degradation of H_2O_2 treated hemoglobin but not control (untreated) hemoglobin has been observed (106). Altogether, these results strongly suggest that dityrosines may serve as signals that "mark" proteins for protein degradation. It is known that *M. tuberculosis* has a bacterial proteasome analogous to that in eukaryotes (116). Based on these facts it is tempting to speculate that a similar phenomena occur in *Mtb* in the infected host. To the extent of our knowledge there is no study of the level of expression and turnover of KatG in infected macrphages but based on these results it is reasonable to think that the turnover rate could be increased presumably due to dityrosine crosslink formation.

In an effort to determine the location of crosslink formation, the 3D structure of KatG was examined. A careful analysis using various protein viewers (Rasmol, Spdb viewer, Pymol) softwares and the Consurf server http://consurf.tau.ac.il/, allowed us to identify Y95, Y210, Y304 and W351 as the most likely residues to be involved in the cross-link formation in KatG (based on their orientation and location in the surface of the protein). Site directed mutagenesis suggests that the residues Y197, Y304, Y28 and Y353 are not sites of cross-link formation. Also, concentration dependence analysis of the oligomerization process strongly suggests that the sites of cross-link are located on the surface of the protein. Unfortunately, the identity of the residues involved in the oligomerization of KatG is still unknown. However, here we propose that tryptic digestion of *M. tuberculosis* KatG pretreated with PAA (under the same conditions used in the cross-link experiments), followed by HPLC separation of the digested peptides and mass spectrometry analysis can be used to identify the residues involved in the cross-links of this protein.

The process of amino acid based radical formation in *M. tuberculosis* KatG as well as a catalytic role for any radicals is still far from being completely understood. The potential catalytic role of amino acid based radicals is an active area of research in KatGs and other peroxidases. Due to the fact that the identity of tyrosyl and tryptophanyl radicals formed during turnover of *M. tuberculosis* KatG after reaction with alkyl peroxides is not proven, site directed mutagenesis and rapid freeze quench EPR studies continue to be important. However, site directed mutagenesis is not always a good way to prove the loci of radical formation based on the fact that once you eliminate a residue where a radical is formed in the native enzyme, a new radical can form at other residues

without significantly altering the overall EPR spectrum or yield of radicals. Evidence that suggested radical formation at residues Y229, W107, and Y353 has already been presented (70,71,74). The residue W91 in *Synechocystis* KatG was also reported as a radical site (117). However, this residue is not involved in radical formation in *Mtb* KatG (71). Additionally, based on coordinates from the crystal structure of *M. tuberculosis* KatG, the software PATHWAYS was used to calculate electron transfer coupling factors between donor amino acid residues and the heme as acceptor. In this approach, the residues Y197, Y28, Y337 and Y413 were predicted as possible radical sites in addition to Y229 and W107 (71). Nevertheless, due to recent results discussed in the following chapter, the role of Y229 and W107 in the process of radical formation in KatG must be reevaluated. Of these residues, only Y353 would be available for cross linking. However, the role as well as the identity of other residues involved in the electron transfer reactions in this protein is far from being completely understood.

A very important conclusion derived from this study is that there are more radical forming residues on the surface of KatG besides Y353. Before these experiments, there was no evidence for any other radical forming residue on the surface of *M. tuberculosis* KatG. Despite the fact that there are several sites of radical formation in *M. tuberculosis* KatG, only Y353 was identified by NO spin trapping experiments. The failure of this approach to identify other sites of radical formation like Y229 and W107 (and any other potential residue involved in this electron transfer pathway between W107 and Y353) can be partially explained by the fact that these residues are deeply buried inside the protein and therefore inaccessible to the NO trap or by a very short lifetime of these amino acid

based radicals. This inaccessibility effect in spin trapping experiments has been reported by others (118).

In summary, here we report the intermolecular crosslink formation of *Mtb* KatG upon reaction with peroxide, the inhibition of this crosslinking process by several peroxidase substrates, the oxidative damage suffered by the protein when it is treated with excess peroxide and proved the existence of at least two sites of radical formation (most likely tyrosine residues) located in the surface of the protein. Also we discussed the possible relationship of this crosslink formation with protein degradation and turnover. One key point here is that a widely used approach to study amino acid radical formation in other reports has relied on using large excess of peroxides shown here to be damaging to the enzyme structure.

Chapter 4. An oxyferrous heme/protein-based radical intermediate is catalytically competent in the catalase reaction of *M. tuberculosis* catalase-peroxidase (KatG)

4.1. Introduction

Heme enzymes such as catalases and peroxidases are ubiquitous in aerobic organisms and are principally responsible for eliminating the potential damaging effects of hydrogen peroxide. The structure and function of the monofunctional enzymes has received abundant attention for many years, while the dual function enzyme, catalase-peroxidase (KatG), found in bacteria and fungi is a relative newcomer and is less well characterized. In the pathogen *M. tuberculosis*, which still infects and kills millions of people each year, KatG is the only catalase and is required for virulence (119,120) . The peroxidase activity of KatG is considered to be responsible for activation of the antiTB therapeutic agent, isoniazid (36,49) and mutations in this enzyme are the principal origin of widespread resistance to this *pro*-drug (47,121).

Investigation of the properties of KatG is of interest because the correlation between unusual features of its structure and particular mechanistic steps is not fully defined or understood. The post-translational modification of residues Met 255, Y229 and W107, the side chains of which form an adduct on the distal side of the heme (Fig. 1, chapter 1. Introduction), is the most intriguing structural feature and is required for catalase but not peroxidase activity (55-58). KatG catalytic function has features in common with classical mono-functional enzymes; for example, an oxoferryl-porphyrin π-cation radical species is formed from resting enzyme in turnover with alkyl peroxides (65,73,122,123) and this intermediate is taken to be common to both peroxidase and catalase reaction paths. Its formation has not been observed in the presence of hydrogen

peroxide however, except in mutants such as W107F and Y229F which lack catalase activity (55,124). Interestingly, a poor rate of reaction with hydrogen peroxide of KatG Compound I (Cmpd I) prepared using alkyl peroxide was recently presented as evidence that the catalase mechanism in KatG diverges from the typical monofunctional enzyme pathway exemplified by bovine liver catalase (34). A reaction between hydrogen peroxide and Cmpd I would be expected to constitute the second phase of the dismutation in which H_2O_2 acts as a two-electron reductant. A mechanism explaining the robust catalase activity exhibited by KatG's is therefore of special interest because novel mechanistic features are likely to be uncovered; Cmpd I is apparently not a catalytically competent intermediate and high activity is absent from other homologous class I peroxidases. The near absence of catalase activity in KatG mutants in which replacements are made in the residues of the Met-Tyr-Trp (MYW) adduct strongly suggests a specific mechanistic role is filled by modification of the distal side residues.

KatG dismutates hydrogen peroxide in a non-scrambling mechanism such that both oxygen atoms of dioxygen derive from the same molecule of hydrogen peroxide (125,126). Unlike classical catalases, however, which do not accumulate intermediates during H_2O_2 turnover because of very rapid rates of both the peroxide reduction and the peroxide oxidation steps, KatG forms a species characteristic of oxyferrous heme (peroxidase Cmpd III) in the presence of high concentrations of peroxide (34,73,127). This intermediate is usually stable in peroxidases and is considered to be catalytically inert, but must be highly unstable in KatG since catalase turnover occurs while the heme is in this form (In CCP oxyferrous heme is unstable because of internal redox chemistry involving W191 but CCP does not exhibit catalase activity (128)) and the catalase

activity of the W321F mutant of *Mtb* KatG is only moderately reduced (50). A protein based radical proposed here to be formed on the distal side amino acid adduct, that co-exists with oxyferrous heme when peroxide turnover occurs, is suggested to be a catalytically competent intermediate in catalase turnover in WT KatG.

Our focus here is on identifying intermediates formed in *Mtb* KatG during catalase turnover. Stopped-flow optical kinetics techniques are applied to follow the changes in heme oxidation state in parallel with RFQ-EPR experiments used to monitor the production and decay of protein based radicals. A heretofore unknown narrow doublet radical is characterized by X-band and D-band EPR spectroscopy. A reaction scheme originally suggested in other work (34) is described, incorporating the new radical proposed to be localized on the MYW adduct into the catalase reaction pathway. A detailed analysis of the catalase reaction mechanism in *Mtb* KatG, the *only* catalase found in *M. tuberculosis*, contributes to our understanding of the biology of this pathogen, which resides in host macrophages upon infection and is subjected to extensive oxidative stress in that environment.

This chapter is an adaptation from the recently published article: Suarez et al. (2009). JBC. *284*, 7017-7029. Due to the various techniques used in this project several people were involved in this research, however, most of the work was done in our lab except for the high field EPR experiments and DFT calculations. For the sake of completeness the whole history is presented here except for the theoretical calculations section done by Professor Andrzej Jarzecki from Brooklyn College. Some of the RFQ and low temperature EPR data was collected with the assistance of Dr. Kalina Ranguelova who was a postdoctoral associate in the laboratory at the time this research

project started. All high field EPR data presented here were collected in Professor Gary Gerfen's laboratory at the Albert Einstein College of Medicine, Bronx, New York. Assistance for sample preparation, and data collection and analysis for these experiments came from Dr. Gerfen, Julia Manzerova (MD/PhD. Student) and Vladimir Krymov (technician).

The tyr mutants described on page 89 (Y28F, Y95F, Y98F, Y113F, Y155S, Y197F, Y229F, Y304F, Y353F, and Y426F) were initially prepared by Dr. Shengwei Yu. Some of the manual mixed EPR data with excess H_2O_2 for all tyr mutants were collected by Abdelahad Khajo (Table 4.1).

4.2. RFQ-EPR and optical stopped-flow experiments

The high catalase activity of *Mtb* KatG is conveniently measured in the presence of millimolar H_2O_2 without enzyme degradation or apparent inhibition. However, recent results data from our lab (not published) show that the hydrogen peroxide concentration conventionally used to measure catalase activity (25 mM, 500,000 fold excess) actually cause some protein damage. Most of the experiments in this study were done at a much lower H_2O_2 concentration (between 1000 and 8000 fold excess). Among the accumulated mechanistic details for this unusual behavior in a Class I peroxidase are the finding of a non-scrambling mechanism shown in isotope-ratio experiments (125), the finding that superoxide is not a product during turnover (125), and the demonstration that mutation of Met255, Y229 or Trp107, the side chains of which form the distal side adduct in KatG shown in Figure 1.9, reduces the rate thousands-fold (55,56,58,124,129-

132). A recent comprehensive kinetic study of heme intermediates formed during catalase turnover (34), and suggestions from that report provided the impetus for the application of RFQ-EPR spectroscopy to probe for protein-based radicals in the catalase reaction pathway in WT KatG and in several mutants. Optical stopped-flow experiments and low temperature EPR were also applied to be able to monitor the kinetics of changes in heme oxidation or spin state.

RFQ-EPR sampling allows mixing of ferric KatG with H_2O_2 followed by freeze-quenching of reactions in the millisecond time range. Fig. 4.1 (top) shows spectra recorded at 77 K in the g = 2 region as a function of incubation time after mixing KatG with a 1000-fold molar excess of H_2O_2 at pH ~ 7 and ~ 8.5. A narrow doublet signal at g = 2.0034 with a principal hyperfine splitting of approximately 11 G appears at the earliest time point accessible here and was the only signal in the g = 2 region in spectra recorded at 77 K. The intensity of the signal was maximal in the sample frozen after 20 ms (approximately 0.1 spins/heme) and decayed thereafter until it was no longer detectable after approximately 200 msec (Fig 4.1 top) for the reaction run at pH ~ 7. The actual spin concentration is likely greater than 0.1 spins/heme because the considerable foaming under these conditions dilutes the solutions; no correction is made for this dilution. At pH 8.5, the narrow doublet signal persisted approximately 8-times longer (up to 1.7 sec) (Fig. 4.2 bottom). When using an 8000-fold molar excess, the narrow doublet signal persists long enough that an EPR sample could be prepared by manually mixing ferric

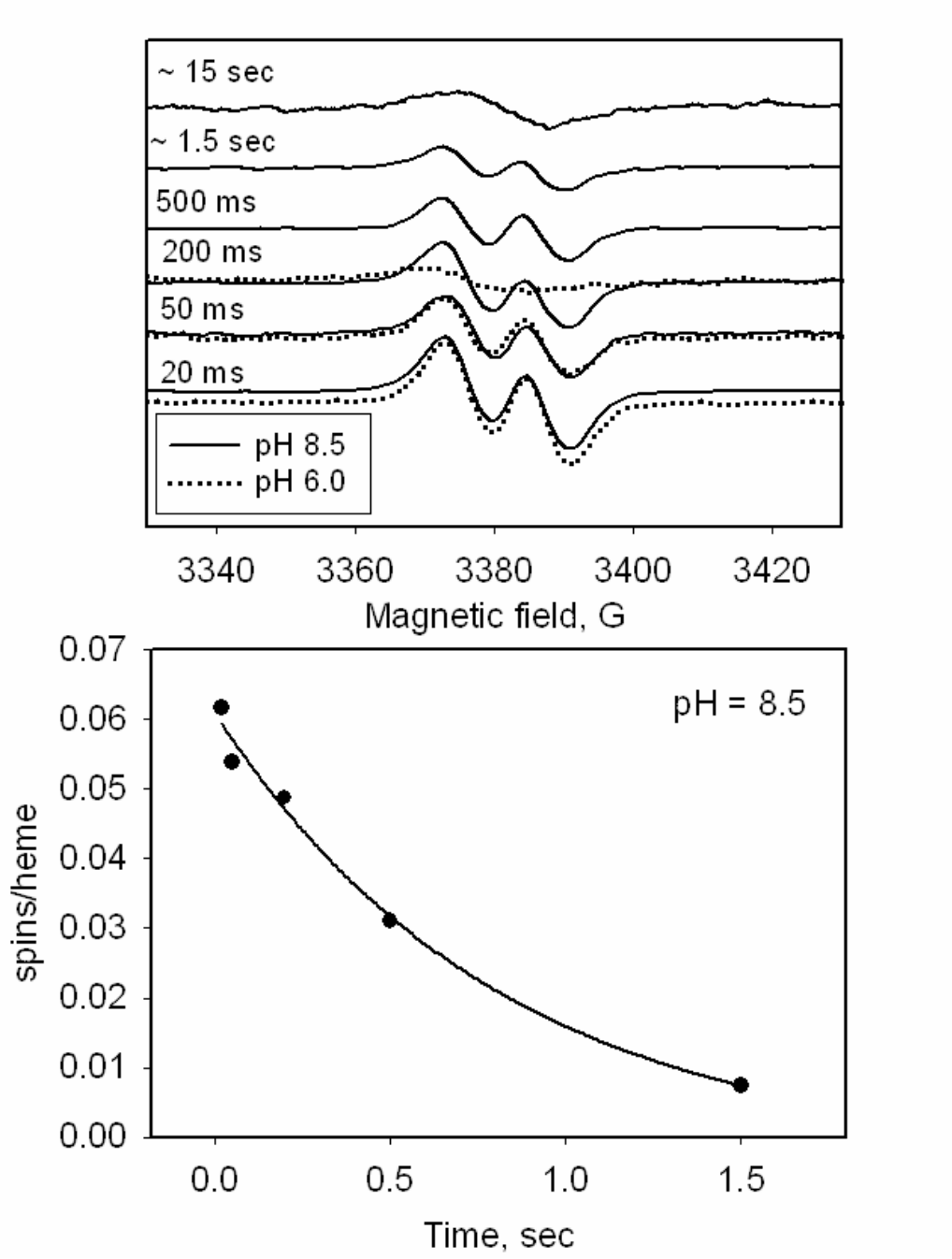

Fig. 4.1. RFQ-EPR of *M. tuberculosis* KatG reacted with H_2O_2. (top) Samples were frozen at the indicated time points after mixing ferric KatG with 1000-fold excess H_2O_2 at pH 7.2 (6.0) or 8.5. Spectra (average of 9 scans) were recorded using the following conditions: T = 77 K, microwave frequency = 9.442 GHz; microwave power = 0.1 mW; modulation amplitude = 1 G. (bottom) Intensity (spins/heme) of the narrow doublet EPR signal as a function of time in RFQ-EPR samples frozen after mixing KatG with 1000-fold excess of H_2O_2 at pH 8.5. The curve is a fit of the data to a single exponential function using Sigma Plot 9.0.

enzyme with peroxide and rapidly transferring and freezing the solution by immersion of the EPR tube in liquid nitrogen. This method for sample preparation was used below for examining radical formation in mutant enzymes.

The catalase specific activity of *Mtb* KatG (~ 4000 U/mg at pH 7 and ~ 439 U/mg at pH 8.5) allows estimation that a 1000-fold excess of peroxide should be completely consumed within ~ 0.2 seconds at pH 6 or 7 and after ~1.6 seconds at pH 8.5. These time intervals correspond very well to the interval during which the radical is present, suggesting that it represents a kinetically competent intermediate of the catalase reaction pathway. The RFQ-EPR conditions are not amenable to optical experiments to directly follow the rate of disappearance of hydrogen peroxide because of active bubbling; therefore no visual comparison in rates is presented for the results using these two techniques.

Stopped-flow optical experiments were performed to record changes in heme species at pH 6 and 8.5. Previous work had shown that small excesses of H_2O_2 do not lead to accumulation of new species (73). Upon mixing of enzyme with 1000-fold molar excess of H_2O_2 at pH 6, a species different from resting enzyme appears at the earliest time point (5 ms) (Fig. 4.2A and 4.2B). This species lacks the CT-bands of the resting (ferric) enzyme at 500 nm and 630-640 nm and has the features of oxyferrous enzyme including a Soret maximum at 413 nm and with β and α bands at 545 nm and 579 nm. The spectrum of oxyferrous heme in *Mtb* KatG (34,73) was confirmed in the companion paper (133). The reaction pathway to oxyenzyme can occur through reduction of Fe(IV) by peroxide, superoxide addition to ferric heme or dioxygen binding to ferrous iron. The finding that this intermediate is observed only when very large excesses of hydrogen

peroxide are present argues for the first pathway, which had been confirmed for *Mtb* KatG[Y229F] (55).

In similar experiments at pH 8.5, a different heme intermediate was found at the earliest time point. (The optical spectrum of the resting enzyme does not change as a function of pH from pH 6 to pH 8.5.) The new species has a Soret maximum at 418 nm, a broad shoulder at 521 nm and no other prominent features in the visible region (Fig. 4.2C). The spectrum of this intermediate decayed sharply after ~1.5 seconds (Fig. 4.2D) and upon reaction of the enzyme with 2000-fold, 4000-fold and 8,000-fold molar excess of hydrogen peroxide persisted for longer periods proportional to the amount of peroxide added (not shown). At pH 7, the optical spectrum formed in the first milliseconds was a mixture of the low and high pH species (not shown). The time interval during which the oxyenzyme intermediate was observed at pH 6 (and also at pH 7) exceeded the time interval during which the narrow doublet EPR signal was detected (Fig. 4.1) and beyond the predicted time interval for complete consumption of peroxide assuming a linear reaction rate throughout. These observations indicate interesting features of the reaction pathway that are addressed in conclusions.

Low temperature EPR spectra of RFQ-EPR samples prepared at pH 7 did not contain a signal in either the g = 6 or the g = 2 regions that could be assigned to a paramagnetic intermediate (Fig. 4.3). This observation is consistent with the optical evidence for oxyferrous heme, which is non-paramagnetic. For the RFQ-EPR samples at pH 8.5, the resting enzyme signals around g = 6 were also absent and a signal consistent with a low-spin ferric heme species was detected in the g = 2 region during the catalase turnover interval. The new signal was broad but two partially resolved features at g =

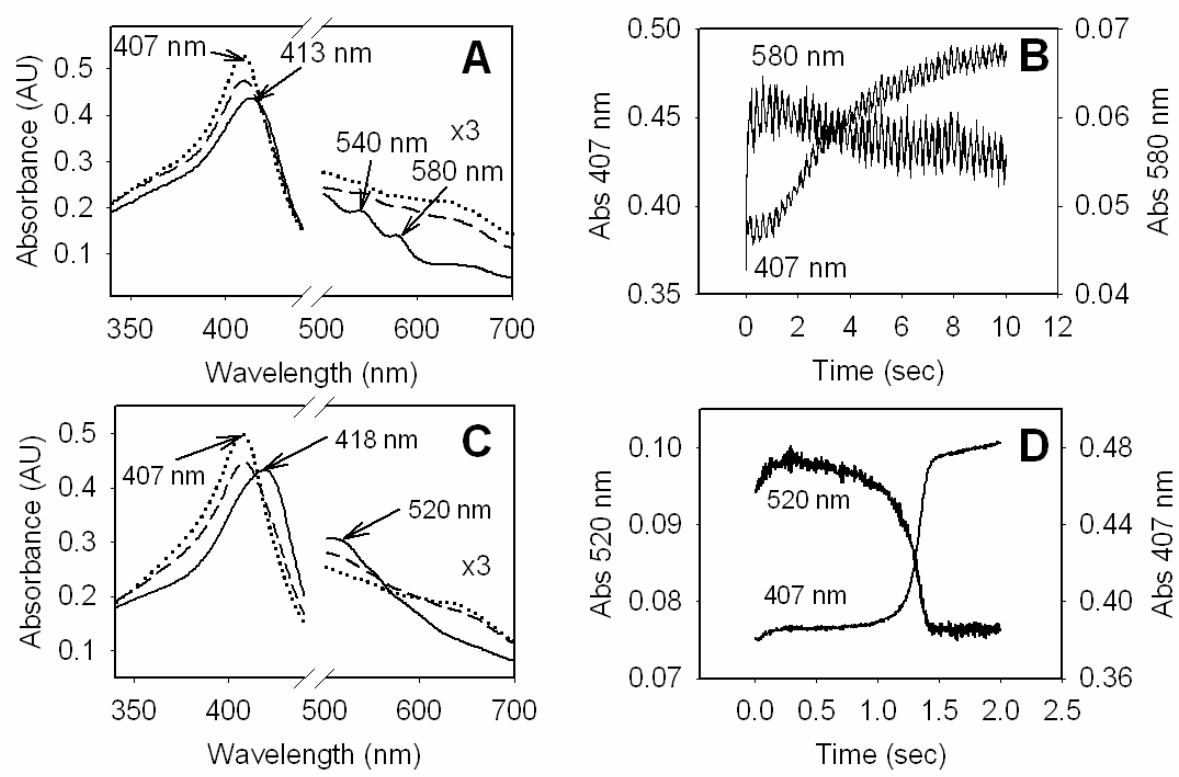

Fig. 4.2. Optical stopped-flow spectra of *M. tuberculosis* KatG reacted with H_2O_2. A) spectrum (solid line) recorded after 5 ms incubation, an intermediate spectrum (dashed line) recorded 3.5 sec after mixing, and a spectrum (dotted line) recorded 10 sec after mixing KatG with 1000-fold excess of H_2O_2 at pH 6. B) time course of the reaction followed at 407 nm and 580 nm (pH 6). C) spectrum (solid line) recorded after 1.3 ms incubation, an intermediate spectrum (dashed line) recorded 1.3 sec after mixing, and a spectrum (dotted line) recorded 2 seconds after mixing KatG with 1000-fold excess of H_2O_2 at pH 8.5. D) time course of the reaction followed at 407 nm and 520 nm. These wavelengths correspond to the Soret maximum at the start of the time course and the new maximum in the visible region of the spectrum of the steady-state species formed at pH 8.5.

2.24 and 2.15 of what could be a rhombic signal were seen. The g-values of the two features are similar to those reported for the deprotonated ferric-peroxo complex of myoglobin (134) or the peroxo-HRP complex (135). A third feature below g = 2 could not be resolved. These results indicate a change in the steady state heme species from the oxyferrous intermediate to a proposed ferric-peroxo species at alkaline pH. Note that the

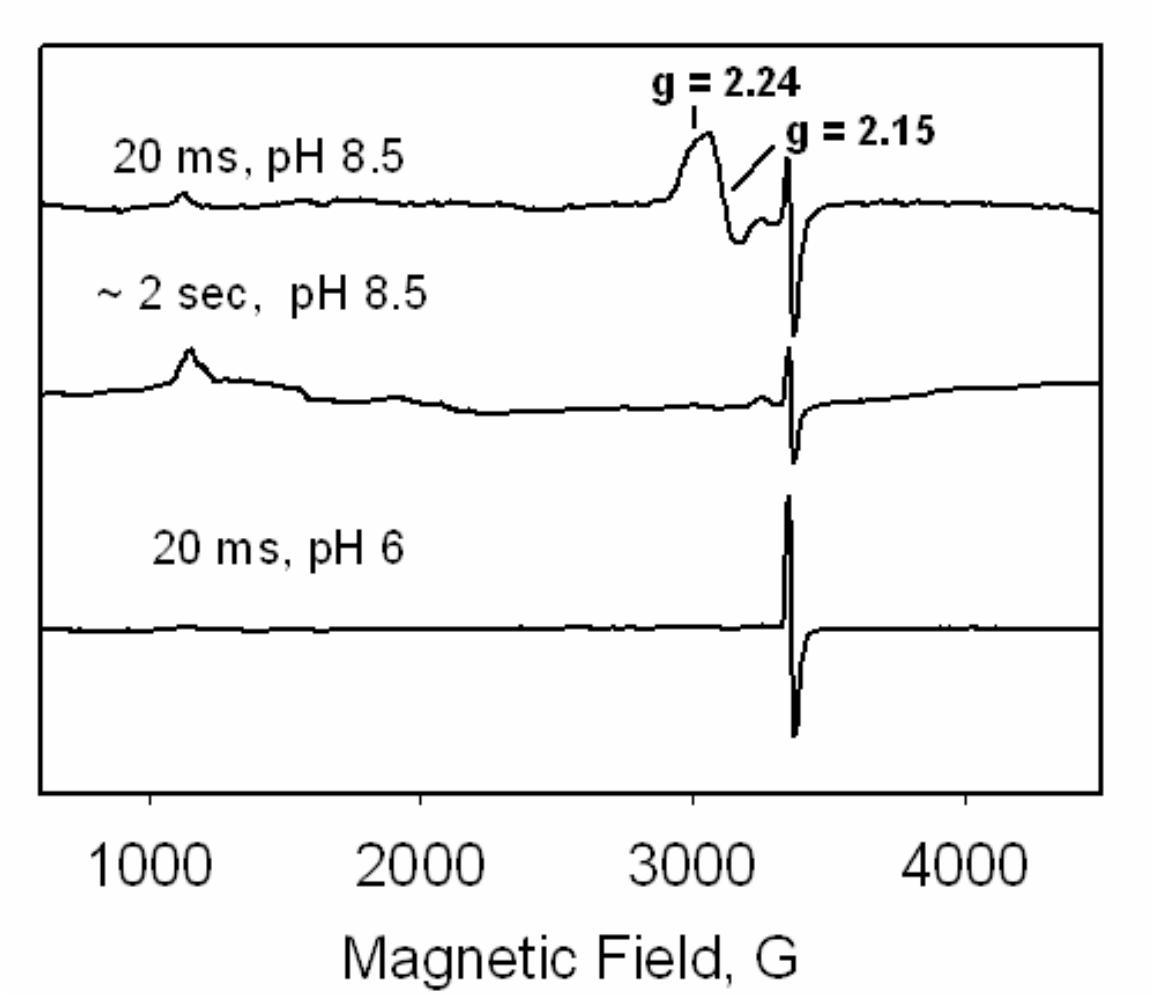

Fig. 4. 3. RFQ-EPR spectra of *M. tuberculosis* KatG reacted with 1000-fold molar excess of H_2O_2 frozen at the indicated time points. Spectra (average of 9 scans) were recorded under the following conditions: T = 4 K; microwave frequency = 9.3879 GHz; microwave power = 1 mW; modulation amplitude = 4 G; A) At pH 8.5, a ferric heme iron intermediate is present (g = 2.24, 2.15,?); B) at pH 7, the only signal present is the narrow doublet signal at g = 2.0034.

actual pH of frozen RFQ-EPR samples in phosphate buffer will be below 7 because of a decrease in pH with temperature for this buffer. This artifact does not have any impact on the narrow doublet radical signal shown in Fig. 4.1 but does remove the signal assigned to a ferric-peroxo species at alkaline pH in tris-maleate buffer (Fig. 4.3), the pH of which is more resistant to changes with temperature.

The optical spectrum of the pH 8.5 samples does not resemble that assigned to the ferric peroxo form of HRP or heme oxygenase (134,135), while the EPR data are clearly consistent with a low spin ferric peroxy heme; the intermediate formed at pH 8.5 at room temperature had been confirmed elsewhere to be a ferric species because in the presence of cyanide, a typical 6-c LS ferric complex was directly formed from it (32). A complete understanding of the identity of all species under these conditions awaits further study.

4.3. Characterization and identification of the radical in WT KatG:

Turnover of KatG with H_2O_2 is expected to generate Cmpd I (oxoferryl porphyrin π-cation radical), which in the experiments above is apparently rapidly reduced by endogenous electron transfer producing a radical on a protein site. The rate of this step is too rapid for finding Cmpd I in either the optical or the EPR data gathered here. In results published earlier, turnover of ferric *Mtb* KatG with alkyl peroxides such as PAA generated Cmpd I and also tyrosyl and tryptophanyl radicals. RFQ-EPR spectra of such samples contain wide doublet, singlet and also a narrow doublet EPR signal (70,71,73) under certain conditions. Wide doublet and singlet signals were found when the enzyme was treated with PAA alone, and a narrow doublet signal was found in the presence of isoniazid. This drug is a peroxidase substrate but is also known to quench the wide doublet radical in *Mtb* KatG (70,71,96). The narrow doublet radical had been suggested to be localized on free Y229, that is, on the tyrosine not incorporated into the MYW adduct in freshly isolated enzyme, and the wide doublet was also considered to represent a radical on this residue having a different ring orientation in the absence of bound

isoniazid (71). Here, we consider the following new interpretation of the earlier findings- the narrow and wide doublet signals may be localized on different sites and the narrow doublet only became evident when the radical giving the wide doublet was quenched by reaction with isoniazid. If this is the case, these two different radicals could be formed in tandem after Cmpd I is produced. A feature consistent with a contribution from the narrow doublet signal can be found superimposed on the wide doublet described in earlier reports (55,71) (Figure 4.4). The important observation for the current results is that a radical species giving a narrow doublet signal is suggested to be produced when ferric KatG is treated with alkyl peroxide or hydrogen peroxide, consistent with its formation from endogenous electron transfer initiated by Cmpd I. Further study is needed to confirm this idea.

Interestingly, turnover of WT KatG with excess H_2O_2 *does not* produce the wide doublet radical signal nor singlet signals seen when Cmpd I is generated by an alkyl peroxide (in the absence of H_2O_2). Also important is the observation that the narrow doublet radical does not propagate to other protein sites; for example, the initial wide doublet produced during reaction with PAA evolves to other species over a period of seconds (70,71). Thus, the species giving the narrow doublet in the presence of H_2O_2 must decay in a reaction with a redox partner that does produce the same secondary protein radicals. These results strengthen the suggestion that the narrow doublet represents an obligatory radical intermediate of the catalase reaction.

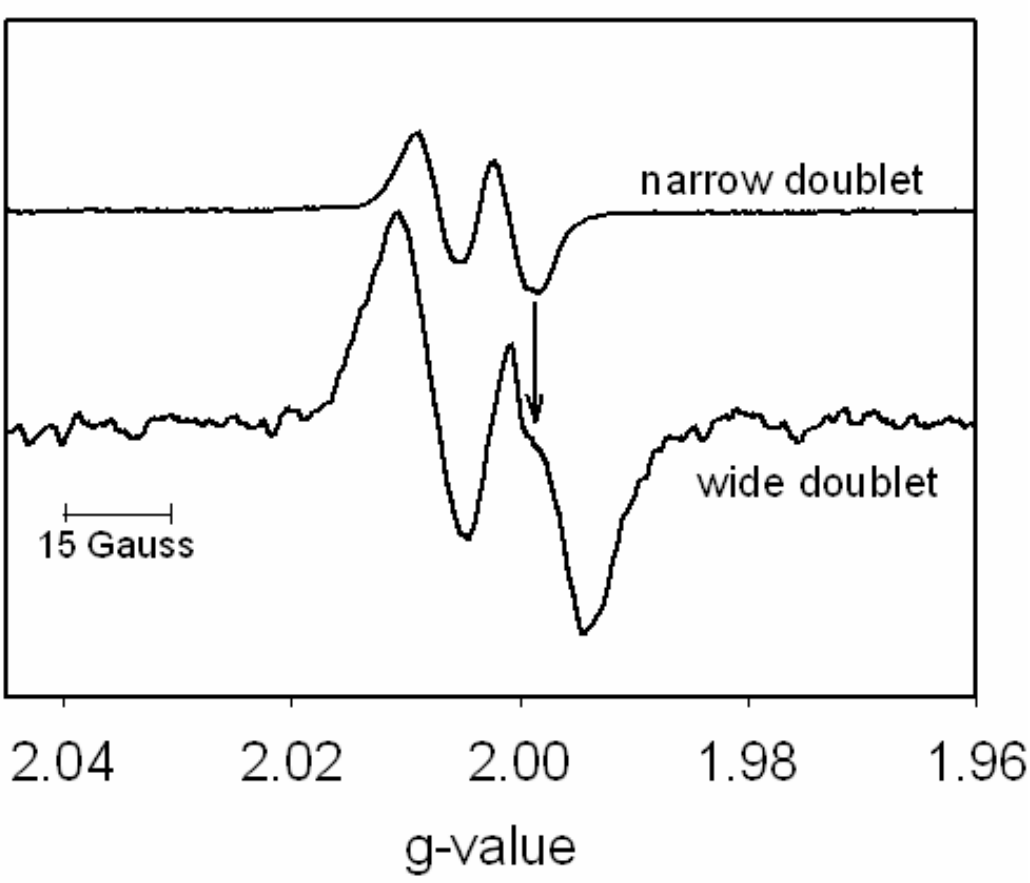

Figure 4.4. RFQ-EPR spectra of *M. tuberculosis* KatG reacted with H_2O_2 or peroxyacetic acid. Narrow Doublet: Sample frozen 20 ms after mixing ferric KatG with 1000-fold excess H_2O_2. Experimental conditions: T = 77 K, microwave frequency = 9.442 GHz, microwave power 0.1 mW, modulation amplitude 1 G; 9 scans. Wide Doublet: Sample frozen 50 ms after mixing ferric KatG with 3-fold molar excess of peroxyacetic acid; experimental conditions: T = 77 K, microwave frequency = 9.486 GHz, microwave power = 0.01 mW, modulation amplitude = 0.5 G; average of 25 scans.

4.4. EPR of distal side mutants:

Mutations in residues of the distal side MYW adduct in KatG are known to disrupt catalase activity but not peroxidase activity (55,124,129). EPR samples were prepared using KatG[Y229F], KatG[W107F] and KatG[M255A] reacted with 8000-fold excesses of H_2O_2. The narrow doublet EPR signal was not formed in any of these

reactions (at pH 8.5) (Fig.4.5). Instead, a very low yield of a singlet EPR signal was observed, as was found in similar experiments with KatG[W107F] and Y229F mutants using PAA (71). These observations are fully consistent with the suggestion that the radical species giving the narrow doublet signal in WT KatG plays a kinetically competent role for catalase turnover. The absence of catalase activity in these mutants could then be due to the loss of the radical or loss of a structural feature particular to the radical form of the WT enzyme. It is important to note that KatG[Y229F], W107F and M255A mutants form oxyenzyme in the presence of excess hydrogen peroxide just as the WT enzyme does, which means that it is not loss of this heme intermediate that is responsible for the loss in catalase function.

4.5. High field RFQ-EPR:

More complete characterization of the structure of the radical giving rise to the narrow doublet EPR signal in WT KatG was pursued using high-field RFQ-EPR spectroscopy. Here, a 4000-fold molar excess of peroxide was used to increase the yield of radical at an early time point and thereby improve the signal-to-noise in D-band experimental data. A rhombic signal with g-values similar to those of tyrosyl radicals was found for samples frozen 35 ms after mixing resting KatG with H_2O_2 (Fig. 4.6A). The principal hyperfine splitting estimated to be 11 G through simulation of the spectrum (see below) demonstrates that this signal represents the same species as that found at X-band. Also, a portion of the identical sample used for the D-band measurements was loaded into a conventional EPR tube and examined at X-band; it exhibited a narrow

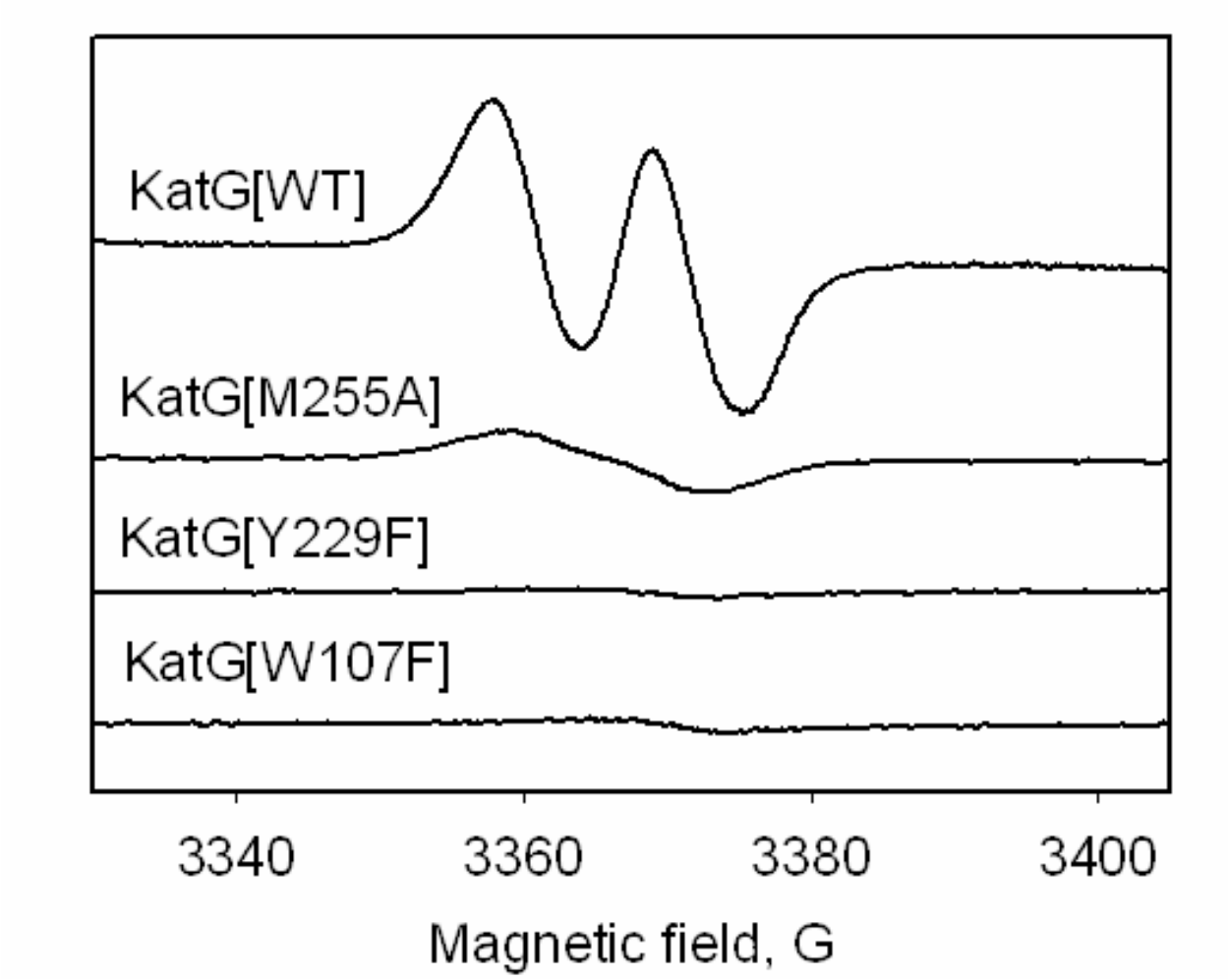

Fig. 4.5. X-Band EPR spectra of manual freeze quench samples of KatG distal side mutants treated with 8000-fold molar excess of H_2O_2 at pH = 8.5. Spectra (average of 9 scans) were recorded under the following conditions: T = 77 K, microwave frequency = 9.442 GHz; microwave power = 0.1 mW; modulation amplitude = 1 G.

doublet radical intensity equal to ~ 20 % of the heme concentration, approximately twice the yield estimated in the X-band data at 20 ms. The slow relaxation characteristics of the two-pulse echo-detected D-band EPR signal suggest that the radical site is isolated from other paramagnetic species. A similar conclusion was drawn based on the power saturation of the narrow doublet signal in X-band spectra (not shown).

Interestingly, simulation of the HF-RFQ-EPR data demonstrates that two different g_x values, equal to 2.00550 and 2.00606, and a single isotropic hyperfine splitting of ~ 11 G were required for simulating the 1:2:1 triplet feature at g_x. The apparent splitting at g_x is not due to the presence of two equivalent I = ½ hyperfine coupling interactions, which could also produce a triplet feature, because the X-band spectrum lacks the multiplicity expected if more than a single 11 G splitting were present. The principal g-values (2.00606/2.00550, 2.00344, 2.00186) obtained by simulation rule out peroxyl (136), glycyl (137,138) tryptophanyl (139-141) and thiyl radicals (142-144).

The presence of multiple g_x values has been documented in HF-EPR spectra of protein-based tyrosyl radicals in which a heterogeneous environment is present at the phenolic oxygen (145-147). The simulation shown in Fig. 4.6A was composed of nearly equal proportions of two rhombic signals differing only in the value of g_x. The proximity of the two g_x values and the similarity of the rest of the spectral features suggest that both signals likely arise from the same species in slightly different environments. The actual g_y and g_z values are quite invariant for known tyrosyl radicals and are in general equal to or larger than 2.0042 and 2.0020, which contrasts with the values here (148-152). The anisotropy of the g-matrix for the new radical signal ($g_x - g_z = 0.00420$ and 0.00364, $g_y - g_z = 0.00158$) however, is near the range typical of tyrosyl radicals ($g_x - g_z \sim 0.007$ to 0.004, $g_y - g_z = 0.002$) (153). In addition, the rhombicity of the g-matrix is similar to that expected for a tyrosyl radical, even though the isotropic g-value is slightly below that previously observed in unmodified tyrosyl radicals. Thus, an electronically modified tyrosyl-like radical is reasonably predicted by these results.

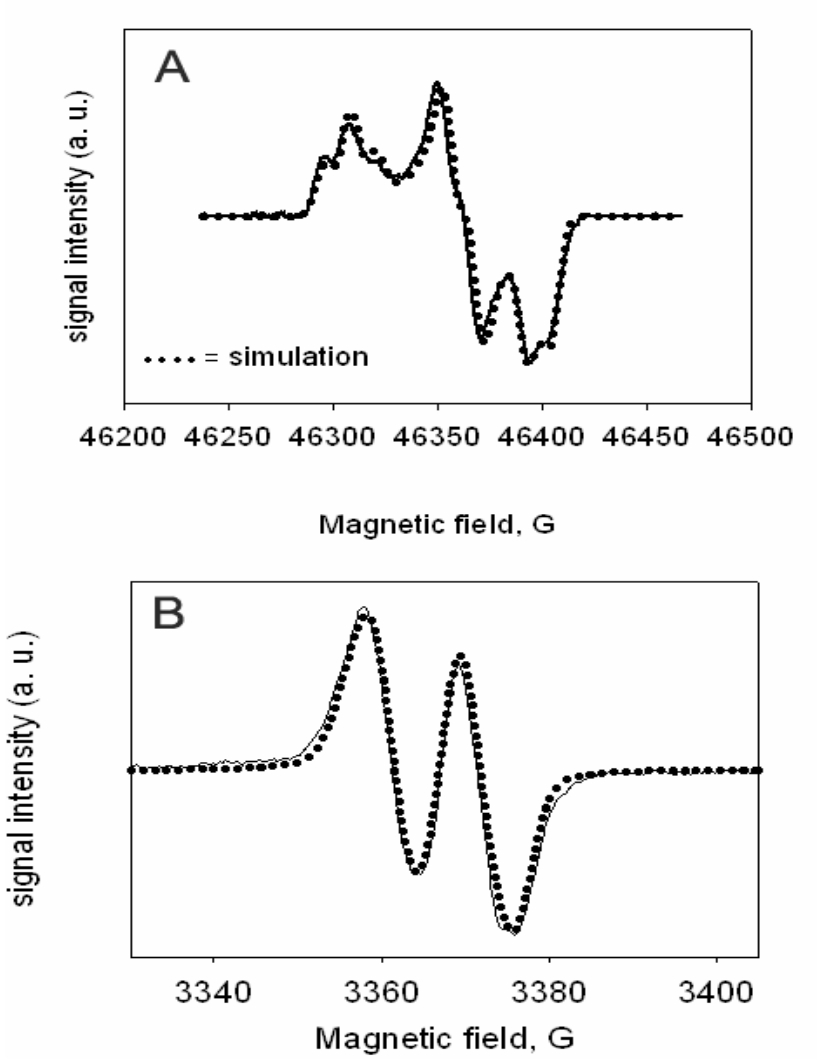

Fig. 4.6. (A) Echo-detected pseudo-modulated D-band (130 GHz) RFQ-EPR spectrum of *M. tuberculosis* KatG frozen 35 ms after mixing resting enzyme with 4000-fold molar excess of H_2O_2 at pH 8.5. Pulse widths: 40 ns and 80 ns; interpulse delay, 120 ns; temperature, 7 K; repetition rate, 10 Hz; averages per point, 30; 16 scans, total scan time 73 minutes. The overlaid simulation (*dotted line*) was generated as described in the text using the following parameters. Species 1 (59% of total simulation): g_x = 2.00606, g_y = 2.00344, g_z = 2.00186, A_x = 11.9 G; A_y = 10.3 G; A_z = 10.3 G;. Species 2 (41% of total simulation): Same parameters as Species 1 except g_x = 2.00550,. Note that the smaller (~2 G) hyperfine coupling required to fit the X-band simulation is unresolved due to inhomogeneous broadening in the D-band spectra. **(B) RFQ X-band EPR spectrum (*solid line*) of WT KatG treated with 1000-fold excess H_2O_2 at pH 8.5 frozen 20 ms after mixing.** Experimental conditions: T = 77 K, microwave frequency = 9.442 GHz; microwave power = 0.1 mW; modulation amplitude = 1 G; average of 9 scans. *Dotted line*, simulation using the following parameters: $g_{1,2,3}$ = 2.00606, 2.00344, 2.00186; $A_{iso}(1)$ = 10.5 G, $A_{iso}(2)$ = 3.2 G; line broadening = 3.6 G (avg.).

4.6. Structural information from the X-band spectrum:

Simulation of the narrow doublet spectrum could be confidently approached adopting the experimentally determined g-values in order to obtain additional hyperfine coupling information. Simulations using a single isotropic hyperfine coupling value of ~11 G to achieve the principal splitting produced a symmetrical line shape unlike that in the X-band spectrum. More satisfactory simulation was achieved by adding in a second weaker isotropic hyperfine coupling. Values of ~10.5 G and ~3.2 G gave the most satisfactory fit to the data (Fig. 4.6B). Inclusion of additional hyperfine interactions with a_{iso} values exceeding approximately 2.5 G decreased the quality of fitting to the experimental spectrum. These observations limit the number and magnitude of interactions that can contribute to the narrow doublet line shape in addition to the main splitting. Note that the X-band experimental spectrum was recorded at very low power and modulation amplitude to ensure against microwave saturation and lineshape distortions, and this spectrum is assumed to optimally indicate all the hyperfine features resolvable at this frequency. The impact on the spectra caused by the two g_x values evaluated at D-band is negligible at X-band.

The two hyperfine interactions used in simulating the X-band spectrum are tentatively assigned to the β-methylene hydrogens of a tyrosyl-like radical. This assignment is consistent with the HF-EPR results demonstrating the isotropic nature of the ~ 11 G hyperfine interactions, which is a feature of such couplings in tyrosyl radicals. Additional hyperfine splittings due to relatively strong anisotropic dipolar interactions for the 3' and 5' ring hydrogens would also be expected in the X-band spectrum if the

species were an unmodified (native) tyrosyl radical, with a_{iso} values around 6-7 G, and with the 2' and 6' hydrogens exhibiting weaker couplings of around 3 G (148,154,155). However, these interactions could not be included in the simulations without severely degrading the quality of the fits (not shown). Couplings in the 6 G range are decidedly absent from the narrow doublet spectrum as they would introduce greater multiplicity in the line. In fact, the upper limit to additional hyperfine coupling interactions was ~2.5 G as stated above. These observations suggest that couplings to ring hydrogens are less than 2.5 G, or that the ring hydrogens are absent from the radical structure.

Further insights can be gained from the isotropic hyperfine coupling values assigned to a pair of β-methylene hydrogens if the spin density in the ring of the tyrosyl-like radical could be estimated. Then a prediction can be made about the couplings expected for the ring hydrogens. A user friendly approach based on the McConnell equation designed for easy analysis of EPR spectra of tyrosyl radicals in proteins (156), which correlates hyperfine couplings with C-1 (Cγ) spin density and phenol ring plane orientation, shows that the experimental couplings of 10.5 and ~ 3.2 G (+/- 0.5) would arise for β-methylene hydrogens when a small ring orientation angle, θ occurs (Fig. 4.7) in a radical in which the spin density on C-1 is ~ 0.2. In this geometry, the weakly coupled hydrogen lies close to the plane of the ring and the strongly coupled hydrogen lies close to the p-π singly occupied orbital direction on C-1 of the phenolic ring. Since there is some error in evaluating the hyperfine couplings by simulation of the X-band spectrum, a small range of θ angles is considered possible here. For ring orientations in a range with $10 > \theta \leq 30$ °, the spin density on carbon-1 of the phenolic ring would remain close to 0.2. An alternative geometry in which θ is close to ~ 66 deg also predicts

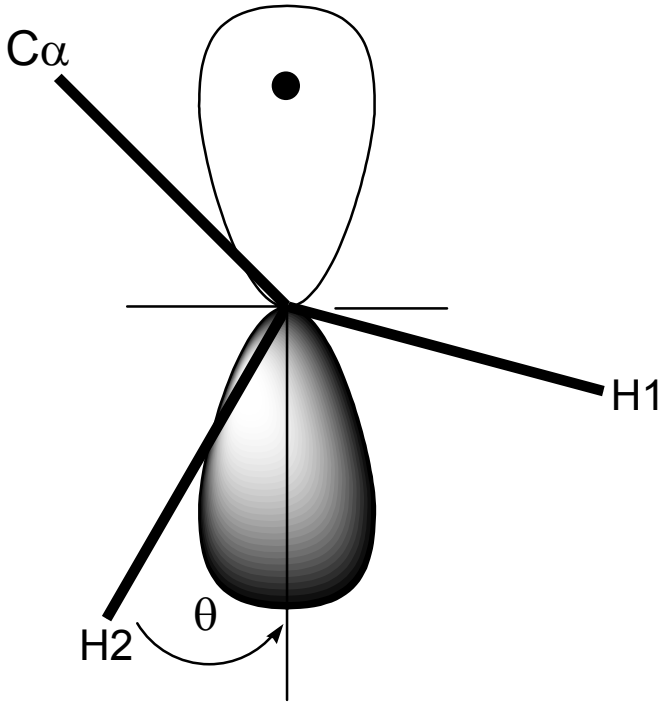

Fig. 4.7. β –methylene hydrogen orientation with respect to the unpaired electron π-orbital perpendicular to the phenol ring plane in a tyrosyl radical. The angle θ is defined for the strongly coupled hydrogen in an arrangement similar to that for Y229 in *Mtb* KatG.

hyperfine couplings near 10.5 and ~ 3.2 G, but in this case the C-1 spin density must be large (~ 0.5). For the narrow doublet signal, this high spin density rules out assignment to a native tyrosyl radical because the EPR spectrum lacks typical hyperfine splittings that would be expected for 3', 5' hydrogens and for 2', 6' hydrogens (154). Furthermore, a spin density greater than ~ 0.4 has not been observed in any tyrosyl radical reported to date nor do calculations predict densities significantly greater than that value (157). Therefore, the analysis points to the conclusion that the narrow doublet signal arises from a tyrosyl-like radical with low spin density at C-1 that may lack 3', 5' hydrogens, or a tyrosyl radical with high spin density that cannot contain ring hydrogens. In either case, the radical giving the narrow doublet EPR signal must be localized on an

electronically and/or structurally modified tyrosine residue according to both HF and X-band EPR analyses.

4.7. An MYW adduct radical?

The only structurally unusual tyrosine residue in KatG is Tyr229 linked within the distal side MYW adduct. Beyond this and upon inspection of the *Mtb* KatG crystal structure, one tyrosine residue that may also have unusual electronic properties is Y390. This residue exhibits a π-cation interaction with Arg 249 (2CCA.pdb) and also happens to have a small θ angle possibly consistent with the structural predictions above. The finding that KatG[Y390F] exhibits the same narrow doublet signal as WT KatG (Figure 4.8) rules out assignment to this residue. There are no other tyrosines in the KatG structure with small θ angles. These observations and the loss of the narrow doublet EPR signal in mutants that lack the distal side adduct (KatG [Y229F], KatG [W107F] and KatG[Met255A]) argues very strongly that this structure is either the site of the radical or is needed to produce the radical on another modified (electronically unusual) tyrosine in KatG.

A range of electronic environments for known tyrosyl radicals in proteins is usually attributed to hydrogen bonding effects at the phenolic oxygen. For example, in cases where there is relatively good hydrogen bonding, a g_x value close to 2.006 is observed while in the absence of hydrogen bonding, this value can be as large as 2.009 (148,150,156,158). Calculations illustrate that the origin of the increased g_x value in the absence of hydrogen bonding is associated with increased unpaired spin density on

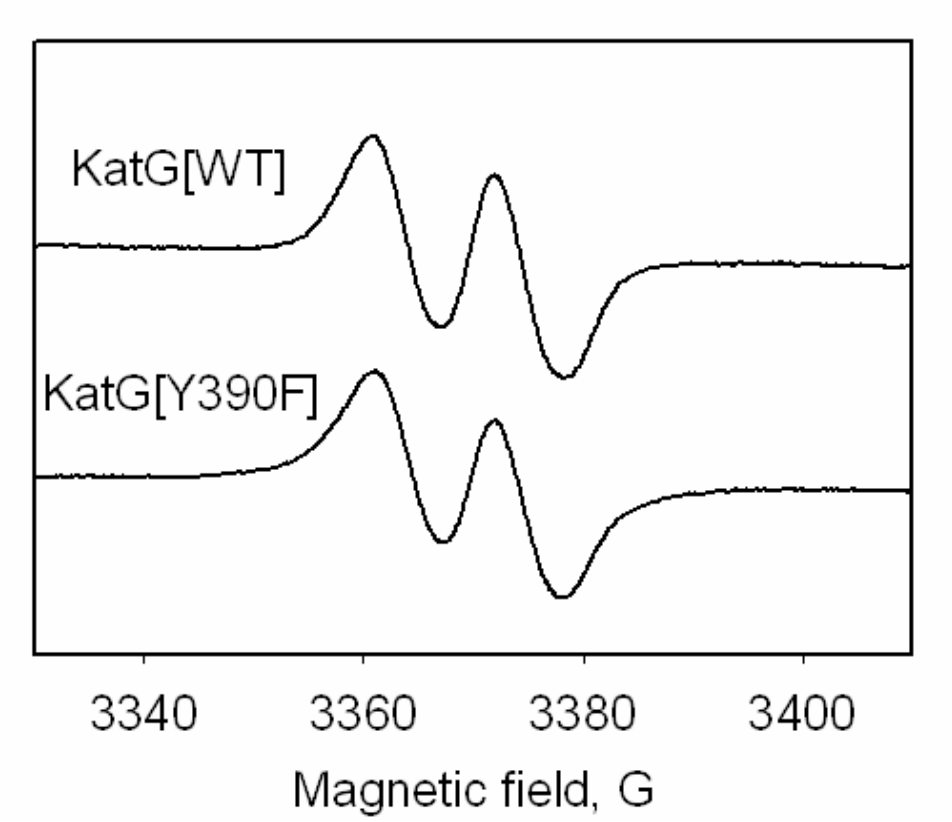

Figure 4.8. EPR spectra of manual freeze-quench samples using 8000-fold molar excess of H_2O_2. Experimental conditions: T = 77 K, microwave frequency = 9.442 GHz; microwave power = 0.1 mW; modulation amplitude = 1 G; average of 9 scans.

oxygen, which coincides with decreased unpaired spin density on C-1 of the ring (157,159). The difference in spin density at C-1, however, is on the order of only 0.03 for the limiting cases in which an isolated tyrosyl radical (no hydrogen bond) is compared to one with a strong hydrogen bonding partner (imidazole) (157). For the narrow doublet here, while the g_x value could be considered consistent with a good hydrogen bond at the phenolic oxygen of a tyrosyl-like radical (for example, the tyrosyl radical in PSII (160)), the predicted spin density at C-1 is much smaller than the typical values whether there is a polarizing interaction at the oxygen or not. Furthermore, the direction for change would be towards increased spin density in the ring with better hydrogen bonding, rather

than an unusually low spin density suggested by the results above. Therefore, a native tyrosyl radical is again ruled out as the species giving the narrow doublet.

The atypical g-values argue for some electronic effect other than hydrogen bonding that alters the spin density at C-1 in the tyrosyl-like radical. Knowledge that *Mtb* KatG treated with excess alkyl peroxide forms dimers due to di-tyrosine cross-links (see chapter 3 and (80)) opens the possibility that modified tyrosines could harbor a radical produced during catalase turnover. However, cross linking of KatG does not occur during turnover of the enzyme with excess hydrogen peroxide, ruling out dityrosine as a locus for the narrow doublet radical.

Mtb KatG contains 21 tyrosine residues. Even though all the evidence presented so far strongly suggests that the narrow doublet radical is located in an electronically or structurally modified tyrosine, the possibility of this radical being located on any of these 21 tyrosines can not be completely ruled out. In order to reduce the ambiguity with respect to the location of this radical, we decided to test for the presence of the narrow doublet signal in 21 single mutant *Mtb* KatGs where each one of the tyrosines is mutated. Due to our previous efforts to study radical formation with alkyl peroxide in KatG, the following mutants were already available for testing here: Y28F, Y95F, Y98F, Y113F, Y155S, Y197F, Y229F, Y304F, Y353F, and Y426F. The remaining 11 tyrosine mutants were prepared in this work (Y64F, Y210F, Y337F, Y339F, Y390F, Y413F, Y597F, Y608F, Y638F, Y678S, and Y711F) and were tested for their catalase and peroxidase activity and for the narrow doublet signal by EPR. The tyrosine mutant Y678F was highly unstable and no protein could be obtained. Due to the instability of Y678F we decided to generate the Y678S mutant. This mutant was also highly unstable but a small

amount of partially purified protein was obtained. This amount was enough to confirm the presence of the ND signal in this mutant enzyme treated with H_2O_2. This tyrosine is located in the carboxy terminus of the protein and its hydroxyl group seems to have key interactions with Arg693 from the same subunit and with Glu294 (through water 442) from the other subunit. These interactions might be necessary for the dimer stability in solution and would explain the high instability of the Y678F mutant. Important to note here is that this tyrosine is not conserved in other KatG enzymes ruling out a role for it in the catalase mechanism. Currently we are working on the generation of mutants other than phenylalanine in the same position to address the structural role of this tyrosine in KatG.

All of the 21 tyrosine mutants studied here have a relatively unaffected catalase activity (except for Y678S) and show the narrow doublet signal just like the wild type protein (Table 4.1). Taken all together these results further confirm our hypothesis of the location of the narrow doublet radical to tyrosine 229 in the MYW adduct.

Tyrosine residue	Catalase Activity (IU/mg)	Peroxidase Activity (IU/mg)	Narrow Doublet EPR signal
Y28F	**3191**	**0.98**	+
Y64F	**3999**	**1.75**	+
Y95F	**3582**	**1.86**	+
Y98F	**3594**	**0.73**	+
Y113F	**3895**	**2.40**	+
Y155S	**3588**	**0.93**	+
Y197F	**3268**	**0.88**	+
Y210F	**3181**	**1.23**	+
Y229F	**2.7**	**2.80**	-
Y304F	**3374**	**1.85**	+
Y337F	**3548**	**1.36**	+
Y339F	**2320**	**0.94**	+
Y353F	**3800**	**1.58**	+
Y390F	**2839**	**0.98**	+
Y413F	**3033**	**1.03**	+
Y426F	**3841**	**2.12**	+
Y597F	**2587**	**1.27**	+
Y608F	**3196**	**1.73**	+
Y638F	**3065**	**1.20**	+
Y678S	**894**	**0.29**	+
Y711F	**2357**	**1.86**	+

Table 4.1. Narrow doublet radical in tyrosine mutants in Mtb KatG

Recently reported DFT calculations for the electronic structure of Cmpd I in KatG suggested localization of a radical mainly on the MYW adduct or on the proximal Trp (W321 in *Mtb* KatG) with a fraction of the electron density located on the porphyrin. The spin density distribution was proposed to be dependent on the protonation state of the tyrosine of the MYW adduct, and/or the conformation of the nearby side chain of Arg 418 and included a radical on the proximal Trp residue in all cases (161). While it would be interesting to compare our results to these calculated predictions, especially to help understand the pH dependence of the catalase reaction, the steady state intermediates under our experimental conditions are different from Cmpd I and an entirely new

mechanism is proposed. One conclusion drawn in the calculations by Vidossich et al., (65) is that a radical should remain in proximity to the heme during the catalase reaction but may move to a new amino acid site when the catalase reaction is suppressed. This idea is in agreement with our experimental observation of only the narrow doublet radical assigned to the MYW adduct during catalase turnover and to "leakage" of this radical to remote sites found during turnover of alkyl peroxides in the absence of hydrogen peroxide. However, a shift in the redox state of the heme to Cmpd III in our model rather than a shift in the electronic properties of Cmpd I is the reason that the MYW radical does not relocate to remote sites. Evidence for a porphyrin π-cation radical and for radical formation on W321 but not on the MYW radical, under non catalytic conditions, was recently published (96). To date, no experimental evidence for a radical on the MYW adduct has been presented under any conditions. The role of Arg 418 in modulating catalytic functions of KatG as a function of pH has also been addressed elsewhere without including the possibility of an MYW adduct radical (131). The results presented here suggest that a reexamination of the structure of intermediates in catalytic functions of KatG is warranted.

4.8. Conclusions

The presence of a tyrosyl-like radical in *Mtb* KatG during catalase turnover has been demonstrated by RFQ-EPR spectroscopy. The persistence of this radical correlates with the amount of H_2O_2 present during catalase turnover and therefore it can be considered a catalytically competent species in the catalase cycle. The arguments in

favor of assignment of the observed narrow doublet radical to the MYW adduct are: 1) the g-tensor anisotropy is within the range of that expected for a tyrosyl radical, but the principal g-values deviate from known unmodified tyrosyl radicals; 2) the narrow linewidth of the signal seen at X-band is consistent with a tyrosyl-like radical having a modified electronic structure; 3) the observation that Y229F, W107F and M255A mutants do not exhibit the WT narrow doublet radical and have negligible catalase activity 4) none of the 21 tyrosine mutants lack formation of the narrow doublet signal have an essentially unaffected catalase activity .

Tyrosyl radicals have been found in the mono-functional catalases from human (162), bovine (163) and *Proteus mirabilis* (65) when treated with alkyl peroxide under conditions in which Cmpd I decays through endogenous electron transfers. No role for these radicals directly related to the dismutation of hydrogen peroxide in the catalase reaction pathway has been assigned. For KatG, since the steady-state form of the heme site during catalase turnover is oxyferrous (at neutral pH), the radical must fulfill a special redox or structural role that ensures release of dioxygen from the enzyme (see Scheme 4.1).

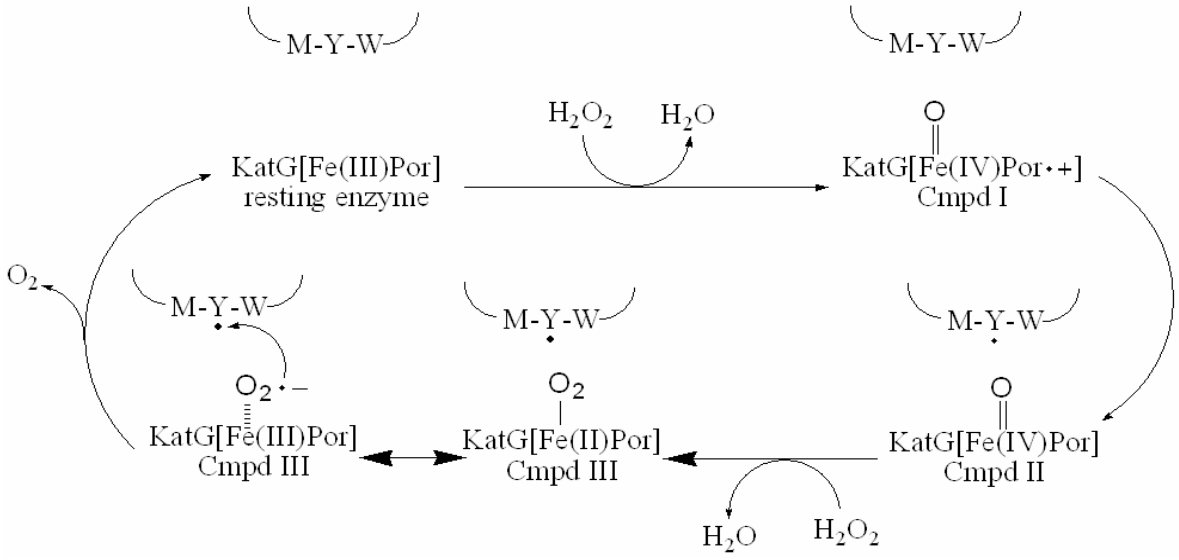

SCHEME 4.1: Proposed catalase reaction pathway.

Treatment of *Mtb* KatG with a high concentration of H_2O_2 does not produce any detectable yield of the dimers and trimers formed upon treatment with alkyl peroxide (Chapter 3). Therefore, the pathway to a surface tyrosyl radical able to produce cross links is absent during catalase turnover. This behavior is expected from the finding of *only* the narrow doublet EPR species in the presence of high H_2O_2 and is considered evidence that: 1) the radical giving the narrow doublet is *not* available for cross linking as a surface radical would be and 2) the radical does not propagate to other sites as seen upon turnover with alkyl peroxide, which ultimately leads to radical formation on residue Y353 (71,74) and others sites. The lack of formation of radicals other than the narrow doublet during catalase turnover is good evidence that it represents an obligatory intermediate of the catalase reaction and that it turns over rapidly enough such that secondary radicals do not form. In the presence of alkyl peroxide, the enzyme cycles through Cmpd I and ultimately returns to ferric enzyme. The MYW radical that must

also be formed under those conditions may be rapidly quenched by electron transfers from other amino acid sites rather than by reaction with a species involved in catalase turnover. This other species is assumed to be superoxide released from oxyferrous heme, an intermediate that is not formed in the presence of alkyl peroxide.

Based on these observations, a scheme for the catalase reaction in KatG that incorporates a radical on the MYW adduct can be drawn similar to suggestions by Jakopitsch et al. (34). The reaction is proposed to proceed via a rapid rate of formation of Cmpd I, its rapid conversion to oxoferryl heme (peroxidase Cmpd II or an isoelectronic species) simultaneous with formation of the MYW radical, followed by a rapid second reaction with hydrogen peroxide to produce oxyferrous heme, which decomposes to ferric enzyme and superoxide, and ultimately dioxygen and the closed shell MYW adduct. At alkaline pH, the reaction is rate limited upon formation of a ferric peroxo heme species (Compound 0) which is the earliest intermediate to appear. The rapid formation of Cmpd III in KatG[W107F] demonstrates that the MYW adduct is not required for the steps leading to the oxyenzyme intermediate (also true for Y229F and M255A) but the distal side structure in the absence of the adduct is partly or entirely responsible for the stabilization of this form in the mutants.

The observation of the persistence of the spectrum of oxyenzyme beyond the time interval expected to be required to consume excess hydrogen peroxide shown in Fig. 4.2B can result from the likely phenomenon that as H_2O_2 is depleted, the rate of the reaction of oxyferryl heme with peroxide assumed to generate the oxyenzyme decreases, and the intermediate that contains the unique radical species can proceed down pathways that deviate from the catalase reaction path due to extraneous electron transfers depleting

this radical in a non-catalytic step. In other words, the rate of internal electron transfers depleting the initial radical begins to outpace the rate of the second reaction with H_2O_2. Without the key radical, oxyenzyme decays too slowly to participate in catalase turnover (on the order of minutes) and this species can accumulate as the level of peroxide falls. Thus, peroxide will be used up with no apparent inhibition for nearly the entire course of catalase turnover, but the enzyme may exhibit the spectrum of the oxy form beyond the catalase turnover interval. At alkaline pH, there is no evidence for the oxyenzyme species because of changes in the rates of one or more steps and the stability of intermediates that cannot be speculated about at this time.

The MYW-O• radical provides a reasonable site for an electron transfer step to enable release of dioxygen from oxyferrous heme, which may be more accurately described as a ferric-superoxo heme complex. As the protein based MYW radical is reduced by dissociated superoxide, the heme returns to a ligand free ferric state, and a cycle is completed with the stoichiometry of peroxide dismutation the same as in the classical monofunctional enzymes. Furthermore, the non-scrambling formation of dioxygen (125) is also explained as both atoms of released dioxygen come from a species in which two oxygen atoms are bound. The outlined mechanism does not invoke any heme intermediates not already recognized in peroxidase catalytic pathways but does not yet account for the proton inventory of the reactions.

One mechanistically critical feature in the Scheme is that electron transfer from superoxide to tyrosyl radical is a reasonable process according to a recent report in which this and other possibilities, such as addition of superoxide to the phenolic ring of tyrosyl radicals, is described (164) Thus, Tyr229 in the MYW adduct of KatG can serve the

function of catalyzing oxygen formation from superoxide dissociating from oxyenzyme during the catalase reaction but importantly, the ring is protected from covalent modification by superoxide because of its incorporation into the MYW adduct.

Chapter 5. Achievements and future research plans

The main focus of my thesis research was the understanding of the origin of antibiotic resistance caused by mutations in *Mtb* KatG and the determination of the location of sites of aminoacid based radicals in this protein. As is usual for this kind of research, several other issues mainly concerning the catalytic mechanisms and some interesting structural features of this enzyme arose as my research project evolved. In summary, the main accomplishments made during my four years of research are the following:

1.- Detailed characterization of the drug resistance mutant KatG[S315G]. This study provided a comprehensive explanation for the low level of drug resistance (8μg/ml) conferred by this mutation. The main conclusion of this research is that a peroxidase cycle "bypass" and a low reactivity of Cmpd I towards INH is responsible for the reduced level of drug activation observed in this mutant.

2.- Study of cyanide binding to WT KatG and several mutants at position 315. This study led to the conclusion that cyanide binds preferably to 6-c heme over 5-c heme. Interesting corollaries about the aging transition from 5-c to 6-c heme in KatG are discussed. (This study is not included here but I contributed to a published paper, "Impact of distal side water and residue 315 on ligand binding to ferric Mycobacterium tuberculosis catalase-peroxidase (KatG)" listed below).

3.- Crosslink formation and identification of sites of radical formation in KatG. During this study several tyrosine and tryptophan mutants were produced and analyzed by RFQ-EPR in an effort to identify possible sites for radical formation. Also crosslink formation upon treatment of KatG with alkyl peroxide and hydrogen peroxide was assessed. The main conclusions from this study are that KatG is able to form protein-protein covalent crosslinks when exposed to peroxide under conditions that disfavor catalase turnover and that there are more radical forming residues in the surface of KatG besides Y353.

4.- The discovery of a new uncharacterized amino acid based radical present only during catalase turnover. The main conclusion from this study is that this radical is localized on the MYW adduct on the distal side of the protein and that this radical is necessary for the catalase activity of the protein through "quenching" of superoxide coming from an oxyferrous intermediate. A new catalytic cycle involving this radical is proposed.

As a result of these five years of research, six papers have been published:

1. Ranguelova, K., Girotto, S., Gerfen, G. J., Yu, S., Suarez, J., Metlitsky, L., and Magliozzo, R. S. (2007) Radical sites in Mycobacterium tuberculosis KatG identified using electron paramagnetic resonance spectroscopy, the three-dimensional crystal structure, and electron transfer couplings, *J. Biol. Chem.* ***282*****,** 6255-6264.
2. Ranguelova, K., Suarez, J., Magliozzo, R. S., and Mason, R. P. (2008) Spin trapping investigation of peroxide- and isoniazid-induced radicals in Mycobacterium tuberculosis catalase-peroxidase, *Biochemistry* ***47***, 11377-11385.
3. Ranguelova, K., Suarez, J., Metlitsky, L., Yu, S., Brejt, S. Z., Brejt, S. Z., Zhao, L., Schelvis, J. P., and Magliozzo, R. S. (2008) Impact of distal side water and residue 315 on ligand binding to ferric Mycobacterium tuberculosis catalase-peroxidase (KatG), *Biochemistry* ***47*****,** 12583-12592.
4. Zhao, X., Yu, S., Ranguelova, K., Suarez, J., Metlitsky, L., Schelvis, J. P., and Magliozzo, R. S. (2009) Role of the Oxyferrous Heme Intermediate and Distal Side Adduct Radical in the Catalase Activity of Mycobacterium tuberculosis KatG Revealed by the W107F Mutant, *J. Biol. Chem.* ***284***, 7030-7037.

5. Suarez, J., Ranguelova, K., Jarzecki, A. A., Manzerova, J., Krymov, V., Zhao, X., Yu, S., Metlitsky, L., Gerfen, G. J., and Magliozzo, R. S. (2009) An Oxyferrous Heme/Protein-based Radical Intermediate Is Catalytically Competent in the Catalase Reaction of Mycobacterium tuberculosis Catalase-Peroxidase (KatG), *J. Biol. Chem.* ***284*****,** 7017-7029.
6. Suarez, J., Ranguelova, K., Schelvis, J. P., and Magliozzo, R. S. (2009) Antibiotic Resistance in Mycobacterium tuberculosis: Peroxidase Intermidiate Bypass Causes Poor Isoniasid Activation by the S315G Mutant of *M. tuberculosis* Catalase-Peroxidase (KatG), *J. Biol. Chem.* ***284*****,** 16146-16155.

The results and conclusions obtained from this research revealed some new (unknown) features of the catalytic cycle of KatG and lead us to suggest a future research plan that will address these new issues:

1. The study of the catalytic activity and binding of iron-binding ligands to the KatG S315G mutant revealed several features that suggest a more "flexible" heme pocket probably due to the lack of hydrogen bonding between the glycine residue and the heme propionate on pyrrole IV. Our next step in this study will be to solve the crystal structure of this mutant enzyme which should reveal structural differences with respect to the WT protein that will help explain/confirm ideas about the unusual catalytic behavior of this mutant. Also, we plan to continue making drug resistant mutants of KatG in an effort to understand how the structural changes imposed by these mutations confer isoniazid resistance. Our next mutant will be W300G which is a recently published drug resistant mutant that confers high level of isoniazid resistance (~128 μg/ml).

2. The two major conclusions from the study of cross-linking in *Mtb* KatG were that KatG forms protein-protein crosslinks upon treatment with peroxide and that there are

more site/sites of radical formation on the surface of KatG besides Y353. In order to determine the location of these sites of crosslink formation we suggest that a trypsin digestion of the crosslinked protein followed by a separation of the resulting peptides by HPLC with a fluorescence detector (which will allow the identification of the crosslinked peptides) and a sequence analysis of the crosslinked peptides by mass spec will allow us to identify the residues involved in the crosslink/radical formation at the surface of KatG. This will prove the location of the tyrosyl radicals involved in the crosslink formation.

Future analysis of the mechanism of turnover of organic substrates by KatG in the presence of alkyl peroxides may confirm a role for surface tyrosyl radicals. Therefore, identification of these residues is considered important.

3. Based on the newly proposed catalase cycle in KatG, several new ideas arise that suggest that a reexamination of previous results is warranted. As an immediate goal, we would like to confirm the location of the new narrow doublet (ND) radical to the MYW adduct, more specifically to Y229. Also we want to prove that the hypothesis that the accumulation of Cmpd III during the catalase cycle is due to the "leakage" of the MYW radical to other sites under conditions of low concentration of H_2O_2. To prove this idea we plan to do several studies of the accumulation of Cmpd III at the "tail end" of the turnover of H_2O_2, when the hydrogen peroxide concentration is reduced and the MYW radical can migrate to other sites. Finally, we want to do a detailed characterization of the R418L mutant (catalase deficient mutant) to understand the role of this residue (which has been proposed to hydrogen bond to Y229) on the catalase cycle.

Appendix A

Experimental procedures

Chapter 2. Antibiotic resistance in *M. tuberculosis*: Peroxidase intermediate bypass causes poor isoniazid activation by the Ser315Gly mutant of *Mtb* catalase-peroxidase (KatG)

All standard chemicals and reagents were obtained from Sigma-Aldrich. INH was re-crystallized from methanol before use. PAA (32%) was diluted to 10 mM in potassium phosphate buffer and was incubated with 780 units/ml bovine catalase (Roche) for 3 h at 37 °C to degrade hydrogen peroxide. After treatment, catalase was removed by ultrafiltration.

The plasmid pKAT II was used as an overexpression vector for KatG (165) as well as a mutagenesis template. *E. coli* strain UM262 (166) was used for overexpression. UM262 and pKAT II were both gifts from Stewart Cole (Ecoles Polytechniques Fédérales de Lausanne). Mutagenesis was performed using the QuickChange II site-directed mutagenesis kit from Stratagene (La Jolla, CA). The pairs of complementary primers (synthesized and purified by Operon Biotechnologies, Inc.) were designed to introduce the S315G mutation. The oligonucleotide pairs (mutated codons are in bold) were: 5'-^{925}GGTAAGGACGCGATCACC**GGC**CGGCATCGAGGTCG^{958}-3' and 5'-^{958}CGACCTCGATGCC**GCC**GGTGATCGCGTCCTTACC^{925}-3'. Mutagenesis was performed according to the manufacturer's protocol and the reaction products were

transformed into the *E. coli* XL1-Blue strain for selection purposes. The presence of the mutated 315 codon in the *katG* gene was confirmed by DNA sequencing (Gene Wiz, Inc.) and the mutated plasmid was electroporated into *E. coli* strain UM262 for protein overexpression. Recombinant KatG[S315G] was purified as previously described for WT KatG (73), in potassium phosphate buffer, pH 7.2. The pure enzyme had an optical purity ratio (A_{405}/A_{280}) of ~ 0.45. The proportion of heme deficient enzyme, which is catalytically active, represented more than half of the total overexpressed enzyme isolated in these experiments. In the case of WT KatG, only a small percentage of total enzyme is found as a heme deficient dimer (73). However, the overexpression conditions are such that polypeptide synthesis outpaces the availability of heme despite supplementation of the medium with the heme precursor δ-ALA. The unknown conditions in *Mtb* carrying KatG[S315G] precludes commenting on the physiological significance of these observations. Here, we have focused only on the properties of the holoenzymes.

Protein concentration was determined using a heme extinction coefficient of approximately 85 mM^{-1} cm^{-1} at 405 nm for the mutant enzyme and 100 mM^{-1} for WT KatG. Catalase and peroxidase activities were determined at 25 °C according to published procedures (83,167) in 20 mM potassium phosphate buffer, pH 7.2 and 50 mM sodium acetate buffer, pH 5.5 respectively. Spectrophotometric measurements were obtained using an NT14 UV-Vis spectrophotometer interfaced to a personal computer (Aviv Associates).

A rapid scanning diode array stopped-flow apparatus (HiTech Scientific Model SF-61DX2) was used for kinetics measurements. Data acquisition and analyses were performed using the Kinet-Asyst software package (HiTech Scientific). All reactions

were carried out at 25 °C in potassium phosphate buffer at pH 7.2. The change in absorbance in the Soret region for the resting enzyme reacted with varying concentrations of PAA was followed for 2 sec and data at selected wavelengths were fit to a single exponential decay function. Observed rates (k_{obs}) were used to calculate second-order rate constants for Cmpd I formation from the plot of k_{obs} vs. PAA concentration. Double-mixing stopped-flow experiments were performed as previously reported (49,73) to follow the reaction of Cmpd I, pre-formed with a small excess of PAA, with INH or PAA as a reducing substrate added in the second mixing step.

The interaction of INH with ferric KatG was analyzed using optical difference spectroscopy in the Soret region similar to published procedures (84,89). The change in the difference in absorbance evaluated between 378 nm and 411 nm was plotted against free isoniazid concentration for titrations conducted at 25 °C in 20 mM phosphate buffer (pH = 7.2). Data were fit to a single site saturation curve using Sigma Plot 8.0 software.

Isothermal titration calorimetry was performed using a MicroCal VP ITC calorimeter. Data analysis was performed using ORIGIN software supplied with the instrument. KatG[S315G] and titrant (INH) solutions were prepared in the same 20 mM potassium phosphate buffer, pH 7.2 to ensure minimal background from buffer mismatch. Reliable titration data were obtained using 20 μM enzyme in the sample cell (1.4 ml) and an INH concentration in the ligand delivery syringe that gave an INH-to-heme ratio of approximately 0.15:1 per injection. A total of 16 injections (10 μl per injection) were made at 10-min intervals because of a very slow equilibration period, and the heat of reaction per injection (microcalories per second) was determined by integration of the peak areas. The software provided the best-fit values for ΔH, ΔS, the stoichiometry of

binding (n) per mole of heme, and the dissociation constant (K_d) from plots of heat evolved per mole of substrate injected *vs.* the drug/heme molar ratio. (ITC titrations of KatG with INH and other hydrazide ligands may overestimate the affinity based on heat released because of background reactions (89)).

IN-NAD formation: The rate of IN-NAD adduct generation catalyzed by KatG[S315G] was examined in a spectrophotometric assay as a function of INH concentration according to a previously published method (59). In this method, KatG (0.5 μM), NAD^+ (50 μM), GOx (10 milliunits/mL), and glucose (5 mM) were incubated in the presence of varying amounts of INH (10, 20, 30, 50, 100 250, 500, 1000 and 2000 μM) and the increase in absorbance at 326 nm due IN-NAD adduct ($\varepsilon_{326\ nm}$ = 6900 M^{-1} cm^{-1}) (71) was recorded for 20 min. The reference cuvette contained all components except NAD^+ to correct for background.

EPR spectroscopy: X-band EPR spectra were recorded using a Bruker E500 EPR spectrometer with data acquisition and manipulation performed using *XeprView* and *WinEPR* software (Bruker). Low temperature spectra were recorded using an Oxford Spectrostat continuous-flow cryostat and ITC503 temperature controller. The spectra of KatG[S315G] (100 μM) were recorded at 4 K in 20 mM potassium phosphate buffer, pH = 7.2. Experimental parameters are given in figure legends.

RFQ-EPR: The RFQ-EPR samples (aerobic) were prepared using an Update Instrument, Inc. Model 1000 chemical-freeze-quench apparatus as described previously

(70). Solutions of enzyme (typically 100 μM heme) and peroxyacetic acid (300 μM) in 20 mM potassium phosphate buffer, pH 7.2, were mixed in a 1:1 ratio, and the mixture was incubated for the indicated time periods followed by freeze-quenching in isopentane at ~130 °C. PAA solutions were freshly prepared before each experiment from H_2O_2-free stock solutions stored at 80 °C. EPR samples were maintained in liquid nitrogen after removal of isopentane and spectra were recorded at 77 K using a finger Dewar held in the EPR cavity. Samples were also prepared anaerobically by thoroughly degassing enzyme and peroxide solutions and filling syringes for the apparatus under continuous argon purging.

Chapter 3. Protein Crosslinks in *M. tuberculosis* catalase-peroxidase KatG.

All standard chemicals and reagents were obtained from Sigma-Aldrich. Commercial PAA was diluted to 10 mM in potassium phosphate buffer and was incubated with 780 units/ml catalase (Roche) for 3 h at 37 °C to degrade hydrogen peroxide. After treatment, catalase was removed by ultrafiltration and the peroxide was stored in small aliquots at -80 °C.

Construction, expression, and purification of the WT and mutant KatG enzymes: The plasmid pKAT II was used as an overexpression vector for KatG (165) as well as a mutagenesis template. *E. coli* strain UM262 (166) was used for overexpression. UM262 and pKAT II were both gifts from Stewart Cole (Institut Pasteur, Paris). Mutagenesis was performed using the QuickChange II site-directed mutagenesis kit from Stratagene

(La Jolla, CA). The pairs of complementary primers (synthesized and purified by Operon Biotechnologies, Inc.) were designed to introduce the following mutations (mutated codons are in bold): **(Y28F)** 5' GGTCATATGAAA**TTC**CCCGTCGAGGGCGGC 3' and 5' CCAGTATACTTT**AAG**GGGCAGCTCCCGCCG 3'. **(Y197F)** 5' GAG CCCGATGAGGTC**TTT**TGGGGCAAGGAAGCC 3' and 5' GGCTTCCTTGCCCCA**AAA**GACCTCATCGGGCTC 3'. **(W204E)** 5' CAAGGAAGCCACC**GAG**CTCGGCGATGAG 3' and 5' CTCATCGCCGAG**CTC**GGTGGCTTCCTTG 3'. **(Y304F)** 5' CTGGAAGAGCTCG**TTT**GGCACCGGAACC 3' and 5' GGTTCCGGTGCC**AAA**CGAGCTCTTCCAG 3'. Mutagenesis was performed according to the manufacturer's protocol and the reaction products were transformed into the *E. coli* XL1-Blue strain for selection purposes. The presence of the mutated codons in the *katG* gene was confirmed by DNA sequencing (Gene Wiz, Inc.) and the mutated plasmid was electroporated into *E. coli* strain UM262 for protein overexpression. Recombinant WT KatG and mutants were purified as previously described (73), in potassium phosphate buffer, pH 7.2. The pure enzymes had an optical purity ratio (A_{405}/A_{280}) of ~ 0.45 – 0.5.

Enzyme assays: Protein concentration was determined using a heme extinction coefficient of 100 mM^{-1} cm^{-1} at 405 nm (73). Catalase and peroxidase activities were determined at 25 °C according to published procedures (83,167) in 20 mM phosphate buffer at pH 7.2 and 50 mM sodium acetate buffer at pH 5.5 respectively.

Spectrophotometric measurements were obtained using an NT14 UV-Vis spectrophotometer interfaced to a personal computer (Aviv Associates).

Crosslink formation reactions (PAA and H_2O_2) and SDS and native PAGE: Crosslink formation experiments were carried out by reacting 10 μM WT KatG with H_2O_2, or t-butyl peroxide in varying concentrations for 15 minutes (PAA, room temperature) or for 1 hour at 37 °C for t-butyl peroxide. Alternatively, reactions were performed under conditions generating a slow flux of H_2O_2 using Glucose/Glucose oxidase; a mixture of 10 μM KatG, 10mM glucose, and 2 or 4 U/ml glucose oxidase was incubated at 37 °C for an hour. All the reactions were stopped by the addition of electrophoresis loading buffer containing SDS and β-mercaptoethanol followed by boiling for 2 min. Gel electrophoresis was carried out under denaturing (SDS-PAGE) and non-denaturing (native PAGE) conditions using an Amersham Biosciences PhastGel system. Gels were stained with Coomassie blue.

Concentration dependence of crosslink formation (intra vs. intermolecular crosslinks): Crosslink formation reactions with PAA under the same conditions described above were performed using KatG concentrations equal to 10, 20, 40, and 80 μM. Reactions were stopped and products were loaded onto SDS gels as described above.

Fluorescence spectrum of KatG: Fluorescence measurements of untreated KatG and KatG treated with 40 fold excess PAA were carried out using a Spex Fluorolog Tau 2 fluorimeter (SPEX-Horiba Instruments, Inc., New Jersey) at room temperature using an excitation wavelength of 315 nm. Using standard right-angle emission optics,

fluorescence intensity measurements were recorded using photon counting mode and corrected for any fluctuations of the 450-watt Xenon lamp source by deflecting a portion of the excitation signal onto a separate photodiode. The measured intensity signals are thus reported in the ratio mode (S/R) as counts per second (S) measured on the emission photomultiplier over the photodiode current (R). Measurements were performed using quartz fluorescence cuvettes with path lengths of 10 mm. These experiments were performed at Professor Lesley Davenport's lab with the assistance of Dr. Yasemin Kopkalli.

Isolation and activity determination of higher molecular weight products: Gel filtration chromatography (Superdex200) was performed to separate the higher molecular weight products formed during peroxide treatment from the native protein; in 20 mM KPI with a flow rate of 1 ml/min. Fractions containing the native and crosslinked protein were concentrated trough amicon column filtration. Catalase and peroxidase activities were measured as described above.

Chapter 4. An oxyferrous heme/protein-based radical intermediate is catalytically competent in the catalase reaction of *M. tuberculosis* catalase-peroxidase (KatG)

M. tuberculosis KatG was prepared from an overexpression system in *E. coli* strain UM262 as previously published (167) and was used usually within a few days of preparation. Mutagenesis was performed using the QuickChange II site-directed

mutagenesis kit from Stratagene (La Jolla, CA). Pairs of complementary primers (synthesized and purified by Operon Biotechnologies, Inc.) were designed to introduce the required mutations. The oligonucleotide pairs (mutated codons are in bold) were: (Y390F) 5'-^{1153}CGGGTGGATCCGATC**TTT**GAGCGGATCACGCGTC^{1186}-3' and 5'-^{1186}GACGCGTGATCCGCTC**AAA**GATCGGATCCACCCG^{1153}-3' (55); (Y64F) 5'-^{192}GTGCGGCGTTCGAC**TTT**GCCGCGGAGGTCGC^{223}-3' and 5'-^{223}GCGACCTCCGCGGC**AAA**GTCGAACGCCGCAC^{192}-3'; (Y210F) 5'-^{630}CGGCGATGAGCGT**TTC**AGCGGTAAGCGGG^{659}-3' and 5'-^{659}CCCGCTTACCGCT**GAA**ACGCTCATCGCCG^{630}-3'; (Y337) 5'-^{1011}CTCGAGATCCTG**TTC**GGCTACGAGTGGGAG^{1041}-3' and 5'-^{1041}GAGCTCTAGGAC**AAG**CCGATGCTCACCCTC^{1011}-3'; (Y339F) 5'-^{1017}GATCCTGTACGGC**TTC**GAGTGGGAGCTGAC^{1047}-3' and 5'-^{1047}GTCAGCTCCCACTC**GAA**GCCGTACAGGATC^{1017}-3'; (Y413F) 5'-^{1239}CGCCAAGGCCTGG**TTC**AAGCTGATCCACCG^{1269}-3' and ^{1269}GCGGTTCCGGACC**AAG**TTCGACTAGGTGGC^{1239}-3'; (Y597F) 5'-^{1791}GATGGCTTCCGAAAC**TTC**CTCGGAAAGGGCAAC^{1824}-3' and 5'-^{1824}GTTGCCCTTTCCGAG**GAA**GTTTCGGAAGCCATC^{1791}-3'; (Y608F) 5'-^{1824}CGTTGCCGGCCGAG**TTC**ATGCTGCTCGACAAG^{1856}-3' and 5'-^{1856}CTTGTCGAGCAGCAT**GAA**CTCGGCCGGCAACG^{1824}-3'; (Y638F) 5'-^{1914}CCTCGGCGCAAAC**TTC**AAGCGCTTACCGC^{1943}3' and 5'-^{1943}GCGGTAAGCGCTT**GAA**GTTTGCGCCGAGG^{1914}-3'; (Y678F) 5'-^{2034}CAGATGACGGGACCT**TCC**AGGGCAAGGATGG^{2065}-3' and 5'-^{2065}CCATCCTTGCCCTGG**AAG**GTCCCGTCATCTG^{2034}-3'; (M255A) 5'-

^{748}GAGACGTTTCGGCGC**GCG**GCCATGAACGACGTC^{780}-3' and 5'-^{780}GACGTCGTTCATGGC**CGC**GCGCCGAAACGTCTC^{748}-3'. Mutagenesis was performed according to the manufacturer's protocol and the reaction products were transformed into the *E. coli* XL1-Blue strain for selection purposes. The presence of the mutated codons in the *katG* gene was confirmed by DNA sequencing (Gene Wiz, Inc.) and the mutated plasmid was electroporated into *E. coli* strain UM262 for protein overexpression. The mutants Y229F and W107F were prepared as previously reported (55,71).

The catalase activity of purified KatG enzymes was evaluated optically based on the disappearance of absorbance due to H_2O_2, at pH 6 or 7 in 20 mM potassium phosphate buffer or in 20 mM sodium borate buffer pH 8.5 according to published procedures (168). No direct comparison is presented for the rate of catalase turnover measured optically and the intensity changes in RFQ-EPR measurements (described below) under identical conditions because of the large difference in sensitivity of the two techniques; high enzyme concentration is needed for detection of the radical in EPR spectra while such conditions produce bubbling in solutions that strongly interferes with absorbance measurements.

RFQ-EPR methodology has been published elsewhere (70,71,74); briefly, enzyme and peroxide solutions are mixed at room temperature in a 1:1 ratio and the mixture is sprayed into a funnel attached to an EPR tube immersed in an isopentane bath held at approximately -130 °C. The frozen powder is packed into precision bore EPR tubes and the packed sample, which retains isopentane, is frozen in liquid nitrogen. For quantitative EPR, signal intensity is based on a copper standard and the total intensity for

RFQ samples is multiplied by 2 to correct for isopentane dilution. The foaming of solutions due to the rapid evolution of dioxygen leads to further dilution by an additional variable amount around 2-fold, but no further correction of EPR signal intensity was made. In some cases (like for the data in figure 4.8), manually-mixed samples were prepared in borate buffer pH 8.5 by mixing protein solution (~100 μM) with an 8000-fold molar excess of H_2O_2, loading the mixture into precision bore EPR tubes and immediately immersing the tube in liquid nitrogen. EPR spectra were recorded on a Bruker E500 ElexSys X-band spectrometer with samples held either in a finger Dewar for spectra at 77 K or in an Oxford liquid helium cryostat for lower temperatures. Signal averaging was employed to improve the signal to noise ratio when needed. Simulation of X-band EPR spectra was performed using SimFonia software (Bruker). Optical stopped-flow spectroscopy was performed using a HiTech 16-DX instrument as described elsewhere (49,55,73) in the buffers listed above.

Crosslink formation: To rule out the formation of dityrosine cross links during catalase turnover, 10 μM WT KatG was incubated with 1000-fold to 8000-fold molar excess of H_2O_2 for 15 minutes at room temperature. SDS-PAGE of KatG from these samples was carried out using an Amersham Biosciences PhastGel system.

High Field-EPR D-band (130 GHz): EPR spectra were obtained using a spectrometer assembled at the Albert Einstein College of Medicine, Bronx, NY, that uses a quadrature detection bridge (100 mW pulsed output) and probe supplied by HF EPR Instruments, Inc. (V. Krymov, New York). Cylindrical resonators operating in the TE_{011} mode

provide typical π/2 pulse widths of 30-50 ns at maximum bridge power. The magnetic field is generated by a specially designed 7 Tesla superconducting magnet with a +/- 0.5 Tesla superconducting sweep/active shielding coil (Magnex Scientific). Frozen RFQ samples were held in quartz capillary tubes with inner and outer diameters of 0.5 mm and 0.6 mm, respectively, and an active volume of 0.2 μL. The frozen sample tubes were loaded into the probe under liquid nitrogen and inserted into the low temperature continuous flow cryostat (Oxford Instruments, Spectrostat Model 86) and were maintained at 7 K to an accuracy of approximately +/- 0.3 K using an ITC503 temperature controller. The magnetic field was calibrated to an accuracy of ~ 2 G using a sample of Mn-doped MgO (169). Field swept-two pulse (Hahn)-echo detected spectra were obtained with 180 degree phase cycling of the first pulse to provide suppression of baseline artifacts. Specific experimental parameters are given in the figure legends.

HF EPR spectra were simulated using software described previously (144,170). The hyperfine interactions were treated to first order and transition probabilities were taken as unity. In order to fit the 130 GHz echo detected spectra, a weighted sum of two simulations having different g_x values was required. Parameters for the simulations are given in the legend to Fig. 5. Uncertainty in the reported g-values is +/- 0.00003 and for the hyperfine coupling value was +/- 0.5 G (152,170).

Preparation of RFQ samples for high–field EPR: The RFQ apparatus and its calibration for preparation of the high frequency EPR samples will be described in detail elsewhere. Briefly, it consists of a System 1000 syringe driving ram (Update Instruments, Madison, WI) and associated reactor hoses to produce a sample frozen at 35

ms, and the following components designed and manufactured in-house: a Wiskind-type mixing chamber, an ejection nozzle, a freezing unit comprising copper-beryllium alloy wheels and a sample collection basin (Manzerova, J., Krymov, V., Gerfen, G., unpublished results). Two syringes of equal volume were mounted on the ram unit; one was filled with the KatG solution (150 μM) and the other with 600 mM H_2O_2. A 25-hole spraying nozzle was attached to the outlet of the aging hose. The reaction mixture was ejected through the nozzle onto the rapidly rotating (1500 rpm) copper-beryllium alloy wheels cooled with liquid nitrogen. The frozen solution was continuously scraped off the wheels by stainless steel blades and was collected as a fine powder under liquid nitrogen. This powder was then divided and packed into either standard size precision bore quartz EPR tubes (4 mm o.d.) for measurements at X-band or into capillaries for D-band measurements. The 4 mm tubes were attached to a glass funnel using heat-shrink tubing and this assembly was immersed in isopentane kept at -140 ˚C; the sample powder was transferred into the funnel with cold metal spatulas and packed using a stainless steel packing rod with a Teflon tip. A packing factor of 0.8 was determined separately by comparing the volume of frozen and then melted contents of a tube. A home-built platform immersed in liquid nitrogen was used to pack D-band capillary tubes.

Appendix B. DNA and amino acid sequence of *M. tuberculosis* catalase-peroxidase KatG (from strain H37Rv)

DNA Sequence:

```
   1 - gtg ccc gag caa cac cca ccc att aca gaa
  31 - acc acc acc gga gcc gct agc aac ggc tgt
  61 - ccc gtc gtg ggt cat atg aaa tac ccc gtc
  91 - gag ggc ggc gga aac cag gac tgg tgg ccc
 121 - aac cgg ctc aat ctg aag gta ctg cac caa
 151 - aac ccg gcc gtc gct gac ccg atg ggt gcg
 181 - gcg ttc gac tat gcc gcg gag gtc gcg acc
 211 - atc gac gtt gac gcc ctg acg cgg gac atc
 241 - gag gaa gtg atg acc acc tcg cag ccg tgg
 271 - tgg ccc gcc gac tac ggc cac tac ggg ccg
 301 - ctg ttt atc cgg atg gcg tgg cac gct gcc
 331 - ggc acc tac cgc atc cac gac ggc cgc ggc
 361 - ggc gcc ggg ggc ggc atg cag cgg ttc gcg
 391 - ccg ctt aac agc tgg ccc gac aac gcc agc
 421 - ttg gac aag gcg cgc cgg ctg ctg tgg ccg
 451 - gtc aag aag aag tac ggc aag aag ctc tca
 481 - tgg gcg gac ctg att gtt ttc gcc ggc aac
 511 - tgc gcg ctg gaa tcg atg ggc ttc aag acg
 541 - ttc ggg ttc ggc ttc ggc cgg gtc gac cag
 571 - tgg gag ccc gat gag gtc tat tgg ggc aag
 601 - gaa gcc acc tgg ctc ggc gat gag cgt tac
 631 - agc ggt aag cgg gat ctg gag aac ccg ctg
 661 - gcc gcg gtg cag atg ggg ctg atc tac gtg
 691 - aac ccg gag ggg ccg aac ggc aac ccg gac
 721 - ccc atg gcc gcg gcg gtc gac att cgc gag
 751 - acg ttt cgg cgc atg gcc atg aac gac gtc
 781 - gaa aca gcg gcg ctg atc gtc ggc ggt cac
 811 - act ttc ggt aag acc cat ggc gcc ggc ccg
 841 - gcc gat ctg gtc ggc ccc gaa ccc gag gct
 871 - gct ccg ctg gag cag atg ggc ttg ggc tgg
 901 - aag agc tcg tat ggc acc gga acc ggt aag
 931 - gac gcg atc acc agc ggc atc gag gtc gta
 961 - tgg acg aac acc ccg acg aaa tgg gac aac
 991 - agt ttc ctc gag atc ctg tac ggc tac gag
1021 - tgg gag ctg acg aag agc cct gct ggc gct
1051 - tgg caa tac acc gcc aag gac ggc gcc ggt
1081 - gcc ggc acc atc ccg gac ccg ttc ggc ggg
1111 - cca ggg cgc tcc ccg acg atg ctg gcc act
1141 - gac ctc tcg ctg cgg gtg gat ccg atc tat
1171 - gag cgg atc acg cgt cgc tgg ctg gaa cac
1201 - ccc gag gaa ttg gcc gac gag ttc gcc aag
1231 - gcc tgg tac aag ctg atc cac cga gac atg
1261 - ggt ccc gtt gcg aga tac ctt ggg ccg ctg
1291 - gtc ccc aag cag acc ctg ctg tgg cag gat
1321 - ccg gtc cct gcg gtc agc cac gac ctc gtc
```

```
1351 - ggc gaa gcc gag att gcc agc ctt aag agc
1381 - cag atc cgg gca tcg gga ttg act gtc tca
1411 - cag cta gtt tcg acc gca tgg gcg gcg gcg
1441 - tcg tcg ttc cgt ggt agc gac aag cgc ggc
1471 - ggc gcc aac ggt ggt cgc atc cgc ctg cag
1501 - cca caa gtc ggg tgg gag gtc aac gac ccc
1531 - gac ggg gat ctg cgc aag gtc att cgc acc
1561 - ctg gaa gag atc cag gag tca ttc aac tcc
1591 - gcg gcg ccg ggg aac atc aaa gtg tcc ttc
1621 - gcc gac ctc gtc gtg ctc ggt ggc tgt gcc
1651 - gcc ata gag aaa gca gca aag gcg gct ggc
1681 - cac aac atc acg gtg ccc ttc acc ccg ggc
1711 - cgc acg gat gcg tcg cag gaa caa acc gac
1741 - gtg gaa tcc ttt gcc gtg ctg gag ccc aag
1771 - gca gat ggc ttc cga aac tac ctc gga aag
1801 - ggc aac ccg ttg ccg gcc gag tac atg ctg
1831 - ctc gac aag gcg aac ctg ctt acg ctc agt
1861 - gcc cct gag atg acg gtg ctg gta ggt ggc
1891 - ctg cgc gtc ctc ggc gca aac tac aag cgc
1921 - tta ccg ctg ggc gtg ttc acc gag gcc tcc
1951 - gag tca ctg acc aac gac ttc ttc gtg aac
1981 - ctg ctc gac atg ggt atc acc tgg gag ccc
2011 - tcg cca gca gat gac ggg acc tac cag ggc
2041 - aag gat ggc agt ggc aag gtg aag tgg acc
2071 - ggc agc cgc gtg gac ctg gtc ttc ggg tcc
2101 - aac tcg gag ttg cgg gcg ctt gtc gag gtc
2131 - tat ggc gcc gat gac gcg cag ccg aag ttc
2161 - gtg cag gac ttc gtc gct gcc tgg gac aag
2191 - gtg atg aac ctc gac agg ttc gac gtg cgc
2221 - tga
```

Amino acid sequence:

```
  1 - VPEQHPPITE TTTGAASNGC PVVGHMKYPV EGGGNQDWWP NRLNLKVLHQ NPAVADPMGA
 61 - AFDYAAEVAT IDVDALTRDI EEVMTTSQPW WPADYGHYGP LFIRMAWHAA GTYRIHDGRG
121 - GAGGGMQRFA PLNSWPDNAS LDKARRLLWP VKKKYGKKLS WADLIVFAGN CALESMGFKT
181 - FGFGFGRVDQ WEPDEVYWGK EATWLGDERY SGKRDLENPL AAVQMGLIYV NPEGPNGNPD
241 - PMAAAVDIRE TFRRMAMNDV ETAALIVGGH TFGKTHGAGP ADLVGPEPEA APLEQMGLGW
301 - KSSYGTGTGK DAITSGIEVV WTNTPTKWDN SFLEILYGYE WELTKSPAGA WQYTAKDGAG
361 - AGTIPDPFGG PGRSPTMLAT DLSLRVDPIY ERITRRWLEH PEELADEFAK AWYKLIHRDM
421 - GPVARYLGPL VPKQTLLWQD PVPAVSHDLV GEAEIASLKS QIRASGLTVS QLVSTAWAAA
481 - SSFRGSDKRG GANGGRIRLQ PQVGWEVNDP DGDLRKVIRT LEEIQESFNS AAPGNIKVSF
541 - ADLVVLGGCA AIEKAAKAAG HNITVPFTPG RTDASQEQTD VESFAVLEPK ADGFRNYLGK
601 - GNPLPAEYML LDKANLLTLS APEMTVLVGG LRVLGANYKR LPLGVFTEAS ESLTNDFFVN
661 - LLDMGITWEP SPADDGTYQG KDGSGKVKWT GSRVDLVFGS NSELRALVEV YGADDAQPKF
721 - VQDFVAAWDK VMNLDRFDVR
```

References

1. Rothschild, B. M., Martin, L. D., Lev, G., Bercovier, H., Bar-Gal, G. K., Greenblatt, C., Donoghue, H., Spigelman, M., and Brittain, D. (2001) *Clin. Infect. Dis.* **33**(3), 305-311
2. Zink, A. R., Sola, C., Reischl, U., Grabner, W., Rastogi, N., Wolf, H., and Nerlich, A. G. (2003) *J. Clin. Microbiol.* **41**(1), 359-367
3. Robitzek, E. H., and Selikoff, I. J. (1952) *Am. Rev. Tuberc.* **65**, 402-428
4. Kochi, A. (1991) *Tubercle* **72**(1), 1-6
5. Phyu, S., Ti, T., Jureen, R., Hmun, T., Myint, H., Htun, A., Grewal, H. M., and Bjorvatn, B. (2003) *Emerg. Infect. Dis.* **9**(2), 274-276
6. Sepkowitz, K. A. (2001) *Emerg. Infect. Dis.* **7**(2), 259-262.
7. Sepkowitz, K. A. (1995) *Clin. Infect. Dis.* **20**(2), 232-242.
8. Hutchison, D. C., Drobniewski, F. A., and Milburn, H. J. (2003) *Respir. Med.* **97**(1), 65-70
9. (2007) *MMWR Morb. Mortal. Wkly. Rep.* **56**(11), 250-253
10. Gandhi, N. R., Moll, A., Sturm, A. W., Pawinski, R., Govender, T., Lalloo, U., Zeller, K., Andrews, J., and Friedland, G. (2006) *Lancet* **368**(9547), 1575-1580
11. Tortora, G. J. F., Berdell R. Case, Christine L. (2007) *Pearson education Inc. San Francisco, CA. Ninth edition*
12. Winder, F. G., and Collins, P. B. (1970) *J. Gen. Microbiol.* **63**(1), 41-48

13. Banerjee, A., Dubnau, E., Quemard, A., Balasubramanian, V., Um, K. S., Wilson, T., Collins, D., de Lisle, G., and Jacobs, W. R., Jr. (1994) *Science* **263**(5144), 227-230

14. Brennan, P. J., and Nikaido, H. (1995) *Annu. Rev. Biochem.* **64**, 29-63

15. Minnikin, D. E., Minnikin, S. M., Goodfellow, M., and Stanford, J. L. (1982) *J. Gen. Microbiol.* **128**(4), 817-822

16. Somoskovi, A., Parsons, L. M., and Salfinger, M. (2001) *Respir. Res.* **2**(3), 164-168

17. Lacave, C., Laneelle, M. A., Daffe, M., Montrozier, H., and Laneelle, G. (1989) *Eur. J. Biochem.* **181**(2), 459-466

18. Takayama, K., and N. Qureshi. (1979) *Proceedings of the 14th U.S.-Japan Tuberculosis Research Conference. U. S. -Japan Cooperative Medical Science Program, NIH/NIAID. National Institutes of Health, Washington, D.C.* , 168-186

19. Claiborne, A., and Fridovich, I. (1979) *Biochemistry* **18**(11), 2324-2329

20. Claiborne, A., Malinowski, D. P., and Fridovich, I. (1979) *J. Biol. Chem.* **254**(22), 11664-11668

21. Nadler, V. G., I. Hochman, A. (1986) *Biochim. Biophys. Acta* **882**, 234-241

22. Loprasert, S., Negoro, S., and Okada, H. (1989) *J. Bacteriol.* **171**(9), 4871-4875

23. Nathan, C., and Shiloh, M. U. (2000) *Proc. Natl. Acad. Sci. U S A* **97**(16), 8841-8848

24. Scanga, C. A., Mohan, V. P., Joseph, H., Yu, K., Chan, J., and Flynn, J. L. (1999) *Infect. Immun.* **67**(9), 4531-4538

25. MacMicking, J. D., North, R. J., LaCourse, R., Mudgett, J. S., Shah, S. K., and Nathan, C. F. (1997) *Proc. Natl. Acad. Sci. U S A* **94**(10), 5243-5248

26. Heym, B., Zhang, Y., Poulet, S., Young, D., and Cole, S. T. (1993) *J. Bacteriol.* **175**(13), 4255-4259

27. Cohn, M. L., Oda, U., Kovitz, C., and Middlebrook, G. (1954) *Am. Rev. Tuberc.* **70**(3), 465-475

28. Ng, V. H., Cox, J. S., Sousa, A. O., MacMicking, J. D., and McKinney, J. D. (2004) *Mol. Microbiol.* **52**(5), 1291-1302

29. McKinney, J. D., Honer zu Bentrup, K., Munoz-Elias, E. J., Miczak, A., Chen, B., Chan, W. T., Swenson, D., Sacchettini, J. C., Jacobs, W. R., Jr., and Russell, D. G. (2000) *Nature* **406**(6797), 735-738

30. Welinder, K. G. (1991) *Biochim. Biophys. Acta* **1080**(3), 215-220

31. Nagy, J. M., Cass, A. E., and Brown, K. A. (1997) *J. Biol. Chem.* **272**(50), 31265-31271

32. Jakopitsch, C., Droghetti, E., Schmuckenschlager, F., Furtmuller, P. G., Smulevich, G., and Obinger, C. (2005) *J. Biol. Chem.* **280**(51), 42411-42422

33. Ivancich, A., Jakopitsch, C., Auer, M., Un, S., and Obinger, C. (2003) *J. Am. Chem. Soc.* **125**(46), 14093-14102

34. Jakopitsch, C., Vlasits, J., Wiseman, B., Loewen, P. C., and Obinger, C. (2007) *Biochemistry* **46**(5), 1183-1193

35. Suarez, J., Ranguelova, K., Jarzecki, A. A., Manzerova, J., Krymov, V., Zhao, X., Yu, S., Metlitsky, L., Gerfen, G. J., and Magliozzo, R. S. (2009) *J. Biol. Chem.* **284**(11), 7017-7029

36. Johnsson, K., King, D. S., and Schultz, P. G. (1995) *J. Am. Chem. Soc.* **117**(17), 5009-5010

37. Vilcheze, C., Wang, F., Arai, M., Hazbon, M. H., Colangeli, R., Kremer, L., Weisbrod, T. R., Alland, D., Sacchettini, J. C., and Jacobs, W. R., Jr. (2006) *Nat. Med.* **12**(9), 1027-1029

38. Middlebrook, G., Cohn, M. L., and Schaeffer, W. B. (1954) *Am. Rev. Tuberc.* **70**, 852-872

39. Heym, B., and Cole, S. T. (1992) *Res. Microbiol.* **143**(7), 721-730

40. Zhang, Y., Heym, B., Allen, B., Young, D., and Cole, S. (1992) *Nature* **358**(6387), 591-593.

41. Zabinski, R. F., and Blanchard, J.S. (1997) *J. Am. Chem. Soc.* **119**, 2331-2332

42. Quemard, A., Dessen, A., Sugantino, M., Jacobs, W. R. J., Sacchettini, J. C., and Blanchard, J. S. (1996) *J. Am. Chem. Soc.* **118**(6), 1561-1562

43. Rawat, R., Whitty, A., and Tonge, P. J. (2003) *Proc. Natl. Acad. Sci. U S A* **100**(24), 13881-13886

44. Rozwarski, D. A., Grant, G. A., Barton, D. H. R., Jacobs, W. R., Jr., and Sacchettini, J. C. (1998) *Science* **279**(5347), 98-102

45. Lei, B., Wei, C. J., and Tu, S. C. (2000) *J. Biol. Chem.* **275**(4), 2520-2526

46. Quemard, A., Sacchettini, J. C., Dessen, A., Vilcheze, C., Bittman, R., Jacobs, W. R., Jr., and Blanchard, J. S. (1995) *Biochemistry* **34**(26), 8235-8241

47. Hazbon, M. H., Brimacombe, M., Bobadilla del Valle, M., Cavatore, M., Guerrero, M. I., Varma-Basil, M., Billman-Jacobe, H., Lavender, C., Fyfe, J., Garcia-Garcia, L., Leon, C. I., Bose, M., Chaves, F., Murray, M., Eisenach, K. D.,

Sifuentes-Osornio, J., Cave, M. D., Ponce de Leon, A., and Alland, D. (2006) *Antimicrob. Agents Chemother.* **50**(8), 2640-2649

48. Cardoso, R. F., Cooksey, R. C., Morlock, G. P., Barco, P., Cecon, L., Forestiero, F., Leite, C. Q., Sato, D. N., Shikama Mde, L., Mamizuka, E. M., Hirata, R. D., and Hirata, M. H. (2004) *Antimicrob. Agents Chemother.* **48**(9), 3373-3381

49. Yu, S., Girotto, S., Lee, C., and Magliozzo, R. S. (2003) *J. Biol. Chem.* **278**(17), 14769-14775

50. Yu, S., Chouchane, S., and Magliozzo, R. S. (2002) *Protein Sci.* **11**(1), 58-64.

51. Wei, C.-J., Lei, B., Musser, J. M., and Tu, S.-C. (2003) *Antimicrob. Agents Chemother.* **47**(2), 670-675

52. Rouse, D. A., DeVito, J. A., Li, Z., Byer, H., and Morris, S. L. (1996) *Mol. Microbiol.* **22**(3), 583-592

53. Zamocky, M., Regelsberger, G., Jakopitsch, C., and Obinger, C. (2001) *FEBS Lett.* **492**(3), 177-182.

54. Dunford, H. B. (1999) *Heme Peroxidases*, Wiley-VCH, New York

55. Yu, S., Girotto, S., Zhao, X., and Magliozzo, R. S. (2003) *J. Biol. Chem.* **278**(45), 44121-44127

56. Regelsberger, G., Jakopitsch, C., Furtmuller, P. G., Rueker, F., Switala, J., Loewen, P. C., and Obinger, C. (2001) *Biochem. Soc. Trans.* **29**(Pt 2), 99-105.

57. Jakopitsch, C., Kolarich, D., Petutschnig, G., Furtmuller, P. G., and Obinger, C. (2003) *FEBS Lett.* **552**(2-3), 135-140

58. Hillar, A., Peters, B., Pauls, R., Loboda, A., Zhang, H., Mauk, A. G., and Loewen, P. C. (2000) *Biochemistry* **39**(19), 5868-5875

59. Zhao, X., Yu, H., Yu, S., Wang, F., Sacchettini, J. C., and Magliozzo, R. S. (2006) *Biochemistry* **45**(13), 4131-4140

60. Kapetanaki, S. M., Chouchane, S., Yu, S., Zhao, X., Magliozzo, R. S., and Schelvis, J. P. (2005) *Biochemistry* **44**(1), 243-252

61. Kapetanaki, S., Chouchane, S., Girotto, S., Yu, S., Magliozzo, R. S., and Schelvis, J. P. (2003) *Biochemistry* **42**(13), 3835-3845

62. George, P., and Irvine, D. H. (1955) *Biochem. J.* **60**(4), 596-604

63. Gibson, J. F., Ingram, D. J., and Nicholls, P. (1958) *Nature* **181**(4620), 1398-1399

64. Barry, B. A., el-Deeb, M. K., Sandusky, P. O., and Babcock, G. T. (1990) *J. Biol. Chem.* **265**(33), 20139-20143.

65. Ivancich, A., Jouve, H. M., Sartor, B., and Gaillard, J. (1997) *Biochemistry* **36**(31), 9356-9364

66. Ivancich, A., Mazza, G., and Desbois, A. (2001) *Biochemistry* **40**(23), 6860-6866.

67. Larsson, A., and Sjoberg, B. M. (1986) *Embo. J.* **5**(8), 2037-2040.

68. Karthein, R., Dietz, R., Nastainczyk, W., and Ruf, H. H. (1988) *Eur. J. Biochem.* **171**(1-2), 313-320.

69. Blodig, W., Smith, A. T., Winterhalter, K., and Piontek, K. (1999) *Arch. Biochem. Biophys.* **370**(1), 86-92.

70. Chouchane, S., Girotto, S., Yu, S., and Magliozzo, R. S. (2002) *J. Biol. Chem.* **277**(45), 42633-42638

71. Ranguelova, K., Girotto, S., Gerfen, G. J., Yu, S., Suarez, J., Metlitsky, L., and Magliozzo, R. S. (2007) *J. Biol. Chem.* **282**(9), 6255-6264

72. Stubbe, J., and Riggs-Gelasco, P. (1998) *Trends Biochem. Sci.* **23**(11), 438-443.

73. Chouchane, S., Lippai, I., and Magliozzo, R. S. (2000) *Biochemistry* **39**(32), 9975-9983

74. Zhao, X., Girotto, S., Yu, S., and Magliozzo, R. S. (2004) *J. Biol. Chem.* **279**(9), 7606-7612

75. Tew, D., and Ortiz de Montellano, P. R. (1988) *J. Biol. Chem.* **263**(33), 17880-17886

76. Giulivi, C., and Davies, K. J. (1993) *J. Biol. Chem.* **268**(12), 8752-8759

77. Spangler, B. D., and Erman, J. E. (1986) *Biochim. Biophys. Acta* **872**(1-2), 155-157

78. Pipirou, Z., Bottrill, A. R., Metcalfe, C. M., Mistry, S. C., Badyal, S. K., Rawlings, B. J., and Raven, E. L. (2007) *Biochemistry* **46**(8), 2174-2180

79. Lardinois, O. M., Medzihradszky, K. F., and Ortiz de Montellano, P. R. (1999) *J. Biol. Chem.* **274**(50), 35441-35448.

80. Ranguelova, K., Suarez, J., Magliozzo, R. S., and Mason, R. P. (2008) *Biochemistry* **47**(43), 11377-11385

81. Mason, R. P. (2004) *Free Radic. Biol. Med.* **36**(10), 1214-1223

82. Parsons, L. M., Clobridge, M. S. A, Dormandy, J., Mirabello, L., Polletta, V. L., Sanic, A., Sinyavskiy, O., Larsen, S. C., Driscoll, J., Zickas, G., and Taber, H. W. (2005) *Antimicrob. Agents Chemother.* **49**, 2218-2225.

83. Saint-Joanis, B., Souchon, H., Wilming, M., Johnsson, K., Alzari, P. M., and Cole, S. T. (1999) *Biochem. J.* **338**, 753-760

84. Wengenack, N. L., Todorovic, S., Yu, L., and Rusnak, F. (1998) *Biochemistry* **37**(45), 15825-15834

85. Metcalfe, C., Macdonald, I. K., Murphy, E. J., Brown, K. A., Raven, E. L., and Moody, P. C. (2008) *J. Biol. Chem.* **283**(10), 6193-6200

86. Chouchane, S., Girotto, S., Kapetanaki, S., Schelvis, J. P., Yu, S., and Magliozzo, R. S. (2003) *J. Biol. Chem.* **278**(10), 8154-8162

87. Ranguelova, K., Suarez, J., Metlitsky, L., Yu, S., Brejt, S. Z., Brejt, S. Z., Zhao, L., Schelvis, J. P., and Magliozzo, R. S. (2008) *Biochemistry* **47**(47), 12583-12592

88. Bertrand, T., Eady, N. A. J., Jones, J. N., Jesmin, Nagy, J. M., Jamart-Gregoire, B., Raven, E. L., and Brown, K. A. (2004) *J. Biol. Chem.* **279**(37), 38991-38999

89. Zhao, X., Yu, S., and Magliozzo, R. S. (2007) *Biochemistry* **46**(11), 3161-3170

90. Wengenack, N. L., Uhl, J. R., St Amand, A. L., Tomlinson, A. J., Benson, L. M., Naylor, S., Kline, B. C., Cockerill, F. R., 3rd, and Rusnak, F. (1997) *J. Infect. Dis.* **176**(3), 722-727

91. Svistunenko, D. A. (2001) *Biochim. Biophys. Acta* **1546**(2), 365-378

92. Kelman, D. J., and Mason, R. P. (1992) *Free Radic. Res. Commun.* **16**(1), 27-33

93. Magliozzo, R. S., and Marcinkeviciene, J.A. (1996) *J. Am. Chem. Soc.* **118**, 11303-11304

94. Ghiladi, R. A., Cabelli, D. E., and Ortiz de Montellano, P. R. (2004) *J. Am. Chem. Soc.* **126**(15), 4772-4773

95. Wengenack, N. L., Hoard, H. M., and Rusnak, F. (1999) *J. Am. Chem. Soc.* **121**, 9748-9749

96. Singh, R., Switala, J., Loewen, P. C., and Ivancich, A. (2007) *J. Am. Chem. Soc.* **129**(51), 15954-15963

97. Singh, R., Wiseman, B., Deemagarn, T., Donald, L. J., Duckworth, H. W., Carpena, X., Fita, I., and Loewen, P. C. (2004) *J. Biol. Chem.* **279**(41), 43098-43106

98. Wengenack, N. L., and Rusnak, F. (2001) *Biochemistry* **40**(30), 8990-8996

99. Broussy, S., Bernardes-Genisson, V., Coppel, Y., Quemard, A., Bernadou, J., and Meunier, B. (2005) *Org. Biomol. Chem.* **3**(4), 670-673

100. Ghiladi, R. A., Medzihradszky, K. F., Rusnak, F. M., and Ortiz de Montellano, P. R. (2005) *J. Am. Chem. Soc.* **127**(38), 13428-13442

101. Argyrou, A., Jin, L., Siconilfi-Baez, L., Angeletti, R. H., and Blanchard, J. S. (2006) *Biochemistry* **45**(47), 13947-13953

102. Argyrou, A., Vetting, M. W., Aladegbami, B., and Blanchard, J. S. (2006) *Nat. Struct. Mol. Biol.* **13**(5), 408-413

103. Kapetanaki, S. M., Zhao, X., Yu, S., Magliozzo, R. S., and Schelvis, J. P. (2007) *J. Inorg. Biochem.* **101**(3), 422-433

104. Kelman, D. J., DeGray, J. A., and Mason, R. P. (1994) *J. Biol. Chem.* **269**(10), 7458-7463

105. Girotto, S. (2004) Application of EPR spectroscopy to study the resting state structure and the mechnism of *Mycobacterium tuberculosis* catalase peroxidase KatG. Ph. D thesis. *The Graduate Center of the City University of New York*

106. Giulivi, C., and Cadenas, E. (1993) *Arch. Biochem. Biophys.* **303**(1), 152-158.

107. Wilming, M., and Johnsson, K. (2001) *FEBS Lett.* **509**(2), 272-276.

108. Malencik, D. A., Sprouse, J. F., Swanson, C. A., and Anderson, S. R. (1996) *Anal. Biochem.* **242**(2), 202-213

109. Lehrer, S. S., and Fasman, G. D. (1967) *Biochemistry* **6**(3), 757-767

110. Boguta, G., and Dancewicz, A. M. (1981) *Int. J. Radiat. Biol. Relat. Stud. Phys. Chem. Med.* **39**(2), 163-174

111. Garcia-Castineiras, S., Dillon, J., and Spector, A. (1978) *Science* **199**(4331), 897-899

112. Giulivi, C., and Davies, K. J. (1994) *Methods Enzymol.* **233**, 363-371

113. Heinecke, J. W. (2002) *Toxicology* **177**(1), 11-22

114. Rivett, A. J. (1985) *J. Biol. Chem.* **260**(1), 300-305

115. Stadtman, E. R., and Wittenberger, M. E. (1985) *Arch. Biochem. Biophys.* **239**(2), 379-387

116. Lin, G., Hu, G., Tsu, C., Kunes, Y. Z., Li, H., Dick, L., Parsons, T., Li, P., Chen, Z., Zwickl, P., Weich, N., and Nathan, C. (2006) *Mol. Microbiol.* **59**(5), 1405-1416

117. Smulevich, G., Jakopitsch, C., Droghetti, E., and Obinger, C. (2006) *J. Inorg. Biochem.* **100**(4), 568-585

118. Goodwin, D. C., Gunther, M. R., Hsi, L. C., Crews, B. C., Eling, T. E., Mason, R. P., and Marnett, L. J. (1998) *J. Biol. Chem.* **273**(15), 8903-8909.

119. Collins, D. M. (1996) *Trends Microbiol.* **4**(11), 426-430

120. Pym, A. S., Domenech, P., Honore, N., Song, J., Deretic, V., and Cole, S. T. (2001) *Mol. Microbiol.* **40**(4), 879-889.

121. Pym, A. S., Saint-Joanis, B., and Cole, S. T. (2002) *Infect. Immun.* **70**(9), 4955-4960

122. Regelsberger, G., Obinger, C., Zoder, R., Altmann, F., and Peschek, G. A. (1999) *FEMS Microbiol. Lett.* **170**(1), 1-12

123. Ivancich, A., Lutz, M., and Mattioli, T. A. (1997) *Biochemistry* **36**(11), 3242-3253

124. Ghiladi, R. A., Knudsen, G. M., Medzihradszky, K. F., and de Montellano, P. R. (2005) *J. Biol. Chem.* **280**(24), 22651-22663

125. Vlasits, J., Jakopitsch, C., Schwanninger, M., Holubar, P., and Obinger, C. (2007) *FEBS Let.t* **581**(2), 320-324

126. Kato, S., Ueno, T., Fukuzumi, S., and Watanabe, Y. (2004) *J. Biol. Chem.* **279**(50), 52376-52381

127. Jakopitsch, C., Wanasinghe, A., Jantschko, W., Furtmuller, P. G., and Obinger, C. (2005) *J. Biol. Chem.* **280**(10), 9037-9042

128. Miller, M. A., Bandyopadhyay, D., Mauro, J. M., Traylor, T. G., and Kraut, J. (1992) *Biochemistry* **31**(10), 2789-2797

129. Jakopitsch, C., Auer, M., Ivancich, A., Ruker, F., Furtmuller, P. G., and Obinger, C. (2003) *J. Biol. Chem.* **278**(22), 20185-20191

130. Ghiladi, R. A., Medzihradszky, K. F., and Ortiz de Montellano, P. R. (2005) *Biochemistry* **44**(46), 15093-15105

131. Carpena, X., Wiseman, B., Deemagarn, T., Herguedas, B., Ivancich, A., Singh, R., Loewen, P. C., and Fita, I. (2006) *Biochemistry* **45**(16), 5171-5179

132. Jakopitsch, C., Obinger, C., Un, S., and Ivancich, A. (2006) *J. Inorg. Biochem.* **100**(5-6), 1091-1099

133. Zhao, X., Yu, S., Ranguelova, K., Suarez, J., Metlitsky, L., Schelvis, J. P., and Magliozzo, R. S. (2009) *J. Biol. Chem.* **284**(11), 7030-7037

134. Garcia-Serres, R., Davydov, R. M., Matsui, T., Ikeda-Saito, M., Hoffman, B. M., and Huynh, B. H. (2007) *J. Am. Chem. Soc.* **129**(5), 1402-1412

135. Denisov, I. G., Makris, T. M., and Sligar, S. G. (2002) *J. Biol. Chem.* **277**(45), 42706-42710

136. DeGray, J. A., Gunther, M. R., Tschirret-Guth, R., Montellano, P. R. O. d., and Mason, R. P. (1997) *J. Biol. Chem.* **272**(4), 2359-2362

137. Miyagawa, I., Kurita, Y., and Gordy, W. (1960) *J. Chem. Phys.* **6**(33), 1599-1603

138. Duboc-Toia, C., Hassan, A. K., Mulliez, E., Choudens, S. O.-d., Fontecave, M., Leutwein, C., and Heider, J. (2003) *J. Am. Chem. Soc.* **125**(1), 38-39

139. Lendzian, F., Sahlin, M., MacMillan, F., Bittl, R., Fiege, R., Pötsch, S., Sjöberg, B.-M., Gräslund, A., Lubitz, W., and Lassmann, G. (1996) *J. Am. Chem. Soc.* **118**, 8111-8120

140. Pogni, R., Baratto, M. C., Giansanti, S., Teutloff, C., Verdin, J., Valderrama, B., Lendzian, F., Lubitz, W., Vaszquez-Duhalt, R., and Basosi, R. (2005) *Biochemistry* **44**(4267-4274), 4267-4274

141. Bleifuss, G., Kolberg, M., Pötsch, S., Hofbauer, W., Bittl, R., Lubitz, W., Gräslund, A., Lassmann, G., and Lendzian, F. (2001) *Biochemistry* **40**, 15362-15368

142. Box, H. C., and Budzinski, E. E. (1976) *J. C. S. Perkins II*, 553-555

143. Kou, W. W. H., and Box, H. C. (1976) *J. Chem. Phys.* **64**(7), 3060-3062

144. Gerfen, G. J., Licht, S., Willems, J.-P., Hoffman, B. M., and Stubbe, J. (1996) *J. Am. Chem. Soc.* **118**, 8192-8197

145. Liu, A., Barra, A.-L., Rubin, H., Lu, G., and Gräslund, A. (2000) *J. Am. Chem. Soc.* **122**, 1974-1978

146. Dorlet, P., Seibold, S. A., Babcock, G. T., Gerfen, G. J., Smith, W. L., Tsai, A. L., and Un, S. (2002) *Biochemistry* **41**(19), 6107-6114

147. Wilson, J. C., Wu, G., Tsai, A.-l., and Gerfen, G. J. (2005) *J. Am. Chem. Soc.* **127**, 1618-1619

148. Gerfen, G. J., Bellew, B.F., Un, S., Bollinger, J.M., Jr., Stubbe, J., Griffin, R.G., and Singel, D.J. (1993) *J. Am. Chem. Soc.* **155**, 6420-6421

149. Ivancich, A., Dorlet, P., Goodin, D. B., and Un, S. (2001) *J. Am. Chem. Soc.* **123**(21), 5050-5058.

150. Un, S., Gerez, C., Elleingand, E., and Fontecave, M. (2001) *J. Am. Chem. Soc.* **123**(13), 3048-3054

151. Andersson, K. K., and Barra, A.-L. (2002) *Spectrochimica Acta Part A: Molecular and Biomolecular Spectroscopy* **58**(6), 1101-1112

152. Gerfen, G. J., Bellew, B. F., Griffin, R. G., Singel, D. J., Ekberg, C. A. and Whittaker, J. W. (1996) *J. Phys. Chem.* **100**, 16739-16748

153. Jeschke, G. (2005) *Biochim. Biophys. Acta* **1707**(1), 91-102

154. Bender, C. J., Sahlin, M., Babcock, G. T., Barry, B. A., Chandrashekar, T. K., Salowe, S. P., Stubbe, J., Lindstroem, B., Petersson, L., Ehrenberg, A., and Sjoberg, B.-M. (1989) *J. Am. Chem. Soc.* **111**(21), 8076-8083.

155. Gunther, M. R., Sturgeon, B. E., and Mason, R. P. (2000) *Free Radic. Biol. Med.* **28**(5), 709-719.

156. Svistunenko, D. A., and Cooper, C. E. (2004) *Biophys. J.* **87**, 582-595

157. Un, S. (2005) *Magn. Reson. Chem.* **43 Spec no.**, S229-236

158. Ivancich, A., Mattioli, T. A., and Un, S. (1999) *J. Am. Chem. Soc.* **121**(24), 5743-5753

159. Farrar, C. T., Gerfen, G. J., Griffin, R. G., Force, D. A., and Britt, R. D. (1997) *J. Phys. Chem. B* **101**, 6634-6641

160. Faller, P., Goussias, C., Rutherford, A. W., and Un, S. (2003) *Proc. Natl. Acad. Sci. U S A* **100**(15), 8732-8735

161. Vidossich, P., Alfonso-Prieto, M., Carpena, X., Loewen, P. C., Fita, I., and Rovira, C. (2007) *J. Am. Chem. Soc.* **129**(44), 13436-13446

162. Putnam, C. D., Arvai, A. S., Bourne, Y., and Tainer, J. A. (2000) *J. Mol. Biol.* **296**(1), 295-309.

163. Anabella Ivancich, H. M. J., and Jacques Gaillard. (1996) *J. Am. Chem. Soc.* **118**(50), 12852 - 12853

164. Winterbourn, C. C., Parsons-Mair, H. N., Gebicki, S., Gebicki, J. M., and Davies, M. J. (2004) *Biochem. J.* **381**(Pt 1), 241-248

165. Johnsson, K., Froland, W. A., and Schultz, P. G. (1997) *J. Biol. Chem.* **272**(5), 2834-2840

166. Loewen, P. C., and Stauffer, G. V. (1990) *Mol. Gen. Genet.* **224**(1), 147-151

167. Marcinkeviciene, J. A., Magliozzo, R. S., and Blanchard, J. S. (1995) *J. Biol. Chem.* **270**(38), 22290-22295

168. Beers, R. F., and Sizers, I. W. (1952) *J. Biol. Chem.* **195**, 133-140

169. Burghaus, O., Rohrer, M., Gotzinger, T., Plato M., and Mobius, K. (1992) *Meas. Sci. Technol.* **3**, 765-774

170. van der Donk, W. A., Stubbe, J., Gerfen, G.J., Bellew, B. F., and Griffin, R. G. (1995) *J. Am. Chem. Soc.* **117** 8908-8916